PhD. Thesis, Harvard Univ., Cambridge, MA. 1977

INFRARED OBSERVATIONS OF GALAXIES

A Thesis presented by
Marc Aaronson
to
the Department of Astronomy
in partial fulfillment of the requirements
for the degree of
Doctor of Philosophy
in the subject of
Astronomy
Harvard University
Cambridge, Massachusetts
August, 1977

Acknowledgements

The data in this thesis could not have been obtained without the aid of a truly vast number of people. I would especially like to thank:

Sallie Baliunas, Phil Marcus, and Steve Perrenod for allowing themselves to be dragged out to Arizona;

Les Wier and the guys in the machine shop for their prompt help when it was really needed, Chip in the shock tube lab for the many leak checks, Bill Grimm for the EE lessons and the pre-amp drawings, John Hamwey and the powers that be for all the wonderful figures, Gerda Schrauwen for the fine tables, Helen Beattie for her good nature, and particularly Val for working overtime during the '75 World Series;

Doug Kleinmann for crucial assistance on the light baffle and external focusing mechanism, the nifty neck tube support, and helpful discussions;

Keith Matthews for discovering (and communicating to me) the wondrous black magic of flashing;

Alex, Al, Herb, Nat, Bob, Peter, Leslie, Vivian, and Ruth for putting up with me and always coming up with the money from somewhere;

John Huchra for obtaining some precious UBV data and for much stimulating conversation;

Bas and Daryl at MHO for the glorious kluges, and also the (too) numerous night assistants at LC, CTIO, and

KPNO;

Bruce Carney for allowing me to squeeze in some galaxy measurements during his telescope time, and for his general goad spirits;

John Mariska for the dart games and for always being a fine source of gossip;

John Danziger and Chris McKee for your early and far too brief support;

Giovani Fazio for having the nerve to became my thesis adviser after the four previous occupants of the job left the Center - his suggestions, encouragement, and support are much appreciated.

Finally, to Eric Persson and Jay Frogel, who more than anyone have taught me the meaning of being an observational astronomer, and who are the guiding lights of this work, thanks seen hardly sufficient.

And to whatever deity sent me only 30% photometric weather far the past two years in Arizona - (expletive deleted)!

Table of Contents

- I. INTRODUCTION
- II. CO AND JHK OBSERVATIONS OF E AND S0 GALAXIES
  - Introduction
  - Observational Procedures and Data Reduction
    - a) Equipment
    - b) Galaxy Observations
    - c) Sources of Error and Instrumental Corrections
    - d) Sources of V Data
    - e) Reddening and K-corrections
    - f) Comparisons with Previous CO Measurements
    - g) Globular Cluster Observations
  - Discussion of the Galaxy Observations
    - a) The Dependence of Color and CO Index on Radius
    - b) Integrated Properties of the Galaxies
    - c) Summary and Conclusions
  - Discussion of the Globular Cluster Observations
  - Comparison of Mean Colors with Stellar Synthesis Models
  - Comparison with Photometric Studies at < 1.0
    - a) The Work of O'Connell
    - b) The Work of McClure and van den Bergh and of Faber
  - Summary and conclusions

- Appendix
- References

- III. OBSERVATIONS OF H_2O ABSORPTION AND THE COOLEST STELLAR COMPONENT OF E AND S0 GALAXIES
  - Introduction
  - Observations
  - The stellar data
  - Discussion of the Galaxy and Globular Cluster Data
  - References

- IV. INFRARED OBSERVATIONS OF BRIGHT GALAXIES ALONG THE HUBBLE SEQUENCE
  - Introduction
  - Observations and Data Reduction
    - a) Equipment
    - b) Galaxy Selection
    - c) Observational Procedure
    - d) Photometric Errors and Instrumental Corrections
    - e) The UVK Colors
    - f) Reddening and Redshift Corrections
    - g) Comparison with Previous Results
  - Results
    - a) Color-Aperture Relations
    - b) Integrated Properties
    - c) Color-Inclination Relations
    - d) Color-Absolute Magnitude Relations
    - e) Color-Color Relationships
  - Discussion
    - a) Integrated Colors
    - b) Color Gradients
  - Non-Stellar Effects
    - a) Dust Absorption
    - b) Dust Emission
    - c) Gaseous Emission
    - d) Non-Thermal Emission
    - e) Discussion
  - Comparison with Stellar Synthesis Models
  - Summary
  - Appendix A. The Stellar Calibration
  - Appendix B. The InSb Detector System
  - Appendix C. Metallicity Calibration and the V - K Color

- References

- V. IDENTIFICATION OF THE NUCLEUS IN THE SPIRAL GALAXY NGC 4631
  - Introduction
  - Observations
  - Discussion
  - References

- VI. CLOSING THOUGHTS

CHAPTER I
Introduction

In recent years many programs have been developed for recovering information about the stellar content of galaxies from their composite light. Such programs usually follow one of two approaches: In empirical models, some mathematical technique is used to find the best fitting mix of stars which matches detailed spectrophotometric or spectroscopic data; while in evolutionary models, an assumed mass function and star formation rate is used to evolve stars along theoretical tracks from which one can then compute integrated colors to compare with observations. In either case, published synthesis work has been based largely on optical data alone. From such data one can learn very little about the presence and nature of the coolest stars since these emit radiation mostly longward of optical wavelengths.

Knowledge of the coolest stellar component in galaxies would set strong constraints on both empirical and evolutionary synthesis models, and would lead to new insight into the relation between systems with different star formation histories. Consequently, I have undertaken a study of the infrared radiation from ordinary galaxies for the purposes of relating such information to the probable components of the stellar population in these systems. That such a study is now possible is due primarily to the recent development of InSb detectors highly sensitive in the 1 - 5 μm region.

The observations presented here consist largely of 1) broad-band magnitude measurements at 1.2 μm, 1.6 μm, and 2.2 μm; and 2) measurements of the 2.3 μm CO absorption band and 1.9 μm H_2O absorption band, features which are sensitive measures of luminosity and effective temperature in late-type stars. Because this study is in some sense a first attempt to obtain infrared photometric data of a quality comparable with that in the optical (i. e., having photometric errors < 0.05 mag), a great deal of attention has been paid to identifying sources of systematic error and making accurate estimates of the true precision obtained.

An endeavor will be made to address a number of questions: giant stars or dwarf stars dominate the 2 μm light? How late in mean spectral type are these stars, and in particular, can limits be placed on the very latest-type stars such as carbons or Miras? Do the infrared colors vary with galaxian luminosity? Do the colors vary with projected aperture size? Does the red stellar component change with galaxian morphology? Are color variations which may be found due primarily to a "pure" population change or to a metallicity-driven population change? Can the interrelations between the various infrared and optical colors be reasonably interpreted? Are there galaxies with non-stellar excesses at 2 μm and if so what are the likely causes of such excesses? How well do the observations support published synthesis models?

The results of this study are presented in Chapters II - V, in the form of four publishable papers. Chapters II and III, which are primarily concerned with the composite light of elliptical galaxies, were written in very close collaboration with Jay Frogel and Eric Persson. The measurements in these papers were obtained mostly with equipment at the Hale Observatories.

The main body of the thesis is Chapter IV, where observations of galaxies with a wide range of morphology are presented and discussed in relation to the data in the previous chapters. In order to obtain the measurements in this paper, I undertook the construction of an InSb detector system, some details of which are given at the end of Chapter IV in Appendix B. It should be noted that a major portion of the work in this thesis went into the building and maintenance of said instrument, which, thank God, worked quite well.

The final paper, in Chapter V, grew out of observations originally obtained for the previous chapter. Although the paper is somewhat tangential to the main themes in the thesis, the results are sufficiently interesting to warrant inclusion anyway.

Chapters II and III have already been submitted to the Ap. J. and are in press. A condensed version of Chapter IV will be submitted to the Ap. J. Suppl., and Chapter V will be sent to the P.A.S.P. Note that in the text, Chapters II, III, and IV are referred to as Papers I, II, and IV.

CHAPTER II
CO and JHK Observations of E and S0 Galaxies

ABSTRACT

New multiaperture infrared photometric observations of the central regions of 51 early-type galaxies and of the integrated light of five globular clusters are presented. These data are compared with selected optical observations and with various model predictions. The main results of the work are: (1) the observed parameters for the brighter galaxies, particularly the CO index and the $V - K$ color, agree with the predictions of stellar synthesis models characterized by giant-dominated populations with $M / L_V < 10$; (2) the galaxian broad-band colors tend to redden with increasing luminosity and decreasing aperture size; (3) for the globular clusters, there is evidence that the integrated colors become redder with increasing metallicity; (4) in bright galaxies the relative changes of $U - V$, $V - J$, and $J - K$ as functions of radius differ from the relative changes as functions of luminosity at a fixed radius.

Subject headings: galaxies: photometry - galaxies: stellar content - globular clusters: photometry - stars: late-type - infrared: general

I. INTRODUCTION

The composite nature of the integrated spectra of elliptical galaxies and the domination of the visible light by late-type giant stars have been known for nearly 30 years (e. g., Stebbins and Whitford 1948; Morgan and

Mayall 1957; Code 1959; reviewed by Whitford 1976). Nevertheless, the lack of luminosity-sensitive indices, particularly in the red and infrared regions of the spectrum, has hindered attempts to build quantitative models of the stellar content of these galaxies. For example, one of the conclusions of a study by Faber (1972), based in part on the observations of Spinrad and Taylor (1971), was that the available optical data could not be used to uniquely determine the proportion of high- and low luminosity red stars. The first broad-band infrared observations of galaxies (Johnson 1966a) showed that the 1.2 - 3.5 μm radiation is contributed mostly by stars cooler than those which dominate the visible light. However, M dwarfs and M giants have similar colors in the infrared, so that Johnson's data were not adequate to determine the relative contributions of the high and low luminosity populations.

Advances in the development of red and infrared sensitive detectors have finally permitted the accurate measurements of both luminosity and temperature-sensitive indices in these spectral regions. Examples of such observations are those of the Ca II + TiO features by O'Connell (1974, 1976a, b), the 2.3 μm CO band by Baldwin et al. (1973a) and Frogel et al. (1975b), and the 9910 Å Wing-Ford band by Whitford (1977). These data are necessary to model the stellar content of elliptical galaxies, and hence to estimate the evolutionary correction to q_0 in the redshift-magnitude diagram (Sandage 1961; Faber 1973b; Tinsley 1973, 1975; Tinsley and Gunn 1976; O'Connell 1976b.

In this paper we present new multiaperture observations of the strength of the CO feature in 51 elliptical and lenticular galaxies. Together with these measurements, we have also obtained magnitudes in the 1.2 μm, 1.6 μm, and 2.2 μm photometric bands (*J*, *H*, and *K*) for the same galaxies. These data are combined with *U* and *V* observations from the literature to examine variations in the relationships between optical and infrared colors from galaxy to galaxy and within individual galaxies. In Section II, the photometric system, observational procedures, and data reduction are described in some detail. The results of the observations are presented in Sections III and IV. In Sections V and VI, the results are compared with published stellar synthesis models and with other photometric studies of galaxies.

Our conclusions are summarized in Section VII. The system of standard magnitudes and colors, and mean photometric relationships for a selection of red giant and dwarf stars are presented in the Appendix.

Paper II of this series (Aaronson, Frogel and Persson 1977) presents observations of the 2.0 μm H_2O absorption band (Baldwin et al. 1973b), which impose additional constrains on the coolest stellar component of the galaxies under investigation. Paper III (Person, Frogel, and Aaronson 1978) presents new multiaperture *UBVR* and *JHK* data for nearly 100 field ellipticals and *JHK* data alone for galaxies in the Virgo and Coma clusters. These data will allow a more thorough investigation of the color-color and color-magnitude relations discussed here.

II. OBSERVATIONAL PROCEDURES AND DATA REDUCTION

a) Equipment

Most of the observations presented in this paper were made during 80 scheduled observing nights at the Hale Observatories in the period 1975 March to 1976 April. The telescopes used were the 24-inch (61 cm), 60-inch (l.5 m), and 100-inch (2.5 m) reflectors on Mount Wilson, and the 200-inch (5 m) Hale reflector. The photometer employed had an offset guider and a star-sky chopper consisting of a rotating sector-wheel mirror

near the focal plane. The measurements were made with an InSb detector cooled to 55° K. A similarly cooled iris diaphragm in the focal plane defined the aperture sizes. All of the filters were cooled to 77° K, and have effective wavelengths and full widths at half maxima as follows: 1.25, 0.24 μm; 1.65, 0.30 μm; 2.20, 0.40 μm; 2.20, 0.11 μm; 2.36, 0.08 μm. The narrow-band 2.20 and 2.36 μm filters define the strength of the 2.3 μm CO absorption band. The fact that these two filters were employed "cold", whereas previously they were mounted outside the dewar (Frogel et al. 1975b) loused a shift in the effective wavelength with a consequent decrease in the measured strength of the CO band in a late-type giant relative to that of α Lyrae. This decrease arises almostentirely from the location of the 2.36 μ filter with respect to the CO absorption band which sets in very abruptly at 2.29 μm .[1] It has been found that the relative CO index is insensitive to small changes in the effective wavelength and bandwidth of the 2.20 μm filter (the continuum filter).

Supplemental infrared observations reported in this paper were made on the 0.9 m, 1.3 m, and 2.1 m telescopes of Kitt Peak National Observatory (KPNO), the 40-inch (1 m) telescope of Las Campanas Observatory, Chile, and the 60-inch (1.5 m) telescopes of Cerro Tololo Inter-American Observatory (CTIO) and of the Smithsonian Astrophysical Observatory on Mount Hopkins, Arizona. These observations were made with two additional and completely independent sets of photometers and filters. Transformations which relate the J - H and H - K colors on the different systems are discussed in the Appendix.

---

[1] Examples of spectra of late-type stars which display the variations of the 2.3 μm CO and 1.9 μm H_2O absorption bands as functions of luminosity and temperature are contained in Moroz (1966), Johnson and Mendez (1970), McCammon, Münch, and Neugebauer (1967), and Frogel (1971). Back.

b) Galaxy Observations

The only galaxies included in the present sample are those early-type systems which were bright enough so that the CO index within a 48" diameter aperture could be measured on a 1.5 m telescope to a statistical accuracy of better than 0.02 mag in 4-6 hours. With improvements in detector sensitivity, this requirement was met for objects as faint as $K \approx 9.5$. The galaxies include most of the ellipticals and lenticulars for which detailed optical-line indices are available from the work of McClure and van den Bergh (1968), Faber (1973b), and O'Connell (1976a). Some bright galaxies from these lists and elsewhere were excluded because they lie too close to the galactic plane ($|b| \leq 20°$) or at too southerly a declination, ($\delta \lesssim -5°$). Because of uncertainties in the K-correction to the CO index, galaxies with redshifts greater than that of the Coma cluster ($z = 0.022$) were not observed. The galaxies observed are listed in Table 1.

All galaxy measurements were made with the focal plane apertures centered on the optical nuclei. Centering was done visually and usually confirmed by maximizing the 1.6 μm signal. The separation of the "signal" and "reference" beams was typically 2 or 3 aperture diameters. The red Palomar Sky Survey prints were checked for the presence of stars in either of the beams. If any were present, they were measured and an appropriate correction was made in the few cases where the stellar signal was more than a few percent of the galaxian signal. Nearly all of the measurements were repeated on two nights, and the CO indices for the fainter galaxies were measured on as many as five nights on the 60-inch telescope. The night-to-night scatter in the CO index and the broad-band magnitudes was found to be consistent with that expected from the statistical and

photometric errors associated with the individual measurements.

c) Sources of Error and Instrumental Corrections

In addition to statistical errors from thermal background radiation from the sky and telescope, and from detector noise, a purely photometric error of ± 0.01 mag at all wavelengths was found from repeated measurements of standard stars.

Aside from random errors, several sources of systematic error exist in the raw data. Orthogonal scans of a star across the focal plane aperture for each of the filters revealed small but measurable differences in the beam profiles for the *J*, *H*, and *K* filters. [2] By convolving a standard galaxy surface brightness profile (de Vaucouleurs and de Vaucouleurs 1964; hereafter RCBG) with an average of the beam profiles through each of the 3 filters we derived corrections to the *J* - *H* and *H* - *K* colors and to the *K*-magnitudes. The corrections to the colors never exceeded 0. 06 mag and were typically 0.02 to 0.03 mag. The corrections to the *K*-magnitudes were typically 0.00 to 0.01 mag and never exceeded 0.02 mag. The errors associated with these corrections and possible other wavelength-dependent irregularities in the beam profiles are thought to be not larger than ± 0.02 mag. No systematic errors of this type greater than ± 0.01 mag in the CO index could be detected either by scanning the beams or by measuring a standard star at several positions in the aperture. [3]

Possible errors from other known instrumental sources are believed to be of the order of 0.01 mag in the mean. These include the correction to the *K*-magnitude for galaxian flux in the reference beam (Frogel et al. 1975c) and nonlinearity in the response of the system to bright and faint standards. An intercomparison of the same standards measured on the 0.6 m, 1.5 m, and 5m, telescopes was used as a monitor of possible; nonlinear response effects. A linearity problem in our previously published CO indices (Frogel et al. 1975b) is discussed in Section f) below.

The observed *K*-magnitudes and colors corrected for the instrumental effects discussed above are given in columns (6), (8), and (9) of Table 1. The CO indices in column (10) have had no instrumental corrections applied. The adopted errors are listed at the bottom of Table 1. These errors are consistent with the scatter in repeated measurements *after* the application of the instrumental corrections.

Table 1. Magnitudes and Colors for E and S0 Galaxies

Galaxy	b^{II}	Tel.	Aper.	Log	Observed *					Corrected for Reddening and Redshift					
Type	z	(inches)	(")	A/D (0)	K	(V-K)	(J-H)	(H-K)	CO	K_c	$(V-K)_c$	$(J-H)_c$	$(H-K)_c$	CO_c	Notes
(1)	(2)	(3)	(4)	(5)	(6)	(7)	(8)	(9)	(10)	(11)	(12)	(13)	(14)	(15)	(16)
NGC 205	-21°	60	48	-0.98	9.22	2.28:	0.61	0.19	0.09	9.20	2.12:	0.59	0.18	0.095	

S0/E5 pec	-0.0008													
NGC 221	-22	60	16	-1.08	6.92	3.15	0.62	0.21	0.15	6.90	3.00	0.60	0.20	0.15
E2	-0.0007	60	48	-0.60	5.98	3.31	0.68	0.21	0.16	5.96	3.16	0.66	0.20	0.16
		24	111	-0.24	5.43	3.28	0.67	0.23	0.14	5.41	3.13	0.65	0.22	0.14
NGC 404	-27	60	48	-0.38	8.57	2.71:	0.67	0.14	0.11	8.56	2.60:	0.66	0.13	0.11
$S0_3(0)$	-0.0001													
NGC 584	-68	60	48	-0.33	7.96	3.28	0.68	0.22	0.12	7.98	3.25	0.68	0.20	0.15
$E3/S0_1$ (3)	0.0061	24	111	+0.04	7.68	3.11	0.68	0.18	0.13	7.70	3.08	0.68	0.16	0.16 ±0.03
NGC 596	-68	60	48	-0.28	8.62	3.18:	0.64	0.18	0.12	8.64	3.14:	0.64	0.16	0.145
E0	0.0068													
NGC 1023	-19	60	48	-0.65	7.23	3.30:	0.71	0.21	0.15	7.22	3.10:	0.69	0.19	0.16
$SB0_1$ (5)	0.0019	24	111	-0.28	6.70	3.36	0.68	0.24	0.14	6.69	3.16:	0.66	0.22	0.15
NGC 1600	-33	200	15	-0.69	9.76	-	0.80	0.31	0.08	9.80	-	0.78	0.26	0.16
E4	0.0161	60	32	-0.35	9.01	3.49	0.78	0.23	-	9.05	.33	0.76	0.18	-
		60	48	-0.18	8.69	3.48	0.69	0.26	0.08	8.73	3.32	0.67	0.21	0.15
		60	53	-0.14	8.66	3.45	0.74	0.25	-	8.70	3.29	0.72	0.20	-
NGC 1700	-28	200	15	-0.75	9.27	-	0.74	0.28	0.12	9.31	-	0.72	0.22	.18
E3	0.0133	40	28.7	-0.46	8.86	3.30	-	-	-	8.90	3.13	-	-	-
		60	48	-0.24	8.56	3.32	0.69	0.25	0.11	8.60	3.15	0.67	0.19	0.165
		40	55.9	-0.17	8.46	3.34	-	-	-	8.50	3.17	-	-	-
NGC 2300	28	200	15	-0.68	9.19	-	0.78	0.27	0.13	9.21	-	0.77	0.23	0.155
E3	0.0066	200	16.5	-0.64	9.07	-	0.77	0.26	0.12	9.09	-	0.76	0.22	0.145
		60	32	-0.35	8.54	3.60:	0.71:	0.24	-	8.56	3.45:	0.70:	0.20	-
		60	48	-0.18	8.23	3.63:	0.74	0.22	0.13	8.25	3.48:	0.73	0.18	0.155
		60	53	-0.14	8.18	3.62:	0.74:	0.22	-	8.20	3.47:	0.73:	0.18	-

		24	111	+0.19	7.87	3.53	0.73	0.19	0.11	7.89	3.38	0.72	0.15	0.14
NGC 2549	34	200	15	-0.88	9.17	-	0.71	0.25	0.15	9.18	-	0.70	0.23	0.165
$S0_1$(7)	0.0036	200	16.5	-0.84	9.08	-	0.73	0.23	0.15	9.09	-	0.72	0.21	0.165
		60	48	-0.38	8.44	3.28	0.59	0.20	0.13	8.45	3.18	0.58	0.18	0.14
NGC 2634	34	200	15	-0.50	10.22	-	0.72	0.25	0.13	10.24	-	0.71	0.22	0.16
El:	0.0066	200	16.5	-0.46	10.10	-	0.70	0.24	0.11	10.12	-	0.69	0.21	0.14 ±0.03
		60	48	+0.01	9.50	-	0.69	0.21	0.10	9.52	-	0.68	0.18	0.12
		60	53	+0.04	9.43	-	0.65	0.27	0.10	9.45	-	0.64	0.24	0.13 +0.03
NGC 2655	33°	200	15	-1.14	8.80	-	0.70	0.26	0.13	8.81	-	0.69	0.24	0.16
SAB (s)0	0.0043	60	48	-0.63	7.93	-	0.69	0.24	0.12	7.94	-	0.68	0.22	0.14
NGC 2672	34	200	15	-0.65	9.82	-	0.76	0.28	0.10	9.86	-	0.74	0.23	0.17
E2	0.0141	200	16.5	-0.61	9.72	3.46:	0.74	0.30	0.09	9.76	3.30:	0.72	0.25	0.15
		60	48	-0.15	8.96	3.35:	0.70	0.24	0.10	9.00	3.19:	0.68	0.19	0.16
NGC 2768	41	200	15	-0.98	9.24	-	0.72	0.25	0.13	9.25	-	0.71	0.23	0.15
E6	0.0047	200	16.5	-0.94	9.09	-	0.75	0.21	0.15	9.10	-	0.74	0.25	0.165
		60	48	-0.48	8.14	3.31	0.71	0.19	0.15	8.15	3.23	0.70	0.17	0.165
		24	111	-0.11	7.48	3.34:	0.69	0.19	0.12	7.49	3.26:	0.68	0.17	0.14 ±0.04
NGC 2974	35	200	15	-0.75	9.08	-	0.76	0.26	0.13	9.09	-	0.75	0.23	0.155
E4	0.0067													
NGC 3115	37	200	15	-1.04	.58	3.56	0.73	0.25	0.15	7.58	3.49	0.72	0.24	0.16
$E7/S0_1$ (7)	0.0022	50	31.6	-0.72	7.02	3.42	0.71	0.24	-	7.02	3.35	0.70	0.23	-
		84	37.5	-0.64	6.89	3.39	0.68	0.24	0.17	6.89	3.32	0.67	0.23	0.17
		60	48	-0.54	6.73	3.39	0.71	0.22	0.18	6.73	3.32	0.70	0.21	0.185
		36	106.4	-0.19	6.27	3.35	0.72	0.23	0.17	6.27	3.28	0.71	0.22	0.175
NGC 3158	55	200	15	-0.56	9.99	-	0.76	0.30	-	10.07	-	0.75	0.22	-

E3	0.0234	200	16.5	-0.52	9.89	-	0.73	0.32	0.05	9.97	-	0.72	0.24	0.16
NGC 3193	55	200	15	-0.78	9.26	-	0.70	0.23	0.14	9.28	-	0.70	0.21	0.16
E2	0.0046	200	16.5	-0.74	9.13	-	0.73	0.24	0.15	9.15		0.73	0.22	0.165
		60	48	-0.28	8.49	3.19	0.67	0.20	0.15	8.51	3.16	0.67	0.18	0.17
NGC 3226	55	200	15	-0.77	9.91	-	0.73	0.24	-	9.93	-	0.73	0.22	-
E2	0.0045	200	16.5	-0.73	9.79	-	0.75	0.26	0.13	9.81	-	0.75	0.24	0.14
		60	48	-0.27	9.11	-	0.68	0.23	0.12	9.13	-	0.68	0.21	0.135
		24	111	+0.10	8.57	-	0.63	0.20	0.11	8.59	-	0.63	0.18	0.12 ±0.05
NGC 3377	58	200	15	-0.90	8.92	3.18	0.70	0.22	0.16	8.93	3.17	0.70	0.21	0.17
E6	0.0024	40	28.7	-0.62	8.52	3.07	-	-	-	8.53	3.06	-	-	-
		40	55.9	-0.33	8.10	3.03	-	-	-	8.11	3.02	-	-	-
NGC 3379	58	200	15	-0.96	8.10	3.34	0.72	0.25	0.14	8.11	3.33	0.72	0.24	0.15
E0	0.0029	50	31.6	-0.64	7.51	3.34	0.70	0.22	-	7.52	3.33	0.70	0.21	-
		60	48	-0.46	7.19	3.39	0.68	0.21	0.15	7.20	3.38	0.68	0.20	0.155
		24	111	-0.09	6.69	3.35	0.68	0.19	0.16	6.70	3.34	0.68	0.18	0.17
NGC 3384	58	200	15	-1.01	8.25	3.28	0.70	0.24	0.15	8.26	3.27	0.70	0.22	0.16
$SB0_1$ (5)	0.0026	40	28.7	-0.73	7.85	3.22	-	-	-	7.86	3.21	-	-	-
		50	31.6	-0.69	7.80	3.22	0.68	0.24	-	7.81	3.21	0.68	0.22	-
		40	55.9	-0.44	7.50	3.18	-	-	-	7.51	3.17	-	-	-
NGC 3607	66°	200	15	-0.83	8.58	3.55:	0.73	0.27	0.15	8.60	3.53:	0.73	0.25	0.16
S03(3)	0.0031	50	31.6	-0.50	8.02	3.40:	0.70	0.25	-	8.04	3.38:	0.70	0.23	-
		60	48	-0.32	7.73	3.37:	0.69	0.22	0.15	7.75	3.35:	0.69	0.20	0.16
		60	53	-0.27	7.62	3.40:	0.67	0.25	0.16	7.64	3.38:	0.67	0.23	0.175
NGC 3608	67	200	15	-0.70	9.36	3.40:	0.70	0.24	0.13	9.38	3.38:	0.70	0.22	0.14
El	0.0040	60	48	-0.20	8.55	3.23	0.70	0.22	0.15	8.57	3.21	0.70	0.20	0.17
		60	53	-0.16	8.47	3.25	0.69	0.22	0.11	8.49	3.23	0.69	0.20	0.125
NGC 3613	55	200	16.5	-0.76	9.20	-	0.72	0.25	0.13	9.23	-	0.72	0.22	0.155

E6	0.0069	60	48	-0.30	8.52	3.20:	0.66	0.20	0.13	8.55	3.15:	0.66	0.17	0.155	
NGC 3842	73	200	16.5	-	10.25	-	0.76	0.30	0.03	10.32	-	0.75	0.23	0.13	1
E	0.0206	60	48	-	9.43	-	0.58	0.26	0.04	9.50	-	0.57	0.19	0.13	
NGC 3998	60	200	15	-0.83	8.46	3.52:	0.73	0.27	0.14	8.47	3.50:	0.73	0.25	0.15	
S01(3)	0.0036														
NGC 4261	67	200	16.5	-0.87	8.83	3.45	0.75	0.28	0.15	8.86	3.41	0.75	0.25	0.175	
E3	0.0073	60	48	-0.41	B.05	3.35	0.70	0.22	0.14	8.08	3.31	0.70	0.19	0.17	
NGC 4278	83	200	7.5	-1.17	9.37	-	0.70	0.25	0.14	9.38	-	0.70	0.24	0.15	
El	0.0021	200	15	-0.87	8.65	-	0.74	0.25	0.14	8.66	-	0.74	0.24	0.145	
		200	16.5	-0.82	8.50	-	0.75	0.24	0.16	8.51	-	0.75	0.23	0.17	
		50	31.6	-0.54	B.10	3.28	0.72	0.17	-	8.11	3.27	0.72	0.16	-	
		60	48	-0.36	7.81	3.29	0.61	0.22	0.14	7.82	3.28	0.61	0.21	0.15	
		60	53	-0.32	7.69	3.35	0.67	0.21	0.19	7.70	3.34	0.67	0.20	0.20	
		24	111	+0.01	7.38	3.23	0.64	0.21	.15	7.39	3.22	0.64	0.20	0.16	
NGC 4283	83	200	16.5	-0.49	9.73	-	0.71	0.25	0.21	9.75	-	0.71	0.23	0.22	
E0	0.0036	60	48	-0.03	9.26	3.24	.62	0.25	0.13	9.28	3.22	0.62	0.23	0.14	
NGC 4365	69	200	15	-1.09	8.73	3.37	0.73	0.26	0.15	8.74	3.35	0.73	0.24	0.16	
E3	0.0039	40	28.7	-0.81	8.20	3.29	-	-	-	8.21	3.27	-	-	-	
		50	31.6	-0.77	8.18	3.25	0.68	0.26	-	8.19	3.23	0.68	0.24	-	
		40	55.9	-0.52	7.59	3.31	-	-	-	7.60	3.29	-	-	-	
NGC 4374	74	200	7.5	-1.28	9.17	-	0.70	0.21	0.15	9.18	-	0.70	0.20	0.16	
El pec	0.0032	200	15	-0.98	8.27	3.47	0.72	0.25	0.10	8.28	3.46	0.72	0.24	0.11	
		50	31.6	-0.66	7.59	3.36	0.69	0.25	-	7.60	3.35	0.69	0.23	-	
		60	48	-0.48	7.29	3.31	0.71	0.21	0.16	7.30	3.30	0.71	0.20	0.165	
		60	53	-0.44	7.15	3.38	0.69	0.24	0.16	7.16	3.37	0.69	0.23	0.17	
NGC 4382	79°	200	15	-1.20	8.62	3.09	0.73	0.23	0.13	8.63	3.08	0.73	0.21	0.135	
$S0_1$(3)	0.0026	40	28.7	-0.92	8.06	3.03	-	-	-	8.07	3.02	-	-	-	
		50	31.6	-0.88	7.95	3.09	0.67	0.25	-	7.96	3.08	0.67	0.23	-	
		40	55.9	-0.63	7.44	3.04	-	-	-	7.45	3.03	-	-	-	

NGC 4406	75	200	7.5	-1.37	9.48	-	0.70	0.20	0.15	9.49	-	0.70	0.19	0.15	
E2	-0.0010	200	15	-1.07	8.75	3.29	0.71	0.26	0.16	8.76	3.28	0.71	0.25	0.16	
		50	31.6	-0.75	8.04	3.21	0.67	0.21	-	8.05	3.20	0.67	0.20	-	
		60	48	-0.57	7.57	3.26	0.68	0.22	0.18	7.58	3.25	0.68	0.21	0.18	
NGC 4459	76	200	15	-0.81	8.76	3.69	0.76	0.29	0.13	8.77	3.67	0.76	0.27	0.14	
S03(3)	0.0037	40	28.7	-0.53	8.35	3.39	-	-	-	8.36	3.37	-	-		
		40	55.9	-0.24	7.84	3.35	-	-	-	7.85	3.32	-	-		
NGC 4464	70	200	16.5	-0.51	10.05	-	0.70	0.20	0.11	10.07	-	0.70	0.18	0.125	
E3	0.0040	60	48	-0.05	9.69	.11:	0.71	0.15	0.17	9.71	3.09:	0.71	0.13	0.18 ±0.04	
NGC 4472	70	200	7.5	-1.56	9.16	-	0.70	0.23	0.16	9.17		0.70	0.22	0.165	
E2	0.0032	200	15	-1.26	8.19	3.42	0.75	0.27	0.16	8.20	3.41	0.75	0.26	0.175	
		200	16.5	-1.21	8.00	3.44	0.75	0.28	0.15	8.01	3.43	0.75	0.27	0.165	
		50	31.6	-0.93	7.37	3.30	0.70	0.24	-	7.38	3.29	0.70	0.23	-	
		60	48	-0.75	6.91	3.32	0.65:	0.22	0.16	6.92	3.31	0.65:	0.21	0.165	
		24	111	-0.38	6.18	3.39	0.68	0.24	0.15	6.19	3.38	0.68	0.23	0.16	
NGC 4478	74	200	15	-0.65	9.54	-	0.69	0.24	0.12	9.55	-	0.69	0.22	0.14	
E2	0.0049	H60	27.4	-0.39	8.92	3.32:	0.63	0.22	-	8.93	3.29:	0.63	0.20	-	
		H60	53.4	-0.10	8.51	3..29	0.64	0.20	-	8.52	3.26	0.64	0.18	-	
NGC 4486	74	200	7.5	-1.48	9.76	-	0.73	0.23	0.15	9.78	-	0.73	0.21	0.165	
E0	0.0042	200	15	-1.18	8.59	3.26	0.76	0.29	0.14	8.61	3.24	0.76	0.27	0.16	
		50	31.6	-0.86	7.60	3.38	0.73	0.24	-	7.62	3.36	0.73	0.22	-	
		60	48	-0.68	7.08	3.42	0.73	0.25	0.16	7.10	3.40	0.73	0.23	0.175	
		24	111	-0.31	6.37	3.41	0.65	0.25	0.15	6.39	3.39	0.65	0.23	0.16	
NGC 4486A	74	200	7.5	-	10.02	-	0.51	0.10	0.09	10.03	-	0.51	0.08	0.11	
	(0.004)	200	15	-	9.52	-	0.52	0.17	0.10	9.53	-	0.52	0.15	0.115	2
NGC 4486B	75	200	7.5	-0.40	10.61	-	0.74	0.16	0.11	10.62	-	0.74	0.14	0.13	
E0	0.0050	200	15	-0.10	10.23	-	0.68	0.21	0.08	10.24	-	0.68	0.19	0.10	

NGC 4494	85	60	48	-0.38	7.96	3.09:	0.68	0.20	0.12	7.98	3.06:	0.68	0.18	0.135
El	0.0044	24	111	-0.01	-	-	-	-	0.10	-	-	-	-	0.115
NGC 4649	74	200	15	-1.10	8.14	3.50	0.73	0.28	0.16	8.16	3.47	0.73	0.26	0.17
E2/S0	0.0042	50	31.6	-0.76	7.34	3.42	0.74	0.24	-	7.36	3.39	0.74	0.22	-
		60	48	-0.60	6.93	3.42	0.65:	0.23	0.16	6.95	3.39	0.65:	0.21	0.175
NGC 4889	88°	200	15	-0.71	9.99	3.41	0.75	0.28	0.08	10.06	3.30	0.74	0.21	0.175
E4	0.0215	200	16.5	-0.66	9.85	3.45	0.72:	0.33	0.07	9.92	3.34	0.71:	0.26	0.17
		60	48	-0.20	9.06	3.41	0.70	0.29	0.06	9.13	3.30	0.69	0.22	0.16
NGC 5813	50	200	15	-0.86	9.36	-	0.71	0.26	0.11	9.39	-	0.71	0.23	0.13
El	0.0063	200	16.5	-0.82	9.22	-	0.72:	0.25	0.11	9.25	-	0.72:	0.22	0.14
		50	31.6	-0.54	8.74	3.46	0.66	0.25	-	8.77	3.39	0.66	0.22	-
		60	32	-0.53	8.72	3.46	0.67	0.25	-	8.75	3.39	0.67	0.22	-
		60	48	-0.36	8.43	3.47	0.71	0.24	0.13	8.46	3.40	0.71	0.21	0.15
		60	53	-0.32	8.32	3.51	0.70	0.26	-	8.35	3.44	0.70	0.23	-
NGC 5846	49	200	16.5	-0.86	9.13	3.54	0.74	0.28	0.15	9.16	3.47	0.74	0.25	0.17
El	0.0059	50	1.6	-0.58	8.46	3.50	0.67	0.25	-	8.49	3.43	0.67	0.22	-
		60	32	-0.57	8.38	3.56	0.67	0.26	-	8.41	3.49	0.67	0.23	-
		60	48	-0.40	8.03	3.53	0.75	0.24	0.13	8.06	3.46	0.75	0.21	0.15
		60	53	-0.36	7.89	3.58	0.72	0.27	-	7.92	3.51	0.72	0.24	-
		24	111	-0.03	7.23	3.59	0.75	0.28	.14	7.26	3.52	0.75	0.25	0.17 ±0.03
NGC 5866	52	100	30	-0.66	7.96	3.42:	0.66	0.32	0.12	7.98	3.40:	0.66	0.30	0.135
$S0_3(8)$	0.0026	50	31.6	-0.64	7.93	3.38:	0.74	0.29	-	7.95	3.36:	0.74	0.27	-
		60	48	-0.46	7.59	3.49:	0.68	0.30	0.16	7.61	3.47:	0.68	0.28	0.17
		60	53	-0.41	7.49	3.50:	0.72	0.30	-	7.51	3.48:	0.72	0.28	-
NGC 5982	47	200	7.5	-0.95	10.02	-	0.71	0.23	0.13	10.06	-	0.70	0.19	0.17
E3	0.0096	200	15	-0.65	9.30	3.40	0.71	0.27	0.13	9.34	3.31	0.70	0.23	0.17
		100	30	-0.35	8.85	3.30	0.67	0.24	0.13	8.89	3.21	0,66	0.20	0.17
		60	48	-0.15	8.59	3.25	0.59:	0.22	0.14	8.63	3.16	0.58:	0.18	0.185
		60	53	-0.11	8.48	3.32	0.66	0.26	0.14	8.52	3.23	0.65	0.22	0.18 ±0.04

		24	111	+0.22	8.22	3.27	0.66	0.20	0.10	8.26	3.18	0.65	0.16	0.14 ±0.06
NGC 6702	20	60	32	-0.15	9.75	3.60:	-	-	-	9.78	3.35:	-	-	-
E2	0.0158	60	48	+0.02	9.53	3.61:	0.73	0.29	0.13	9.56	3.36:	0.70	0.23	0.21
		60	53	+0.06	9.51	3.57:	0.72	0.30	-	9.54	3.32:	0.69	0.24	-
NGC 7619	-48	60	16	-0.63	9.27	-	0.69	0.25	0.11	9.32	-	0.68	0.20	0.17
E3	0.0125	60	48	-0.16	8.53	3.59:	0.71	0.26	0.11	8.58	3.49:	0.70	0.21	0.17
		24	111	+0.21	8.09	3.42:	0.75	0.24	0.10	8.14	3.32:	0.74	0.19	0.16 ±0.05
NGC 7626	-48	60	48	-0.12	8.70	3.50	0.71	0.23	0.11	8.74	3.41	0.70	0.19	0.17
El	0.0112													

* The assigned nominal errors are ± 0.03, ± 0.10, ± 0.04, ± 0.03, and ± 0.02 for K, (V-K), (J-H), (H-K), and CO, respectively. A colon indicates that the error for that measurement may be as much as twice the nominal value. CO index errors larger than ± 0.02 are indicated in the body of the table. NOTES: 1. The galaxy is from the list of Gunn and Oke (1975). 2. The redshift was assumed to be the same as for N4486.

---

[2] The usual character of the profiles was that the *K*-filter beam was relatively flat while that of the *J* filter was peaked in the middle. This arises from the wavelength-dependent properties of the silicon field lens. Back.

[3] The measurements made on the 1.3 m telescope at KPNO employed an off-axis field mirror rather than a field lens. Thus, the beam profiles were the same at all wavelengths, and no corrections to the colors were required. Corrections to the *K*-magnitudes were found to be of order -0.03 mag. Back.

d) Sources of V Data

The visual magnitudes used in column (7) of Table 1 are based largely upon a compilation from the literature by Sandage (1976). We have also included data from Tifft (1969, 1973). As described in Frogel et al. (1975c), values for *V* at apertures corresponding to those at which the infrared measurements were made were interpolated from the tabulated data. Errors in *V* - *K*, from uncertainties in combining measurements made with different aperture sizes, and from scatter in the published V data, are estimated to be ± 0.10 mag. A colon after a *V* - *K* color in Table 1 indicates that the scatter in the published *V* data is exceptionally large; for these cases we adopt an error in *V* - *K* of ± 0.2 mag. In addition, a systematic error could be present in the 200-inch *V* - *K* colors which depend on a relatively limited amount of published small-aperture *V* data. A few galaxies had no appropriate *V* measurements available from the literature. Data for some of these were taken from *UBVR*

measurements made on the 0.9 m and 1.5 m telescopes: at CTIO (Paper III). Clearly, the use of such a heterogeneous body of *V* data will hinder our examination of variations in the *V* - *K* color within galaxies since these variations are small to begin with (cf. Frogel et al. 1975c).

e) Reddening and K-corrections

To obtain the reddening and extinction corrections, the absorption-free polar-cap model for A_V given by Sandage (1973) was used together with the Van de Hulst reddening law (Johnson 1968). Values of E_{J-H} / A_V, E_{H-K} / A_V, E_{V-K} / A_V, E_{U-V} / A_V, and E_{CO} / A_V used are 0.10, 0.06, 0.91, 0.56, and 0.00, respectively. Since the largest value of A_V was only 0.21 mag, errors which may arise from the inapplicability of either the polar-cap model or the Van de Hulst reddening law cannot affect the conclusions of this paper.

The K-corrections to the *V*-magnitudes are from Schild and Oke (1971) and Whitford (1971). (For the limited redshift range of the galaxies considered here, the results of both authors are identical.) For the *U* - *V* colors obtained from the literature, the K-correction is from Table 3 of Sandage (1972). Heliocentric redshifts (column [2], Table 1) are from de Vaucouleurs and de Vaucouleurs (1964).

Separate procedures were followed for determining the K-correction for the infrared broad-band data and for the CO index. The stratoscope balloon scans of several late-type stars (Woolf, Schwarzchild, and Rose 1964) were convolved with the transmission curves of the *JHK* filters and redshifted. The resulting K-corrections as functions of *z* were quite similar for α Tau (K5 III), μm Gem (M3 III), and α Ori (M2 I) - the spread at $z = 0.03$ was only 0.01 to 0.02 mag in the *J* - *H* and *H* - *K* colors and *K*-magnitudes. Since the CO indices of nearby galaxies are most similar to those of a late K III star, the values for α Tau were used to correct the broad-band galaxy measurements. The K-corrections are approximately linear with increasing *z*; for $z = 0.03$ they are -0.02, -0.10, and +0.10 for *J* - *H*, *H* - *K* , and *K*, respectively.

Redshift corrections to the CO index were first determined numerically by convolving the transmission curves of the two filters with the high resolution spectra of several stars observed by Frogel (1971). For K2, K5, and M2 giants, the corrections were similar out to a *z* of 0.012. Beyond this they diverged rapidly, the spread becoming nearly 0.04 mag at $z = 0.022$. Uncertainty in the choice of a realistic starting point (i.e., a model stellar population) therefore made it necessary to derive empirically the K-correction to the CO index at large redshift. We show below that the CO index depends only weakly on galaxian luminosity or radius for the brighter nearby galaxies. Thus the *observed* CO indices of the intrinsically brightest galaxies were plotted against redshift, and a straight-line fit to the data was made. The K-correction found in this way, and adopted for all galaxies, is given by $K_{CO} = +4.8z$. Out to $z = 0.012$ the empirical relation agreed with the mean computed relation for the three stars to better than ± 0.01 mag. Although the empirical relation is based on observations of the most luminous galaxies, no systematic error is introduced in the results for fainter galaxies, since they are all at small values of *z*. (See Lasker 1970 for a discussion of this point.) *Note that for galaxies in the Coma cluster the K-correction is two-thirds of the final CO index.*

f) Comparisons with Previous CO Measurements

The CO observations presented in this paper were made on the photometric system described above and defined by the standards listed in Table A1. By reobserving with the new ("cold") system. many of the stars used to

define Figure 1 of Frogel et al. (1975b) (the old, "warm" system), and by making simultaneous observations on both old and new systems for 16 giant stars, the transformation of the CO index from the warm to the cold system was determined to be

CO index:	Warm - Cold = 0.1 × Warm	Warm $\leq$ 0.2
	Warm - Cold = 0.02	Warm > 0.2

i.e., the sense of the transformation is that the CO indices for the giants and supergiants in Figure 1 of Frogel et al. (1975b) become *smaller*. The error in the transformation as determined from the scatter of stellar measurements is of the order of the size of the transformation. *This transformation applies only to giants and supergiants.*

All of the galaxies measured on the old system were remeasured with the new system. For the data obtained with the 5 m telescope, a comparison with the measurements reported in Table 1 of Frogel et al. (1975b) revealed that *even after the old CO indices were transformed*, the resulting values for the CO index were larger than the new values by 0.04 mag in the mean. Reexamination of the old data indicated that the source of most of this systematic difference was due to saturation of the continuum from bright standards. The continuum filter (2.20 μm) gave a signal nearly three times as strong as the CO filter, and the signal through the former was clipped by about 0.03 mag. The effect of this was to assign too strong a CO index to the galaxies. Old measurements made with the 1.5 m telescope (Frogel et al. 1975b plus unpublished data) were also transformed to the "cold" system and compared with measurements reported here. No statistically significant differences were found. We emphasize that the systematic differences in the 200-inch measurements *in no way affect the main conclusion of the earlier paper.* The one consequence of the error in these measurements was to give a false impression of the existence of a radial gradient in the CO index (Frogel et al. 1975a, b). The galaxy data presented here supersede these previously published CO data.

The *K*-magnitudes of all galaxies in Frogel et al. (1975c) were remeasured in the course of this work. There is no systematic difference larger than 0.01 mag in the mean between these two independent sets of data.

g) Globular Cluster Observations

The integrated infrared light of five globular clusters was observed with the KPNO 0.9 m and the CTIO 1.5 m telescopes. Reference beam corrections were derived by using the multiaperture photometry of Kron and Mayall (1960) with the assumption of no radial color dependence. For M13, the correction to the *K*-magnitude was -0.11 mag, and for the other clusters, it was between -0.03 and -0.05 mag. Corrections to the infrared measurements for nonuniformity in the beam profiles were calculated in a manner similar to that employed for the galaxy measurements, and amounted to a few hundredths of a magnitude. *V* - *K* colors were formed using *V* magnitudes interpolated from the data of Kron and Mayall (1960) and transformed to the Johnson *V* system (Peterson and King 1975). Values of $E_{(B-V)}$ are from van den Bergh (1967) for M69 and M15, and are those recommended by Sandage (1970) for the others. *U* - *V* values are also from van den Bergh (1967), although not at the same aperture sizes as the infrared measurements. Final values with all corrections applied are presented in Table 2.

Table 2. Globular Cluster Data

Cluster	Aper	[Fe/H] †	Observed *			Reddening Corrected					CO
			K	*J-H*	*H-K*	*K*	*U-V*	*V-K*	*J-H*	*H-K*	
M3	105.	-1.5	5.23	0.49	0.08	5.23	0.78	2.16	0.49	0.08	0.01
M13	105.	-1.6	5.05	0.54	0.09	5.04	0.66	2.41	0.53	0.08	0.03
M15	105.	-1.9	4.97	0.49	0.09	4.94	0.55	1.82	0.46	0.07	0.01
M69	66.4	> - 0.4	5.62	0.70	0.17	5.57	1.15	2.59	0.64	0.13	0.08
M92	105.	-2.2	5.25	0.47	0.08	5.25	0.61	2.15	0.47	0.07	-0.01

* The "observed" values have been corrected for beam profile and reference beam flux as discussed in the text. The CO values did not require any corrections.

† For M3, M13, M15, and M92, [Fe/H] is from Hesser, Hartwick, and McClure (1976). For M69, [Fe/H1] is an estimate based on the results of Hartwick and Sandage (1968).

III. DISCUSSION OF THE GALAXY OBSERVATIONS

Table 1 contains the final colors and magnitudes of the galaxies corrected for reddening and redshift. Many of the morphological types are from Sandage (1976). Values of log A / $D(0)$ refer to the aperture size in units of the major diameter $D(0)$ (RCBG). We first consider the variations of the different photometric indices within individual galaxies. This then permits discussion of the average galaxian colors within a standard projected aperture size. The reader should bear in mind the restricted nature of the sample of galaxies, particularly with regard to their absolute magnitude. Also, multiaperture observations such as those presented here are not ideal for a study of color gradients within galaxies. Since such gradients are expected to be in most cases, and since the accuracy of photometric measurements is never better than a couple of percent, the galaxies can be treated only in a statistical sense and not examined individually. A much better technique is to displace the measuring aperture from the center of the galaxy (e.g., Strom et al., 1976, 1977).

a) The Dependence of Color and CO Index on Radius

Figure 1 displays all the galaxy observations from Table 1 as a function of log A / $D(0)$.

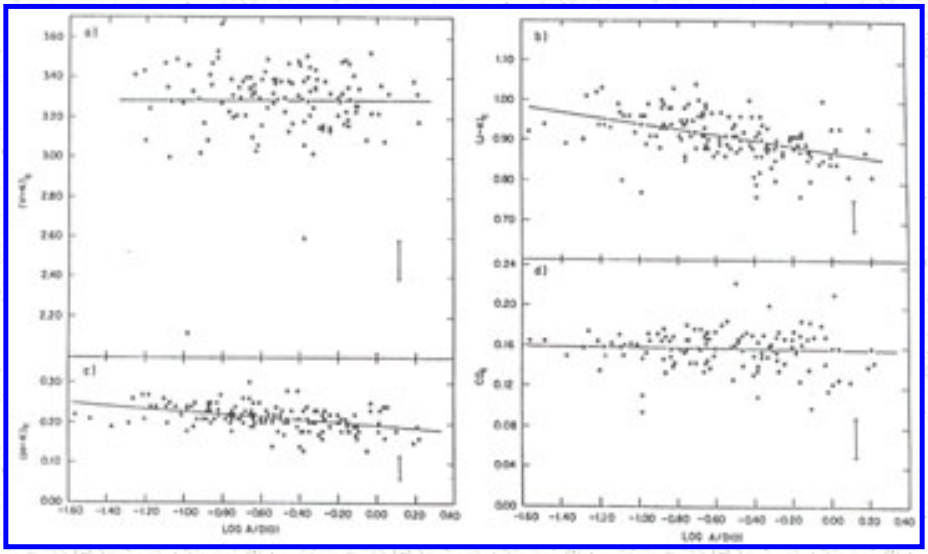

Figure 1. All the corrected colors and CO indices from Table 1 are plotted as a function of log *A* / *D*(0). The linear least-squares fit to these data points is shown by the solid line and is discussed in the text.

Table 3 presents least-squares solutions for radial color gradients found in two ways. First, linear fits (color versus log *A* / *D*(0)) were made to all of the data in Table 1 treated simultaneously; these fits are plotted in Figure 1. Second, slopes and errors were found for each galaxy individually, and then a weighted average was taken. Owing to the magnitude limited nature of the sample, selection effects could influence the first solution, and only the solutions on the right hand side of Table 3 have physical significance. As mentioned above, the 5 m *V* - *K* colors may contain a small systematic error. Although exclusion of these data does not produce a statistically significant change in the mean *V* - *K* gradient, the uncertainty in the gradient for this solution becomes as large as the gradient itself.

Table 3.RADIAL COLOR GRADIENTS

	All Points Solution (Fig. 1)				Average of Individual Radial Gradients			
Color	*N*	Slope	$\pm \sigma_m$	*r*	*N*	Slope	$\pm \sigma_m$	$\pm \sigma_e$
CO	120	-0.002	(0.01)	-0.05	33	0.00	(0.01)	0.02
V-K	120	0.00	(0.03)	0.00	32	-0.11	(0.04)	0.05
J-H	148	-0.04	(0.01)	-0.34	37	-0.08	(0.01)	0.04
H-K	148	-0.04	(0.01)	-0.43	37	-0.04	(0.01)	0.03
J-K	148	-0.07	(0.01)	-0.48	37	-0.12	(0.02)	0.04

The All Points Solution on the left gives the slope Δ color / $\Delta \log A / D(0)$ for galaxies in Table 1 and Figure 1. *r* is the correlation coefficient. The averages of individually determined color gradients are given on the right. 1n the last two columns are listed the purely statistical errors (σ_m), and our estimated errors (σ_e) in the slope values. The estimated errors include contributions from possible systematic beam profile effects as discussed in the text.

Two important results from Table 3 are (1) the broad-band colors become bluer with increasing aperture size, and (2) there is no radial gradient in the CO index. The latter result differs from the tentative conclusion of Frogel et al. (1975b), as discussed in Section II f). The former result for the *V* - *K* color is consistent, to within the errors, with that of Frogel et al. (1975c). Note, however, that to within the errors, the mean radial change in *V* - *K* can be entirely accounted for by the change in *J* - *K*. The variances of the fits are consistent with the measuring errors for *J* - *H*, *H* - *K*, and CO, while for *V* - *K* it is about twice the estimated errors.

The dependence of *V* - *K* on aperture size is not well established by the data of this paper. At least part of the problem lies in the heterogeneous nature of the *V* data as mentioned above. Also, we cannot rule out a large dispersion in the *V* - *K* gradients of individual galaxies. The average *J* - *K* gradient (Table 3) is large, however, and would argue that any such dispersion would have to occur shortward of 1 μm.

Another estimate of the *average* dependence of *V* - *K* color on aperture size can be made by comparing *V* and *K* growth curves. Figure 2 displays the *K* growth curve obtained from the present data (see Section III (b), below). This curve was compared with a *V* growth curve constructed from data to be presented in Paper III. This latter curve is based on a *homogeneous* set of multiaperture observations made at CTIO of about 100 E and S0 galaxies. In terms of the distribution in absolute magnitude this sample is similar to the sample studied here. It differs, however, in consisting primarily of field galaxies. Such a comparison results in a change of *V* - *K* of -0.12 ± 0.03 for a change in *A* / *D*(0) from 0.1 to 1.0. This is consistent with the value in Table 3.

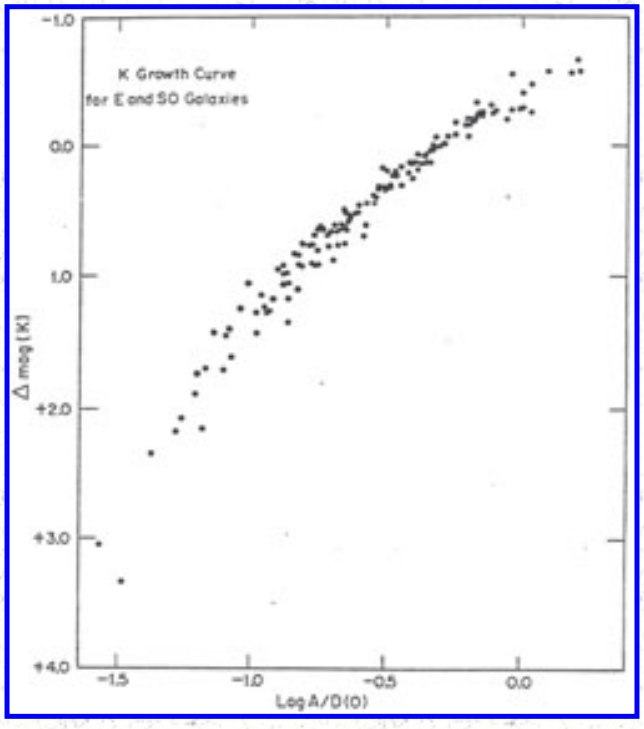

Figure 2. The *K* growth curve -based on the data of Table 1 and derived as discussed in the text. Normal points for the mean curve are given in Table 5.

b) Integrated Properties of the Galaxies

In order to study the integrated properties of the galaxies, we assigned to each galaxy representative values of the observed quantities, corrected for reddening and redshift at a projected aperture size of $A / D(0) = 0.5$. This value was chosen as it involves the least extrapolation of the data. The adopted values are contained in Table 4, and were derived as follows: for the CO index, any radial variations are masked by the measuring errors, and a weighted average of all the CO observations for a given galaxy was formed. These are given in column (2) of Table 4. (Values at 7".5 and 111" were excluded from the average because they are available for only a few galaxies). All observations of galaxies having *K*-magnitudes measured at both $A / D(0) \gtrsim 0.5$ were combined into a preliminary growth curve. This curve determined ΔK between $A / D(0) = 0.25$ and 0.75 and allowed the addition of nearly all the remaining galaxies. The data are presented in Figure 2 and representative values for the growth curve am given in Table 5. Column (7) of Table 4 gives *K*-magnitudes ($K_{0.5}$) at $A / D(0) = 0.5$ for the galaxies based either on interpolation between observed points or extrapolation via the growth curve. A similar procedure was followed to obtain $(J - K)_{0.5}$ and $(H - K)_{0.5}$. Values of $(V - K)_{0.5}$ in column (4) of Table 4 were obtained either by interpolating between the values given in Table 1 or in a few cases by extrapolating from available *V* and *K* growth curves. The values of $(U - V)_{0.5}$ were taken from the sources used for the *V*-magnitudes or from Paper III. In a few cases it was necessary to extrapolate available $(U - V)$ measurements to $A / D(0) = 4.5$ by use of the mean slope $\Delta(U - V) / \Delta \log A / D(0) = - 0.13$ (Paper III).

Table 4. Fully Corrected Colors and Magnitudes for E and S0 Galaxies

		Values at $A / D(0) = 0.5$					Values at $A / D(0) = 1.0$			
Galaxy	CO	$(U - V)_{0.5}$	$(V - K)_{0.5}$	$(J - K)_{0.5}$	$(H - K)_{0.5}$	$K_{0.5}$	$V_{1.0}$	$M_{V_{1.0}}$	$M_{K_{1.0}}$	Notes
(1)	(2)	(3)	(4)	(5)	(6)	(7)	(8)	(9)	(10)	(11)
NGC 205	0.095	0.81	2.12	0.71	0.15	7.9	8.72	-15.38	-16.6	2, 5, 6
NGC 221	0.155	1.31	3.14	0.87	0.21	5.50	8.16	-15.94	-19.02	1, 5
NGC 404	0.11	1.03	2.60	0.78	0.13	8.44	10.44	-13.66	-16.08	2, 5, 6
NGC 584	0.15	1.52	3.24	0.88	0.20	7.95	10.81	-22.11	-25.39	1
NGC 596	0.145	1.43	3.14	0.80	0.16	8.65	11.42	-21.50	-24.69	1, 2, 6
NGC 1023	0.16	1.46	3.15	0.88	0.22	6.72	9.44	-21.06	-24.20	
NGC 1600	0.155	1.53	3.33	0.93	0.20	8.93	11.75	-23.16	-26.40	1
NGC 1700	0.17	1.38	3.15	0.87	0.19	8.68	11.41	-23.03	-26.18	1

NGC 2300	0.15	1.64	3.46	0.92	0.19	8.45	11.52	-21.88	-25.37	1
NGC 2549	0.155	1.49	3.18	0.75	0.17	8.26	11.28	-20.39	-23.83	
NGC 2634	0.14	-	-	0.89	0.20	9.92	-	-	-	
NGC 2655	0.15	-	-	0.87	0.21	7.38	10.27	-21.79	-25.10	
NGC 2672	0.16	1.53	3.22	0.90	0.21	9.25	12.10	-22.42	-25.69	
NGC 2768	0.16	1.50	3.24	0.87	0.17	7.82	10.57	-22.06	-25.23	1
NGC 2974	0.155	1.54	3.43	0.94	0.21	8.3	11.26	-21.52	-24.9	2,4,6
NGC 3115	0.17	1.59	3.30	0.93	0.22	6.33	9.33	-20.29	-23.71	1
NGC 3158	0.16	1.62	3.44	0.94	0.22	9.5	12.59	-23.15	-26.7	1, 2, 4, 6
NGC 3193	0.165	1.46	3.16	0.65	0.18	8.53	11.24	-20.66	-23.79	1
NGC 3226	0.14	1.48	3.32	0.89	0.21	9.17	11.85	-20.05	-23.15	4
NGC 3377	0.17	1.22	3.02	0.85	0.19	7.99	10.68	-20.20	-23.31	6
NGC 3379	0.155	1.63	3.36	0.87	0.19	6.97	9.87	-21.01	-24.33	
NGC 3364	0.16	1.45	3.15	0.87	0.22	7.20	10.20	-20.68	-24.10	1, 6
NGC 3607	0.165	1.52	3.36	0.90	0.21	7.70	10.64	-20.97	-24.33	1
NGC 3608	0.145	1.48	3.24	0.90	0.20	8.73	11.45	-20.16	-23.30	1
NGC 3613	0.155	1.47	3.15	0.83	0.17	8.55	11.19	-21.68	-24.74	
NGC 3842	0.13	-	-	-	-	-	-	-	-	3
NGC 3998	0.15	1.50	3.50	0.93	0.23	7.5	10.83	-21.02	-24.8	1, 2, 6
NGC 4261	0.175	1.60	3.29	0.88	0.22	7.88	10.86	-22.32	-25.72	
NGC 4278	0.165	1.45	3.29	0.86	0.20	7.68	10.62	-20.73	-24.09	1
NGC 4283	0.18	1.37	3.22	0.90	0.23	9.56	12.50	-18.85	-22.21	
NGC 4365	0.16	1.57	3.29	0.90	0.24	7.29	10.03	-21.70	-24.86	1
NGC 4374	0.15	1.56	3.33	0.89	0.21	7.00	9.87	-21.86	-25.15	1
NGC 4382	0.135	1.41	3.05	0.85	0.21	6.89	9.40	-22.33	-25.26	1
NGC 4406	0.17	1.52	3.23	0.88	0.21	7.15	9.79	-21.94	-25.00	1
NGC 4459	0.14	1.53	3.33	0.98	0.25	8.02	10.82	-20.91	-24.13	1, 6
NGC 4464	0.145	1.41	3.09	0.86	0.16	9.91	12.79	-18.94	-22.24	
NGC 4472	0.17	1.64	3.38	0.90	0.19	6.12	8.89	-22.84	-26.03	1

NGC 4478	0.14	1.28	3.28	0.83	0.20	8.80	11.67	-20.06	-23.35	1
NGC 4486	0.17	1.55	3.39	0.88	0.19	6.45	9.27	-22.46	-25.70	3
NGC 4486A	0.115	-	-	-	-	-	-	-	-	
NGC 4486B	0.10	1.62	3.6	0.88	0.17	10.49	13.66	-18.07	-21.66	1, 4
NGC 4494	0.135	1.34	3.06	0.85	0.18	7.83	10.43	-20.92	-23.94	1, 2, 6
NGC 4649	0.17	1.70	3.39	0.91	0.19	6.45	9.29	-22.44	-25.70	
NGC 4889	0.17	1.0	3.31	0.92	0.23	9.29	12.08	-23.54	-26.75	
NGC 5813	0.14	1.59	3.40	0.91	0.20	8.35	11.16	-21.62	-24.85	1
NGC 5846	0.16	1.66	3.50	0.96	0.23	7.81	10.73	-22.05	-25.39	1
NGC 5866	0.15	1.41	3.47	0.98	0.28	7.37	10.32	-21.03	-24.40	
NGC 5982	0.155	1.49	3.21	0.85	0.20	8.83	11.62	-22.18	-25.39	1
NGC 6702	0.21	1.46	3.35	0.96	0.24	9.97	13.0	-22.01	-25.5	1, 2, 6
NGC 7619	0.17	1.73	3.49	0.90	0.20	8.80	11.70	-22.68	-26.00	
NGC 7626	0.17	1.65	3.41	0.91	0.20	9.0	11.95	-22.43	-25.8	1, 2, 6

NOTES:

1. Value of $V[A / D(0) = 1]$ not from RCBG.
2. Value of $K[A / D(0) = 0.5]$ is extrapolated using growth curve.
3. No value for $D(0)$ available.
4. No overlap of V and K data, so use growth curves to get $(V - K)_{0.5}$
5. Local Group: $(m - M) = 24.1$.
6. Value of (J-K) extrapolated using mean slope of -0.12 (only one observation).

To obtain absolute magnitudes, we used values of $V_{1.0}$ from the RCBG, with changes made when new data from the literature or Paper III were available. Mean redshifts corrected for solar motion relative to the Local Group of galaxies from the RCBG, and a Hubble constant of 50 km s^{-1} Mpc^{-1} was adopted. For those galaxies identified as being in small groups (de Vaucouleurs 1976), the mean redshift of the group was used; all galaxies considered to be in the Virgo cluster were assigned the same redshift. For Local Group members in the vicinity of M31 an M33, with NGC 404 included, a value of $(m - M)_0 = 24.1$ was used (van den Bergh 1976). The absolute K-magnitudes $M_{K_{1.0}}$ were derived from $(K_{0.5} - K_{1.0}) = 0.42$ mag (Table 5).

Table 5. Adopted K Growth Curve

Log A/D(0)	Δ Mag (K)	Log A/D(0)	Δ Mag (K)
-l. l.	+1.57	-0.4	+0.16
-1.0	+1.34	-0.3	0.0
-0.9	+1.13	-0.2	-0.15
-0.8	+0.91	-0.1	-0.29
-0.7	+0.70	0.0	-0.42
-0.6	+0.50	+0.1	-0.55
-0.5	+0.33		

i) Color-Color Relationships

In Figures 3 - 5, we present the interrelationships between the CO index and the broad-band colors, and we list in Table 6 some least squares fits to the data points. The points for the globular clusters in these figures have not been included in the least squares solutions. These data will be discussed in Section IV below. Several basic results are apparent from Figures 3 and 4. First, the location of the points in a CO index versus color diagram reiterates our previous conclusion that the light of early-type galaxies is dominated by giant stars (Frogel et al. 1975a, b). Second, the CO index shows no significant dependence on color for the galaxies in this sample. In fact, with a few exceptions, the observed dispersion in the CO index is consistent with that expected from the measuring errors alone. Third, the *average* broad-band colors indicate a mean spectral type which depends on wavelength. This is the same effect noted by Stebbins and Whitford (1948); viz, the light of elliptical galaxies is of a composite nature, and as the observational baseline shifts to the red, we sample, in the mean, a later and later component of the stellar population. *H* - *K*, the reddest color, corresponds to that of an M star.

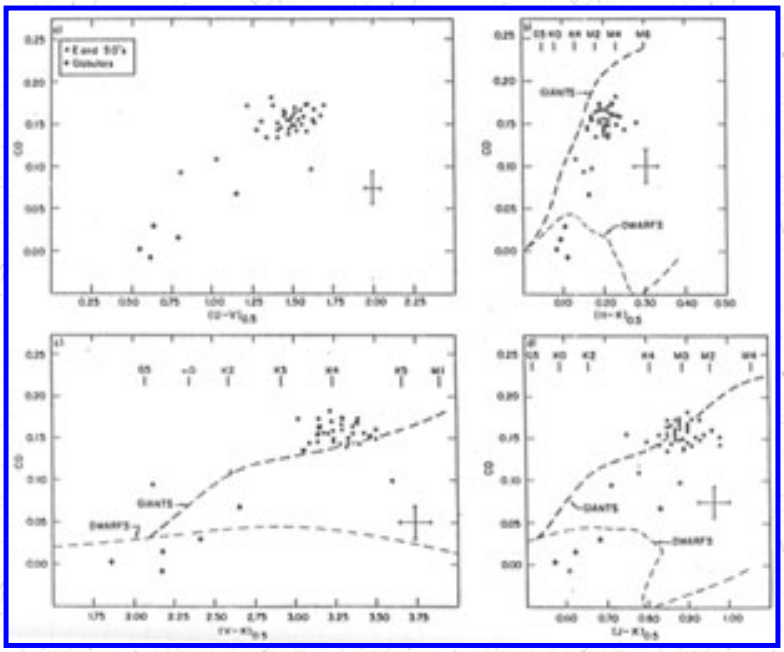

Figure 3. The average CO index for a galaxy as a function of several colors determined at a characteristic value of $A / D(0) = 0.5$. All the data points from Table 4 are plotted. The *dashed lines* are the mean relationships for field giants and dwarfs from Appendix A. The *circles* represent the globular cluster observations from Table 2. The indicated spectral types refer to the mean giant relationship.

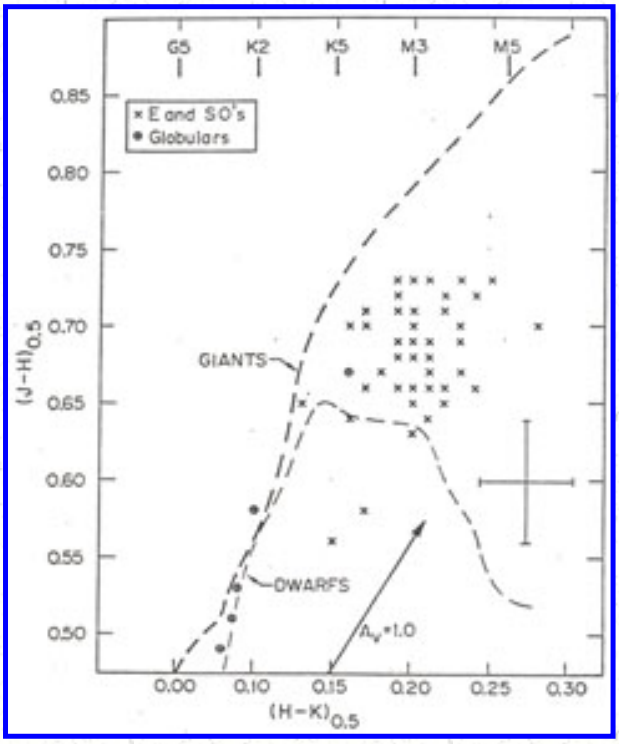

Figure 4. The *J* - *H*, *H* - *K* relation for the data from Table 4. The symbols are the same as in Fig. 3.

In Figure 5 we plot *V* - *K* and *J* - *K* against *U* - *V*. The *V* - *K* color is strongly correlated with *U* - *V*, in agreement with the results of Strom et al. (1976). These correlations are discussed further below.

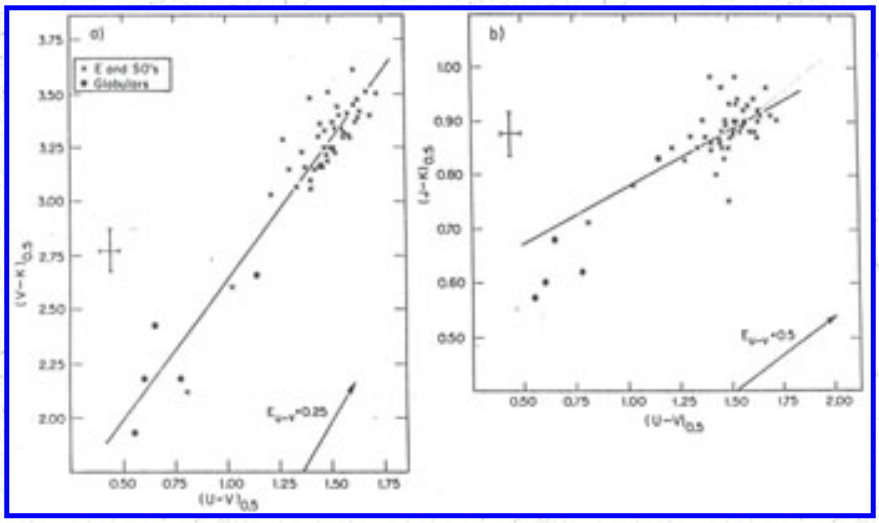

Figure 5. All the galaxies from Table 4 are plotted. The open symbols represent the globular cluster data from Table 2. The solid lines are the linear least-squares fits to the galaxy data only.

ii) Color - Absolute Magnitude Relationships

Figure 6 displays the colors and the CO index as functions of absolute magnitude; the least squares solutions from Table 6 are also shown. That a strong correlation exists between U - V and $M_{V_{1.0}}$ is well known (e.g., de Vaucouleurs 1961). The value for the slope agrees with that found from the data of Sandage (1972). As expected from Figure 5, V - K also correlates with $M_{V_{1.0}}$. The extinction vectors suggest that part of the scatter in Figure 6 could arise from uncertainties in the reddening. Any significant dependence of CO index on luminosity is not established by the present data.

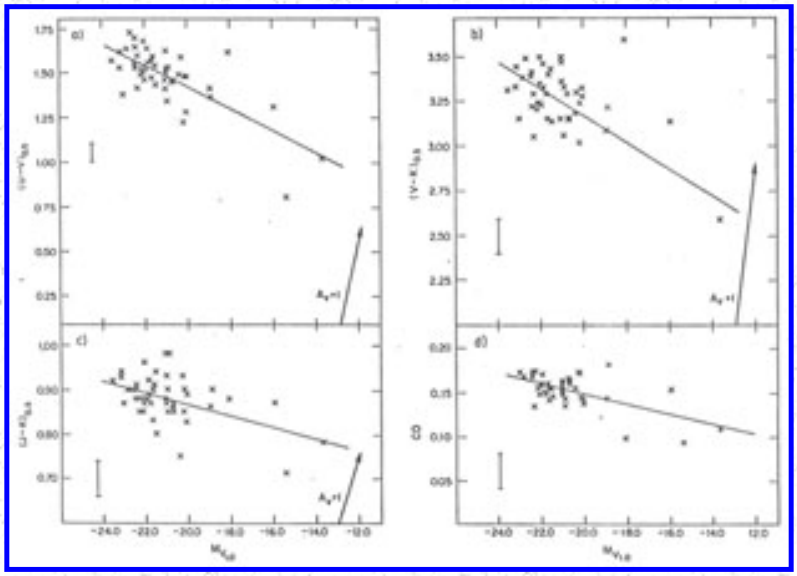

Figure 6. Corrected colors and CO indices for all galaxies from Table 4 are shown as functions of absolute magnitude. The linear least-squares fits are also indicated.

In order to reduce the scatter in the color - absolute magnitude relationships, the observations of galaxies with well-determined distances (i.e., those in groups or clusters) were binned in unit absolute magnitude intervals (Table 7). This table shows evidence for the $V - K$ color of the brightest galaxies to be relatively independent of luminosity compared to the fainter groups. A relative flattening in color - magnitude plots was first noted by Lasker (1970); this point is discussed further in Section VI (a) and in Paper III.

Table 6. Color-Color and Color-Magnitude Relations of the form $Y = A + BX$

X	Y	N	$A(\pm\sigma)$	$B(\pm\sigma)$	r	s
$(U - V)_{0.5}$	$(V - K)_{0.5}$	47	1.35 (0.14)	+1.28 (0.09)	+0.89	0.11
$(U - V)_{0.5}$	$(J - K)_{0.5}$	47	0.57 (0.07)	+0.21 (0.05)	+0.65	0.04
$M_{V_{1.0}}$	$(U - V)_{0.5}$	47	0.22 (0.32)	-0.06 (0.02)	-0.73	0.11
$M_{V_{1.0}}$	$(V - K)_{0.5}$	47	1.69 (0.35)	-0.07 (0.02)	-0.09	0.19
$M_{V_{1.0}}$	$(J - K)_{0.5}$	48	0. 60 (0.32)	-0.01 (0.02)	-0.51	0.05
$M_{V_{1.0}}$	CO*	41	0.03 (0.34)	-0.006 (0.016)	-0.60	0.02

* Galaxies with $z \geq 0.012$ have been excluded from the CO solution. s is the variance of the fit. The assumed uncertainties in the quantities are ± 0.03,± 0.10,± 0.04,± 0.02, and ± 0.2 mag for $(U - V)$, $(V - K)$, $(J - K)$, CO and $M_{V_{1.0}}$, respectively.

Table 7. Galaxies in Clusters and de Vaucouleurs' Groups with Well-determined Distances

		Mean Colors					
$M_{V_{1.0}}$	No.	$(U - V)_{0.5}$	$(V - J)_{0.5}$	$(V - K)_{0.5}$	$(J - H)_{0.5}$	$(H - K)_{0.5}$	CO*
$M_V < -22.8$	3	1.57	2.44	3.36	0.70	0.22	-
$-22.8 \leq M_V < -21.8$	13	1.58	2.43	3.33	0.69	0.21	0.16
$-21.8 \leq M_V < -20.8$	10	1.50	2.40	3.30	0.68	0.22	0.15
$-20.8 \leq M_V < -19.8$	8	1.43	2.36	3.22	0.67	0.20	0.16
$-19.8 \leq M_V < -18.8$	3	1.39	2.27	3.15	0.68	0.20	0.14

* Galaxies with $z \geq 0.012$ were excluded from the average CO values.

iii) Ratios of Color Variations

An interesting result is found when changes in the colors within galaxies are compared with changes from galaxy-to-galaxy. Within individual galaxies, the average change in $U - V$ is given by $\Delta(U - V) / \Delta \log A / D(0) = - 0.13 \pm 0.02$, a result which is based on the measurements of Paper III, and which agrees with that of Sandage (1976). We now combine this with the results of Tables 3 and 6 to arrive at the following values shown in Table 8. Taken at face value, these results show that if the 0.5 - 2.2 μm spectral region is divided in two, then radial changes of the stellar population (due to luminosity function and/or metallicity changes) within galaxies are most evident at wavelengths *longward* of 1.2 μm. On the other hand, from one galaxy to another such changes are evident primarily at wavelengths *shortward* of 1.2 μm.

Table 8. Ratios of Color Variations

Color Ratio	Within Galaxies	Between Galaxies
$\Delta(V - K) / \Delta(U - V)$	0.9 ± 0.5	1.3 ± 0.1
$\Delta(J - K) / \Delta(U - V)$	0.9 ± 0.4	0.2 ± 0.1
$\Delta(V - J) / \Delta(U - V)$	0.0 ± 0.5	1.1 ± 0.2

The measurements made with the J filter were subject to the largest corrections due to the beam profile effects noted in Section II(c). Since the average value of $\Delta \log A / D(0)$ for the determination of $\Delta(J - K) / \Delta \log A / D(0)$ is 0.6, any residual systematic error in the $J - K$ color will be doubled. As an example, a systematic error of 0.02 mag would change $\Delta(J - K) / \Delta(U - V)$ within galaxies by nearly 0.3. Another potential difficulty with the interpretation of these numbers is that the slope *within* galaxies is determined mainly from observations of the brighter galaxies, whereas the determination of the slopes *between* galaxies is weighted toward the few galaxies of lower luminosity.

A proper resolution of the question of the color-color relationships within galaxies and between galaxies awaits detailed off-axis photometry, free of systematic beam profile effects.

c) Summary and Conclusions

The results presented above can be summarized as follows:

(1) In combination with the reddest broad-band colors, the CO data show that the infrared light. of the inner regions of early-type galaxies is dominated by the light of M giant stars.

(2) The strength of the CO absorption remains constant out to a projected aperture diameter $A / D(0)$. A significant dependence of CO index on absolute magnitude is not established by the data.

(3) The observed dispersion in the *UVJHK* colors is clue, in part, to a dependence of the colors both on the fraction of the galaxy being measured on the galaxian luminosity. The sense of the dependences is for the colors to be redder near the nucleus and in galaxies of higher luminosity.

(4) There is evidence for differences in the ratios of color variations between galaxies and within galaxies.

It should be noted that the above conclusions are based on data from a sample of galaxies having a limited range in luminosity. Furthermore, averages have been taken over a sample which is inhomogeneous in several respects: a number of S0 galaxies, several local group dwarfs, and two possibly tidally stripped objects, NGC 221 and 4486B (Faber 1973a) have been included, and the galaxies are members of both rich and sparse groups. However, none of the correlations presented above are changed in a statistically significant way when various subsets of the data are excluded from the solutions. These points are explored in detail in Paper III, where a larger sample of galaxies is studied.

IV. DISCUSSION OF THE GLOBULAR-CLUSTER OBSERVATIONS

Our preliminary study of globular clusters is based on the integrated light data presented in Table 2. The colors are compared with those of the galaxies in Figures 3 - 5. M15 and M92 are examples of stellar systems with extreme metal deficiencies, M3 and M13 of moderate metal deficiencies, and M69 of only a small metal deficiency (Sandage 1970; Hartwick and Sandage 1968, and references therein). It is apparent from the color - color plots (Figs. 4 and 5) that these five clusters extend the sequences defined by the E and S0 galaxies and, in fact, overlap the two faintest galaxies NGC 205 and 404. This behavior is similar to that found from studies of optical colors and indices (e.g., McClure and van den Bergh 1968; Faber 1973b). Furthermore, *the ordering of these clusters by their infrared colors corresponds approximately to an ordering by metallicity in the sense that redder colors are associated with higher (Fe/H).* [4] This result differs from the finding of Grasdalen (1974), who derived $V - K$ colors for a number of highly reddened distant clusters.

The location of the clusters relative to the galaxies on plots of CO versus color (Fig. 3) may differ from the relative locations on color-color plots. There is evidence that for a given color, the CO strengths in globular clusters are weaker than would be estimated from a linear extrapolation of-the available galaxy data. Alternatively, the possibility exists that the CO index for galaxies turns sharply downward below $V - K = 3.0$.

---

[4] Observations of individual stars in clusters (Cohen, Frogel, and Persson 1978) in fact shows that for a constant effective temperature the CO index decreases with decreasing metallicity. Back.

V. COMPARISON OF MEAN COLORS WITH STELLAR SYNTHESIS MODELS

Recently, attempts have been made by several authors (Tinsley and Gunn 1976; O'Connell 1976b; Whitford 1977) to model photometric and spectrophotometric observations of the central regions of bright elliptical galaxies. In this section, we ask how well these published models agree with our new data for bright galaxies. Detailed model fitting is deferred to a later paper.

Two models are chosen as examples: Model "A" of Tinsley and Gunn (1976, TG) in which the slope of the

initial mass function x equals zero; and model "C" of O'Connell (1976b, OC) with a flat luminosity function φ (M dwarfs), which corresponds to an x of about 0.5. The published luminosity function of TG and unpublished values from O'Connell (1976c) were combined with the stellar calibrations of Appendix A and of Johnson (1966b), and the colors for these two models were calculated. (Johnson's J - K colors were transformed to the system of this paper as discussed in Appendix A). The results are given in Table 9, where the observed values are for the galaxies in the second group of Table 7. The OC model gives an excellent fit to the average galaxy colors, while the TG model has colors which are too blue and a CO index which is too weak. OC's model fit is probably fortuitous, however, because of the sensitivity of the infrared indices to the luminosity function of the giant branch (see Table A3) combined with the coarseness of OC's bins for giants. The origin of the difference between the two models lies in the choice of the relative shape of the giant branch luminosity function, and in the assumed values of M_V for giants (which differed by up to l mag). For the OC model, about 35 percent of the light at 2 μm comes from the M6 III bin whereas these stars contribute only 12 percent of the 2 μm light in the TG model. Nevertheless, the model fitting work of TG (and references therein), OC, and Frogel et al. (1975a) has established that *the V - K color and the CO index provide strong constraints on both the dwarf-to-giant ratio and the shape of the giant branch - V - K is effective for the latter and the CO index for the former.* Any significant increase in the number of late-type dwarf stars beyond those already contained in the models drives the CO index to unacceptably low values and begins to make V - K too red. The J - H color is mildly sensitive to the giant-to-dwarf ratio since dwarf stars do not exhibit J - H colors greater than 0.7 (e. g., Mould and Hyland 1976). H - K provides a weak constraint on the giant branch luminosity function as can be seen from Figure 4 : stars later than M3 III must be present to provide the red H - K color.

Table 9. Comparison Between Models and Observations

Parameter	TG	OC	Obs.
V - K	2.97	3.29	3.33
J - H	0.59	0.7	0.70
H - K	0.22	0.2	0.20
CO	0.14	0.16	0.16
M / L_V	3.0	2.4	-

VI. COMPARISON WITH PHOTOMETRIC STUDIES AT λ < 1.0 μm

In this section we compare our results with those of three previous photometric studies of the nuclei of early-type galaxies and of the integrated light of globular clusters -- O'Connell (1976a), Faber (1973b), and McClure and van den Bergh (1968).

a) The Work of O'Connell

Nineteen E and S0 galaxies were observed photoelectrically by O'Connell (1976a) in the extreme red region of the optical spectrum, mostly through a 12" diameter aperture. The results of immediate interest here may be

summarized as follows: $A(1.0 - 0.74)_0$ color, which is insensitive to blanketing effects, shows a "mild color-luminosity dependence" over the range $-22 < M_V < -16$. However, if the faintest galaxies are excluded, then O'Connell's data are consistent with a constant $(1.0 - 0.74)_0$ color for $M_V < -19$. This color is "equivalent to an M0-1 III star." O'Connell also found that the strength of the Ca II+TiO λ 8542 feature (which is positively correlated with luminosity in giant stars), rather than increasing monotonically with absolute galaxian magnitude, reaches a maximum near $M_V = -20$, and then declines with increasing luminosity. He interprets this as a decrease in the luminosity of the late M giants in the brightest galaxies due to the increased metal content of these systems.

All but one of O'Connell's galaxies were observed by us through either a 15" or a 16".5 diameter aperture. These observations were taken from Table 1 and divided into the same three luminosity groups used by O'Connell. The colors and CO index showed no statistically significant variation from group to group. These results did not change when other galaxies with 15" or 16".5 observations from Table 1, and having reliable distance estimates, were included in the averaging.

To carry this comparison further, we use the averaged colors from Table 7. Although these measurements refer to a much larger fraction of the light than that measured by O'Connell, these data are expected to have smaller uncertainties than the small aperture data, and they substantially increase the sample size. From the decrease in Ca II + TiO strength for $M_V < -20$, one might expect to see some effect in the infrared colors, especially in $V - K$. Table 7 shows no evidence that any of the colors become bluer with increasing luminosity. A much larger sample of galaxies is needed to proceed further with this puzzling comparison (cf. Paper III).

b) The Work of McClure and van den Bergh and of Faber

McClure and van den Bergh (1968) and Faber (1973b) observed the central regions of a number of E/S0 galaxies and the integrated light of globular clusters with sets of narrow bandpass filters chosen to isolate specific spectral features primarily in the blue and visible. The UV blanketing feature measured by McClure and van den Bergh (1968) (defined by them as C^* [38 - 45]) was found to be strongly correlated with Q, the reddening-free metallicity index. Based on these results and on model fitting, they concluded that dwarf ellipticals consist primarily of metal-deficient stars, that the cores of giant ellipticals consist of metal-rich stars with strong CN bands, and that these cores are embedded in a metal-poor halo. Additional evidence for the presence of a stellar population with strong CN bands in the nuclei of galaxies has been presented by McClure (1969), Spinrad et al. (1971), Welch and Forrester (1972), and Spinrad, Smith, and Taylor (1972), among others.

Faber's (1973b) observations of galaxies and globulars led her to the following conclusions: (a) all of the colors depend on only one parameter -- the luminosity of the galaxy; (b) the scatter in the data at a given M_V comes mostly from residual reddening errors and from observational errors; and (c) a monotonic increase in mean metallicity with luminosity seemed the most likely explanation for the observed variation in the various indices.

In Figure 7 we compare the values of $(U - V)_{0.5}$, $(V - K)_{0.5}$, $(J - K)_{0.5}$, and CO for the galaxies and the globulars from Tables 2 and 5 with the CN_0 - Mg_0 line index of Faber (1973b). Some of the measurements of McClure and van den Bergh were transformed to the CN_0 - Mg_0 index via a comparison of objects in common and were added to Figure 7. The correlations seen in Figure 7 are in qualitative agreement with those expected from the

relations between Faber's line index and absolute magnitude and from our own results in Figure 6, in that the colors and CO index are seen to increase monotonically with increasing CN_0 - Mg_0. A slight curvature may be present in Figure 7 (c), and this could be another piece of evidence for a relative insensitivity of the infrared colors of brighter galaxies to changes in M_V. Aside from this, latter point, though, the data in Figures 5, 6, and 7 are in basic agreement with Faber's (1973b) main conclusions.

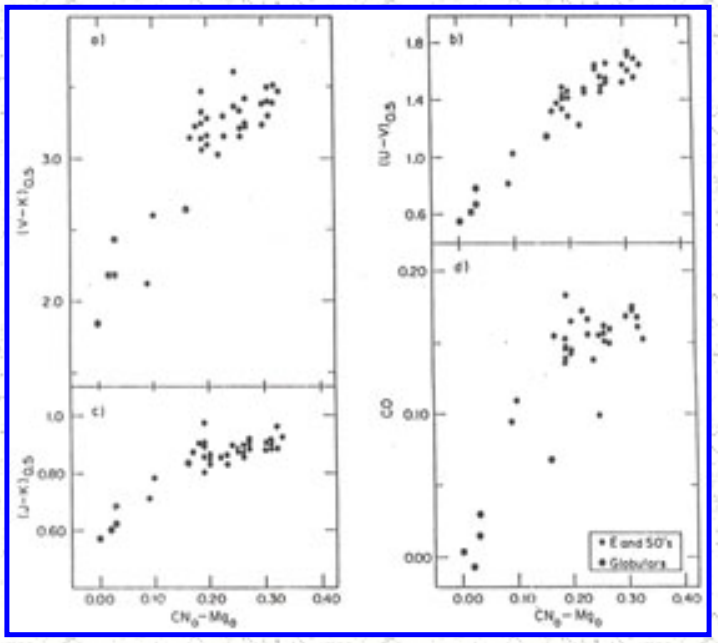

Figure 7. Colors and CO indices for galaxies from Table 4 and for globular clusters from Table 2 are shown as functions of Faber's (1973b) CN_0 - Mg_0 index.

VII. SUMMARY AND CONCLUSIONS

In this paper we have presented new broad-band infrared colors and CO indices for early-type galaxies and globular clusters. We have compared our data with recent stellar synthesis models of bright ellipticals and can conclude that the only models which are consistent with the present observations are those with rich giant branches and relatively flat main-sequence luminosity functions. A detailed quantitative comparison is made difficult, however, because of the sensitivity of the predicted infrared colors to the numbers and luminosities of M giants, combined with the observational uncertainties in these latter quantities.

We have examined the dependence of the various colors on absolute galaxian luminosity and on measuring aperture size. The broad-band colors tend to redden with increasing luminosity and with decreasing aperture size. Since we find evidence for the infrared colors and the CO index to be redder and stronger, respectively, in globular clusters of high mean metallicity as opposed to those of low metallicity, it is reasonable to conclude that the changes observed in the integrated light of galaxies also have, as their underlying cause, changes in the mean metallicity of the stellar population. A change in the metallicity acts both directly via a change in the CO strength for stars of the same effective temperature and indirectly via a change in the relative populations of the principal sequences of a color-magnitude diagram. Of particular note is the evidence that the relative changes of the *U* - *V*, *V* - *J*, and *J* - *K* colors within galaxies differ from those between galaxies. It may be possible to

understand this result qualitatively if some fraction of the changes in the optical parameters arises from changes in CN blanketing rather than from changes in [Fe/H] alone (Peterson 1976a, b). This may, mean that *U* - *V* cannot be used as a pure indicator of the mean metallicity of a composite system. The color changes in systems consisting of metal-rich and metal-poor stars may also be important in understanding the interplay of *U* - *V* and *V* - *K*. Stellar synthesis models of a complexity greater than any heretofore reported in the literature, and which include a certain amount of chemical evolution, will be required to quantitatively interpret these and other recent photometric observations of galaxies.

Acknowledgements

This program would not have been possible without the generous allotment of observing time made available to us, particularly at the Hale Observatories, or without the collaboration of Eric Becklin and Gerry Neugebauer. We are grateful to Allan Sandage for allowing us to have access to his compilation of published optical photometry and for his continued interest in this work. We acknowledge helpful conversations with Beatrice Tinsley and Robert O'Connell. Special assistance was provided by d. Walker and G. Livet. An anonymous referee made several critical comments on an earlier version of this paper. This work was supported in part by NSF grant AST 74-18555 A2 and NASA grant NGL 05-002-207.

APPENDIX

Although the *J* and *K* filters used in this study are similar to those employed in the original infrared photometric system as described by H. L. Johnson and others, the need for a high degree of internal accuracy required the determination of a new set of standard magnitudes. Twenty-one stars, selected so that a reasonably large range of brightness and color could be spanned were set up as standards.

Individual standards were typically observed on 10-20 different nights with between one and three observations per night. The system was closed once around the sky, and no systematic closure errors were found. We estimate that the *internal* accuracy of the system is ± 0.01 mag at *H*, *K*, and in the CO index; and ± 0.03 mag at *J*. A combination of the transmission characteristics of the J filter, the atmosphere, and the field lens, and the rounded nature of the beam profile, causes the *J* measurements to have the largest uncertainty.

Table Al contains the *J* - *H* and *H* - *K* colors, *K*-magnitudes, and CO indices for our grid of standards. The zero-point of this system is set by defining the magnitudes and colors of α Lyr to be 0.00 at all wavelengths. If allowance is made for the fact that Johnson (1966b and references therein) takes *K*(α Lyr) = + 0.02, there is no systematic difference between the magnitude scales of Johnson and of Table Al based on a comparison of 16 stars. Thus, except for the zero-point shift, the *V* - *K* values in this paper are on the system of Johnson. Because the effective wavelength of our *J*-filter is different from that of Johnson, a small transformation exists between the two systems. To transform the *J*-magnitudes of this paper to the Johnson (1966b) system, the following equation is adequate

$$J_J = 1.09(J - H) + H \qquad \text{(A1)}$$

i. e., the *J* - *K* colors in this paper are systematically blue compared with Johnson's. We caution other observers

using the photometric system defined by these stars to check carefully for the presence of a color equation, particularly at 1.2 μm.

Table A1. Standard Stars

Name	Sp. Type	V	K	J-H	H-K	CO
BS 117	MO III	5.71	1.87	0.74	0.16	0.155
BS 134	KO III	6.30	4.07	0.45	0.08	0.04
BS 718	B9 III	4.28	4.38	-0.05	-0.02	0.00
BS 923	KO III	5.99	3.74	0.49	0.08	0.05
BS 1552	B2 III	3.69	4.14	-0.04	-0.05	0.00
BS 1698	K3 III	4.46	1.84	0.53	0.10	0.095
BS 3304	KS III	5.63	2.37	0.66	0.13	0.15
BS 3403	K2 III	4.59	1.88	0.54	0.06	0.08
BS 3427	KO III	6.39	4.25	0.48	0.07	0.04
BS 4039	dF5	5.82	4.49	0.28	0.03	-0.005
BS 4550	G8 VI	6.45	4.42	0.44	0.06	0.005
BS 4608	G8 III	4.13	1.89	0.47	0.05	0.05
BS 4689	A2 V	3.88	3.77	-0.05	-0.01	-0.005
HD 107906	K	-	7.04	0.39	0.05	0.035
HD 132950	K	-	6.33	0.51	0.07	0.04
BS 5634	F5 V	4.92	3.88	0.22	0.02	0.00
BS 6092	B5 IV	3.89	4.30	-0.06	-0.05	0.01
BS 6136	K4 III	5.39	2.02	0.66	0.14	0.145
BS 6228	K5 III	5.16	1.44	0.72	0.15	0.165
BS 7001	AO V	0.00	0.00	0.00	0.00	0.00
BS 8498	K3 II-III	4.12	0.99	0.62	0.13	0.15
BS 8551	KO III-IV	4.80	2.29	0.53	0.09	0.07

Table A2 contains measurements of selected high luminosity late-type stars. These data were used to define mean relationships between colors, CO index, and spectral type, and can be employed to establish transformations from the present photometric system to any other system. The three supergiants in Cygnus, plus the stars identified with BD numbers, are heavily reddened (Lee 1970).

Table A2. Selected M Giants and Supergiants

Name	Sp. Type	K	J-H	H-K	CO

BS 3027	M2 II-III	2.01	0.83	0.20	0.20
BS 3705	M0 III	-0.61	0.84	0.16	0.17
BS 4008	MO III	2.10	0.80	0.17	0.20
BS 4069	MO III	-0.84	0.79	0.15	0.18
BS 4336	M2 III	1.44	0.79	0.18	0.20
BS 4902	M3 III	0.14	0.82	0.20	0.20
BS 4910	M3 III	-1.25	0.80	0.18	0.21
BS 5879	gMl	0.05	0.82	0.17	0.19
BS 7139	M4 II	-1.17	0.85	0.21	0.26
BS 7157	M5 III	-2.06	0.83	0.26	0.25
BK Vir	M7 III	-0.91	0.89	0.33	0.25
SW Vir	M7 III	-1.88	0.91	0.34	0.27
RT Vir	M8 III	-1.18	0.90	0.36	0.24
BC Cyg	M4 Ia	0.25	1.17	0.54	0.33
AZ Cyg	M2 Ia	1.31	0.97	0.38	0.34
KY Cyg	M4 Ia	1.54	1.27	0.59	0.30
+9° 3920	M2 III	4.37	0.85	0.22	0.21
+29° 3730	M4 III	1.95	0.85	0.24	0.21
+35° 4138	M3 III	3.89	0.86	0.23	0.20
+59° 2541	M2.5 III	4.46	0.85	0.26	0.18
+64° 1842	M2 II	3.11	1.03	0.33	0.19
+42° 1065	MO III	5.66	0.83	0.20	0.14

Table A3 gives the adopted mean relationships based on the system of Tables Al and A2. The *V* - *K* and *J* - *K* colors as functions of spectral type for the giants are transformed from Johnson (1966b) for stars earlier than M0 and from Lee (1970) for MO-M6. The *H* - *K* colors and CO indices of the giants are from the data of Tables Al and A2 and from additional unpublished measurements. All of the mean values for the dwarf's are based on our own infrared measurements plus *V*-magnitudes from the literature. The agreement with most of the recently published infrared photometry of dwarfs (e.g., Mould and Hyland 1976) is generally better than ± 0.02 mag at all wavelengths. A complete discussion of our observations of late-type dwarfs will be presented elsewhere.

Table A3. Adopted Mean Colors

	Giants				Dwarfs			
Sp. Type	V-K	J-H	H-K	CO	V-K	J-H	H-K	CO

G5	2.08	0.47	0.05	0.03	1.25	0.26	0.04	0.01
G8	2.16	0.49	0.06	0.04	1.50	0.32	0.05	0.02
KO	2.35	0.51	0.08	0.07	1.75	0.37	0.06	0.02
K1	2.48	0.54	0.09	0.09	2.00	0.42	0.07	0.03
K2	2.59	0.56	0.10	0.11	2.25	0.47	0.08	0.04
K3	2.92	0.62	0.12	0.12	2.50	0.52	0.09	0.04
K4	3.24	0.68	0.13	0.14	2.75	0.56	0.10	0.04
K5	3.67	0.73	0.15	0.15	3.00	0.59	0.11	0.04
MO	3.74	0.74	0.16	0.17	3.25	0.63	0.13	0.04
M1	3.90	0.76	0.17	0.18	3.50	0.65	0.14	0.04
M2	4.16	0.77	0.18	0.19	3.75	0.65	0.16	0.03
M3	4.63	0.79	0.20	0.21	4.00	0.63	0.21	0.02
M4	5.34	0.81	0.23	0.22	4.25	0.60	0.22	0.00
M5	6.20	0.86	0.26	0.23	4.50	0.57	0.24	-0.02
M6	7.20	0.89	0.30	0.24	4.75	0.54	0.25	-0.03
M7	-	0.91:	0.33:	0.25:	5.00	0.53	0.26	-0.04
M8	-	0.89:	0.37:	0.26:	5.25	0.52	0.28	-0.05
					5.50	0.53	0.29	-0.05
					5.75	0.54	0.31	-0.04
					6.00	0.55	0.32	-0.04
					6.25	0.57	0.33	-0.03
					6.50	0.59	0.35	-0.03
					6.75	0.61	0.36	-0.02
					7.00	0.62	0.37	-0.02
					7.25	0.63	0.38	-0.01
					7.50	0.65	0.39	-0.01

REFERENCES

1. Aaronson, M., Frogel J. A., and Persson, S.E. 1977, Ap. J. (Paper II).
2. Baldwin, J. R., Danziger, I. J., Frogel, J. A., and Persson, S. E. 1973a, Ap. Letters, 14, 1.
3. Baldwin, J. R., Frogel, J. A., and Persson, S. E. 1973b, Ap. J., 184, 427.
4. Code, A. D. 1959, Pub. A.S.P., 71, 118.
5. Cohen, J. G., Frogel, J. A., and Persson, S. E. 1978, Ap. J., to be submitted.
6. de Vaucouleurs, G. 1961, Ap. J. Suppl., 5, 233.
7. de Vaucouleurs, G. 1976, in Stars and Stellar Systems, vol. 9, Galaxies and the Universe, ed. A. and M. Sandage, and J. Kristian (Chicago: University of Chicago Press), p. 557.
8. de Vaucouleurs, G. and de Vaucouleurs, A. 1964, Reference Catalogue of Bright Galaxies (Austin:

University of Texas Press).
9. Faber, S. M. 1972, Astr. and Ap., 20, 361.
10. Faber, S. M. 1973a, Ap. J., 179, 423.
11. Faber, S. M. 1973b, Ap. J., 179, 731.
12. Frogel, J. A. 1971, Ph.D. thesis, California Institute of Technology.
13. Frogel, J. A., Persson, S. E., Aaronson, M., Becklin, E. E., and Matthews, K. 1975a, presented at Tercentenary Symposium of the Royal Greenwich Observatory.
14. Frogel, J. A., Persson, S. E., Aaronson, M., Becklin, E. E., Matthews, K., and Neugebauer, G. 1975b, Ap. J. (Letters), 195, L15.
15. Frogel, J. A. Persson, S. E., Aaronson, M., Becklin, E. E., Matthews, K., and Neugebauer, G. 1975c, Ap. J. (Letters), 200, L123.
16. Grasdalen, G. L. 1974, A. J., 79, 1047.
17. Hartwick, F. D. A., and Sandage, A. 1968, Ap. J., 153, 715.
18. Hesser, J. E ., Hartwick, F. D. A., and McClure, R. D. 1976, preprint.
19. Johnson, H. L. 1966a, Ap. J., 143, 187.
20. Johnson, H. L. 1966b, Ann. Rev. Astr. and Ap. 4, 193.
21. Johnson, H. L. 1968, in Stars and Stellar Systems, vol. 7, Nebulae and Interstellar Matter, ed. B. M. Middlehurst, and L. H. Aller (Chicago; University of Chicago Press), p. 167.
22. Johnson, H. L., and Mendez, M. E. 1970, A. J., 75, 785.
23. Kron, G. E., and Mayall, N. U. 1960, A. J., 65, 581.
24. Lasker, B. M. 1970, A. J., 75, 21.
25. Lee, T. A. 1970, Ap. J., 162, 217.
26. McCammon, D., Münch, G., and Neugebauer, G. 1967, Ap. J., 147, 575.
27. McClure, R. D. 1969, A. J., 74, 50.
28. McClure, R. D., and van den Bergh, S. 1968, A. J., 73, 313.
29. Morgan, W. W., and Mayall, N. U. 1957, Pub. A.S.P., 69, 291.
30. Moroz, V. I. 1966, Soviet Astron. - AJ, 10, 47.
31. Mould, J. R., and Hyland, A. R. 1976, Ap. J., 208, 399.
32. O'Connell, R. W. 1974, Ap. J. (Letters), 193, L49.
33. O'Connell, R. W. 1976a, Ap. J. (Letters), 203, L1.
34. O'Connell, R. W. 1976b, Ap. J., 206, 370.
35. O'Connell, R. W. 1976c, private communication.
36. Persson, S. E., Frogel, J. A., and Aaronson, M. 1978, Ap. J. (Paper III, to be published).
37. Peterson, R. 1976a, Ap. J. Suppl., 30, 61.
38. Peterson, R. 1976b, Ap. J. (Letters), 210, L123.
39. Peterson, C. J., and King, I. R. 1975, A. J., 80, 427.
40. Sandage, A. 1961, Ap. J., 134, 916.
41. Sandage, A. 1970, Ap. J., 162, 841.
42. Sandage, A. 1972, Ap. J., 176, 21.
43. Sandage, A. 1973, Ap. J., 183, 711.
44. Sandage, A. 1976, private communication.
45. Schild, R., and Oke, J. B. 1971, Ap. J., 169, 209.

46. Spinrad, H., Gunn, J. E., Taylor, B. J., McClure, R. D., and Young, J. W. 1971, Ap. J., 164, 11.
47. Spinrad, H., Smith, H. I., and Taylor, D. J. 1972, Ap. J., 175, 649.
48. Spinrad, H., and Taylor, B. J. 1971, Ap. J. Suppl., 22, 445.
49. Stebbins, J., and Whitford, A. E. 1948, Ap. J., 108, 413.
50. Strom, S. E., Strom, K. M., Goad, J. W., Vrba, F. J., and Rice, W. 1976, Ap. J., 204, 684.
51. Strom, K. M., Strom, S. E., Jensen, E. B., Moller, J., Thompson, L. A., and Thuan, T. X. 1977, Ap. J. (to be published).
52. Tifft, W. G. 1969, A. J. 74, 354.
53. Tifft, W. G. 1573, Pub. A.S.P., 85, 283.
54. Tinsley, B. M. 1973, Ap. J. (Letters), 184, L41.
55. Tinsley, B. M. 1975, Ann. N.Y. Acad. Sci., in press.
56. Tinsley, B. M., and Gunn, J. E. 1976, Ap. J., 203, 52.
57. van den Bergh, S. 1967, A. J., 72, 70.
58. van den Bergh, S. 1976, in Stars and Stellar Systems, vol. 9, Galaxies and the Universe, ed. A. and M. Sandage, and J. Kristian (Chicago: University of Chicago Press), p. 509.
59. Welch, G. A., and Forrester, W. T. 1972, A. J., 77, 333.
60. Whitford, A. E. 1971, Ap. J., 169, 215.
61. Whitford, A. E. 1976, in Stars and Stellar Systems, vol. 9, Galaxies and the Universe, ed. A. and M. Sandage, and J. Kristian (Chicago: University of Chicago Press), p. 159.
62. Whitford, A. E. 1977, Ap. J., 211, 527.
63. Woolf, N. J., Schwarzchild, M., and Rose, W. K. 1964, Ap. J., 140, 833.

CHAPTER III
Observations of H_2O Absorption and the Coolest Stellar Component of E and S0 Galaxies

ABSTRACT

Multiaperture observations of the H_2O absorption feature near 2.0 microns are presented for the nuclei of 37 early-type galaxies, 5 globular clusters, and for a selection of stars. The H_2O absorption is a sensitive function of effective temperature, and provides a strong constraint on the contribution of the very coolest stars to integrated galaxian light. In combination with the luminosity-sensitive CO absorption, the large H_2O absorption found in galaxies indicates that at two microns a significant contribution from a stellar giant component at least as late as M5 in spectral type is present. For our limited data sample, the amount of H_2O absorption shows no dependence on absolute magnitude for galaxies with $M_V \leq -20$, and no dependence on projected aperture size in the range $1.0 \geq A / D(0) \geq 0.1$. The observations are compared with recently published synthesis models of Tinsley and Gunn and of O'Connell; better agreement is found with the latter author's models. It does not appear that a significant contribution of carbon stars can account for the discrepancy between the infrared data and the models of Tinsley and Gunn.

I. INTRODUCTION

Observations and stellar synthesis models of early-type galaxies have shown that most of the visible and infrared light from these galaxies is supplied by a giant-dominated stellar population (O'Connell 1974, 1976b; Tinsley and Gunn 1976; Whitford 1977; Frogel et al. 1975a, b, 1977, hereafter referred to as Paper I). The various photometric indices used by these authors establish that the contribution of main sequence stars to the total flux at 2 μm is less than 10%. However, the detailed structure of the giant branch remains uncertain. As an example, M6 III stars contribute 37% of the flux at 2.2 μm in the model of O'Connell (1976b) that fits the infrared data best, but only 12% in the best-fitting model of Tinsley and Gunn (1976). Yet, the CO indices of these models differ by only 0.02 mag (Paper I).

A spectral feature which is sensitive to effective temperature in late-type stars, and can therefore set constraints on the luminosity function of the giant branch is the broad stellar absorption band due to H_2O centered at 1.9 μm (Johnson and Mendez 1970; Frogel 1971; Baldwin, Frogel, and Persson 1973). In this paper we first discuss the dependence of the H_2O absorption on stellar effective temperature and luminosity. We then present multiaperture H_2O observations of the nuclei of 37 early-type galaxies and 5 globular clusters, and compare the data with those of Paper I and with the results of stellar synthesis models.

II. OBSERVATIONS

The equipment and techniques used for these observations are described fully in Paper I. Briefly, all measurements were made with an InSb detector cooled to 55° K. To measure the strength of the H_2O absorption, two filters cooled to either 77° K or 55° K were used. They have effective wavelengths and full widths at half maximum of 2.00(0.08 μm) and 2.20(0.11 μm); the latter filter is the "continuum" filter used in measuring the CO index (Paper I). Thirty-seven galaxies selected from Paper I were observed in the spring of 1976 with the 60-inch (1.5 m) and 100-inch (2.5 m) telescopes on Mount Wilson, and the 200-inch (5 m) Hale reflector. Most of these observations were made at the same time as the CO and JHK observations of Paper I. The stellar calibration of the H_2O index was determined with these telescopes and with the 60-inch (1.5 m) Tillinghast reflector of Mount Hopkins, Arizona. Several globular clusters were observed on the 1.3 m telescope of Kitt Peak National Observatory and the 1.5 m telescope at Cerro Tololo Interamerican Observatory. As in Paper I, all measurements were made with the focal plane apertures centered on the optical nuclei and the visual centering was confirmed by maximizing the infrared signal. Sky chopping was always in the north-south direction with the "reference" beam typically 2 to 3 aperture diameters away from the "signal" beam. Most of the measurements were made on only one night. Repeatability of the standards, however, shows that the combined error from uncertainties in the calibration, statistical measurement error, and systematic errors arising from beam profile effects are on the order of 0.02 mag. A full discussion of the sources of error in the measurements of the CO index was given in Paper I, and applies equally well here.

III. THE STELLAR DATA

A grid of 17 standard stars was set up in a manner similar to that described in Paper I. The H_2O indices of these stars are referred to that of α Lyrae, which is defined equal to 0.00, and are given in the first part of Table 1. The internal accuracy of the grid is judged to be close to ± 0.01 mag. The second part of Table 1 lists values of the H_2O index for high luminosity stars, and can facilitate transfer between ours and other photometric systems. Similar observations of dwarf stars are presented by Persson, Aaronson and Frogel (1977). In the last part of

Table 1, CO and H_2O indices of a few Mira and carbon stars are listed. Although high resolution scans (Johnson and Mendez 1970; Frogel and Hyland 1972) show that carbon stars have very strong CO and no H_2O absorption, the extremely red continua of these stars causes our measured indices to indicate the opposite.

Table 1. H_2O Indices of Stars

Standards			Selected High Luminosity Stars			OTHER LATE-TYPE STARS			
HR	Spectral Type	H_2O Index	Name	Spectral Type	H_2O Index	Name	Spectral Type	H_2O Index	CO Index
0134	KO III	0.025	HR 3027	M2II-III	0.04	R Aur	Mira	0.29	0.45
0923	KO III	0.025	HR 4008	M0 III	0.05	U Ori	Mira	0.60	0.31
1552	B2 DI	0.00	HR 4336	M2 III	0.06	W Ori	C5,3	0.19	0.04
1698	K3 III	0.03	HR 4902	M3 III	0.08	T Cnc	C4,5	0.23	-0.06
3304	K5 III	0.035	BK Vir	M7 III	0.35				
3403	K2 III	0.035	RT Vir	M8 III	0.37				
3427	KO III	0.03	BC Cyg	M4 Ia	0.20				
4039	d F5	0.02	AZ Cyg	M2 Ia	0.18				
4550	G8 VI	0.02	KY Cyg	M4 Ia	0.21				
4608	GO III	0.02	+9° 3920	M2 III	0.06				
4689	A2 V	0.00	+29° 3730	M4 III	0.10				
6092	B5 IV	-0.01	+35° 4138	M3 III	0.06				
6136	K4 III	0.02	+59° 2541	M2.5 III	0.07				
6228	K5 III	0.04	+64° 1842	M2 II	0.10				
7001	AO V	0.00	+42° 1065	MO III	0.06				
8498	K3 II - III	0.03							
8551	KO III - IV	0.02							

HD 132950	K	0.035

Table 2 gives the adopted mean relationships between the H_2O index and color and spectral type for giant and dwarf stars. They are based on the data of Table 1 and on unpublished observations of more than 50 other stars. Values of *V* - *K* are from Paper I. It is apparent from Table 2 that for K and M dwarfs and giants, the H_2O index depends strongly on effective temperature. Furthermore, for stars with spectral types between MO and M6, it depends strongly on luminosity, but in the opposite sense to that of the CO index; viz., the H_2O index is stronger in dwarfs than in giants.

Table 2. Adopted Mean H_2O Indices

GIANTS			DWARFS		
Spectral Type	*V* - *K*	H_2O Index	Spectral Type	*V* - *K*	H_2O Index
G5	2.08	0.02	F8	1.25	0.02
G8	2.16	0.02	G5	1.50	0.02
KO	2.35	0.03	KO	1.75	0.03
K1	2.48	0.03	K1	2.00	0.03
K2	2.59	0.03	K2	2.25	0.03
K3	2.92	0.03	K3	2.50	0.04
K4	3.24	0.03	K5	2.75	0.04
K5	3.67	0.04	K6	3.00	0.05
MO	3.74	0.05	K7	3.25	0.06
Mi	3.90	0.05	MO	3.50	0.08
M2	4.16	0.06		3.75	0.11
M3	4.63	0.08	Ml	4.00	0.13
M4	5.34	0.10	M2	4.25	0.17
M5	6.20	0.12 ± 0.03	M3	4.50	0.19
M6	7.20	0.20 ± 0.05	M4	4.75	0.21
M7	-	0.36 ± 0.05	M5	5.00	0.22
				5.25	0.23
			M6	5.50	0.24
				5.75	0.25
				6.00	0.2G
			M7	6.25	0.27
				6.50	0.28

		6.75	0.30
	M8	7.00	0.31
		7.25	0.32
		7.50	0.34

Note: Owing to the small number of giant stars observed with spectral types M6 and later, we attach an uncertainty of ± 0.05 mag, to the mean H_2O indices. In addition, we find evidence for a substantial dispersion in the H_2O index at a given color for these late stars. The uncertainties arc approximately ± 0.02 mag elsewhere.

IV. DISCUSSION OF THE GALAXY AND GLOBULAR CLUSTER DATA

The observed values of the H_2O index for the galaxies and globular clusters are presented in Tables 3 and 4, respectively. Unless noted otherwise, the 1 terrors in the photometry are ± 0.02 mag. For the values of A_v appropriate to the objects in these tables, no reddening corrections need be applied to the H_2O indices. Unlike the *K*-correction for the CO index where the absorption feature is shifted out of the filter bandpass for $z > 0$, the center of the H_2O band is shifted into the filter bandpass for $z < 0.05$. An analytic redshift correction based on stellar observations could not be determined, as in Paper I, because the data requires significant extrapolation past the wavelength of atmospheric cutoff. An attempt to derive the *K*-correction empirically as was done in Paper I for the CO index is hampered by the more limited sample of galaxies and the apparently small size of the correction. Since the indicated result was $0 \leq K_{H_2O} < 1.3z$, and only 5 galaxies in Table 3 have redshifts $z > 0.01$ (the largest being $z = 0.022$), we have chosen to apply no redshift correction to the data.

Table 3. H_2O Indices in Early-Type Galaxies

Galaxy/Type	Telescope (inches)	Aperture Diameter (arc sec)	Log A/ D(0)	H_2O Index
(1)	(2)	(3)	(4)	(5)
NGC 1600	200	15	-0.69	0.14
E4				
NGC 1700	200	15	-0.75	0.125
E3				
NGC 2300	200	15	-0.68	0.135
E3	60	48	-0.18	0.11
NGC 2549	200	15	-0.88	0.115
$S0_1(7)$	60	48	-0.38	0.115

NGC 2634	200	15	-0.50	0.145
El:	60	48	+0.01	0.105 ± 0.04
NGC 2655	200	15	-1.14	0.11
SAB(s) 0	60	48	-0.63	0.105
NGC 2672	200	15	-0.65	0.135
E2				
NGC 2768	200	15	-0.98	0.115
E6	60	48	-0.48	0.115
NGC 2974	200	15	-0.75	0.135
E4				
NGC 3115	200	15	-1.04	0.13
E7/$S0_1$(7)	84	37.5	-0.64	0.13
	60	48	-0.54	0.135
	36	106.4	-0.19	0.145
NGC 3193	200	15	-0.78	0.10
E2				
NGC 3377	200	15	-0.90	0.10
E6				
NGC 3379	200	15	-0.96	0.11
E0	60	48	-0.46	0.1.05
NGC 3384	200	15	-1.01	0.10
$SB0_1$(5)				
NGC 3607	200	15	-0.83	0.115
$S0_3$(3)				
NGC 3608	200	15	-0.70	0.10
E1				
NGC 3998	200	15	-0.83	0.12
$S0_1$(3)				
NGC 4278	200	7.5	-1.17	0.16
E1	200	15	-0.87	0.145
	200	16.5	-0.82	0.105
	60	48	-0.36	0.09
NGC 4283	100	30	-0.23	0.07
E0				
NGC 4365	200	15	-1.09	0.125

E3				
NGC 4374	200	7.5	-1.28	0.12
E1 pec	200	15	-0.98	0.09
	60	48	-0.48	0.115
NGC 4382	200	15	-1.20	0.11
$S0_1(3)$				
NGC 4406	200	7.5	-1.37	0.095
E2	200	15	-1.07	0.115
	60	48	-0.57	0.135
NGC 4459	200	15	-0.81	0.12
$S0_3(3)$				
NGC 4472	200	7.5	-1.56	0.15
E2	200	15	-1.26	0.125
	200	16.5	-1.22	0.105
	60	48	-0.75	0.10
NGC 4478	200	15	-0.65	0.125
E2				
NGC 4486	200	7.5	-1.48	0.145
E0	200	15	-1.18	0.125
	60	48	-0.68	0.105
NGC 4486A	200	7.5	--	0.085
	200	15	--	0.075
NGC 4486B	200	7.5	-0.40	0.12
EO	200	15	-0.10	0.065
NGC 4494	100	30	-0.58	0.13 ± 0.04
E1				
NGC 4649	200	15	-1.10	0.12
E2/S0				
NGC 4889	200	15	-0.71	0.125
E4				
NGC 5813	200	15	-0.86	0.095
E1	100	30	-0.56	0.095
NGC 5846	100	30	-0.60	0.155
E1	60	48	-0.40	0.11
NGC 5866	100	30	-0.66	0.135

$S0_3(8)$				
NGC 5982	200	7.5	-0.95	0.095
E3	200	15	-0.65	0.125
	100	30	-0.35	0.135
NGC 6702	100	30	-0.18	0.075
E2				

NOTE. - The values of log A / $D(0)$ refer to the aperture size in units of the major diameter $D(0)$ (de Vaucouleurs and de Vaucouleurs 1964). The morphological types were made available to us by Dr. A. Sandage (1977 private communication). One σ_m errors in the H_2O indices are ± 0.02 mag unless noted otherwise.

Table 4. H_2O Indices in Globular Clusters

Cluster	Aperture Diameter (arcsec)	[Fe/H][1]	H_2O Index
M3	105.	-1.5	0.01
M13	105.	-1.6	0.035
M15	105.	-1.9	0.035
M69	66.4	> -0.4	0.07
M92	105.	-2.2	0.025

[1] For M3, M13, M15, and M92, [Fe/H] is from Hesser, Hartwick, and McClure (1976). For M69, [Fe/H] is an estimate based on the results of Hartwick and Sandage (1968).

In Figure l the data from Table 3 are plotted as a function of log A / $D(0)$. No obvious dependence of the H_2O index on radius is seen in this diagram. As was done for the CO data of Paper I, a least squares fit to the multiaperture data for each galaxy was made, and the resulting values for the individual slopes were averaged. The mean change in the H_2O index per unit change in log A / $D(0)$ is -0.04± 0.02 mag. Thus for our limited sample we find no significant dependence of the H_2O index on radius.

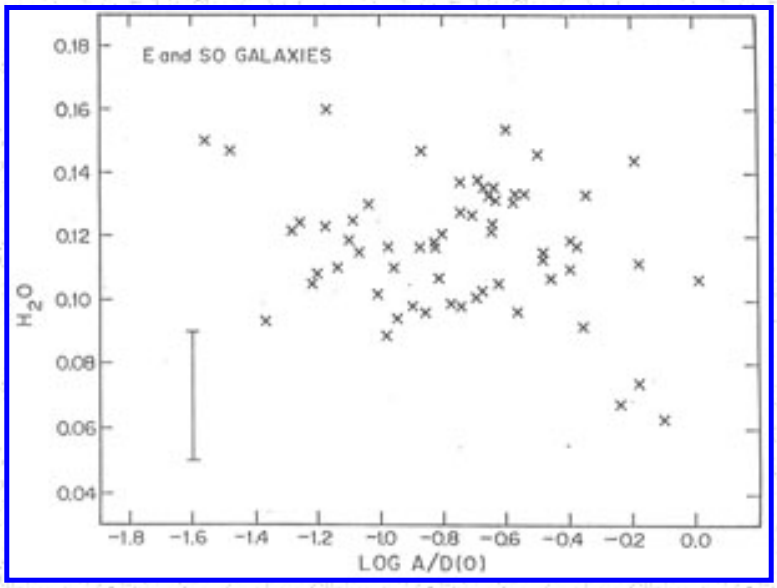

Figure 1. The H_2O indices from Table 3 are plotted as a function of log A / $D(0)$.

We have also searched for a dependence of the H_2O index on galaxian absolute magnitude. Table 5 presents a binning of the 15" aperture data into the same M_V bins as in Paper I. It is apparent that no significant dependence of H_2O index on M_V exists for $M_V < -19$. Although the ordering by M_V is also an ordering by increasing z, and no redshift correction has been applied, the largest allowable correction will not significantly affect this conclusion. This result differs from that of O'Connell (1976a), who found that a Ca II + TiO index, which also increases toward late spectral type for M giants, decreases with increasing galaxian luminosity for $M_V < -19$. Radial gradients in either index are not likely to affect this comparison since the aperture size used by O'Connell is close to ours. This difference remains if we restrict our sample to only those 10 galaxies observed in common with O'Connell. This and other absolute magnitude effects will be discussed further in Paper III (Persson, Frogel, and Aaronson 1977).

Table 5. Mean H_2O Indices for Galaxies with Well-Determined Distances

$M_{V_{1.0}}$ Limits	NO.	<z>	H_2O Index *
$M_V < -22.8$	3	0.0170	0.13 (± 0.01)
$-22.8 \leq M_V < -21.8$	9	0.0058	0.12 (± 0.02)
$-21.8 \leq M_V < -20.8$	8	0.0037	0.115 (± 0.01)
$-20.8 \leq M_V < -19.8$	8	0.0033	0.115 (± 0.02)

* Indices for an aperture diameter of 15" were averaged. The errors in parentheses are the dispersions.

Figure 2 displays the relationship between the H_2O data of Tables 3 and 4 and the corrected CO and broad-band color data from Paper I for the same or similar aperture size. Also shown are the mean relationships from Table 2. The relative location of the galaxies on the H_2O versus V-K, J-H, and H-K plots is determined by the fact that we are sampling the light of a composite stellar population. Thus, as was pointed out in Paper I, the V-K color is dominated by a hotter population of stars than is the H-K color. This accounts qualitatively for the relatively large displacement of the galaxy data from the mean relation for giants in the H_2O versus V-K plot. Now the data of Paper I showed that the 2.2 μm radiation from these galaxies is dominated by giant stars. Since the measured strength of the H_2O indices for these galaxies corresponds to that of an M5 III star, we conclude that late M giants must also make a significant contribution to the infrared light of early-type galaxies. O'Connell (1976a, b) came to a similar conclusion on the basis of his Ca II + TiO measurements.

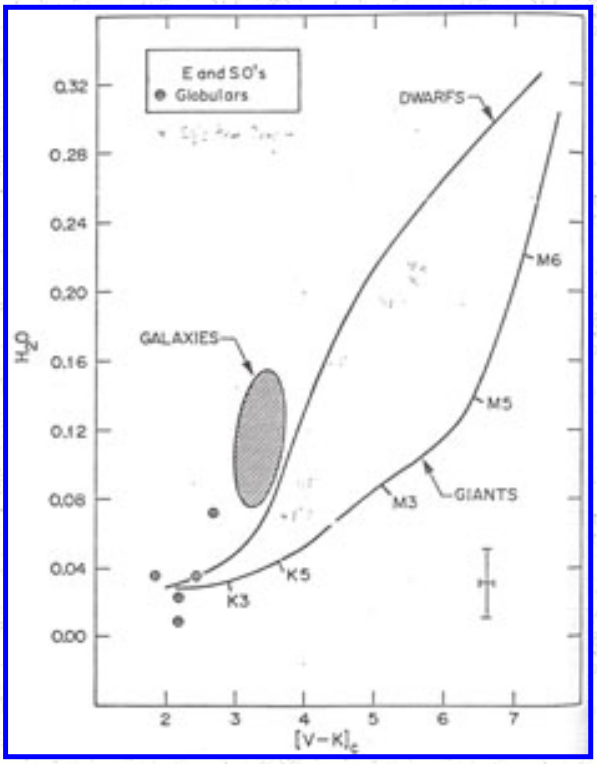

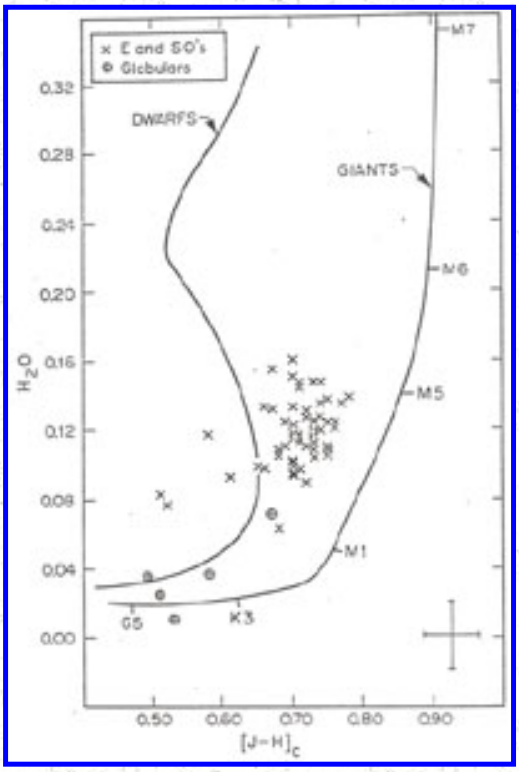
× E and SO's
● Globulars
DWARFS
GIANTS
M7
M6
M5
M1
G5
K3
0.32
0.28
0.24
0.20
0.16
0.12
0.08
0.04
0.00
H_2O
0.50
0.60
0.70
0.80
0.90
$[J-H]_C$

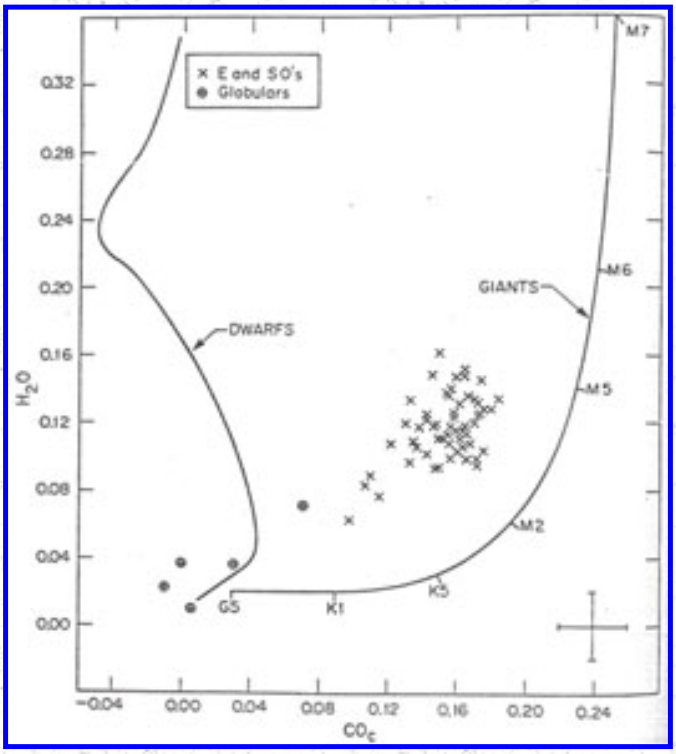
× E and SO's
● Globulars
DWARFS
GIANTS
M7
M6
M5
M2
G5
K1
K5
0.32
0.28
0.24
0.20
0.16
0.12
0.08
0.04
0.00
H_2O
-0.04
0.00
0.04
0.08
0.12
0.16
0.20
0.24
CO_C

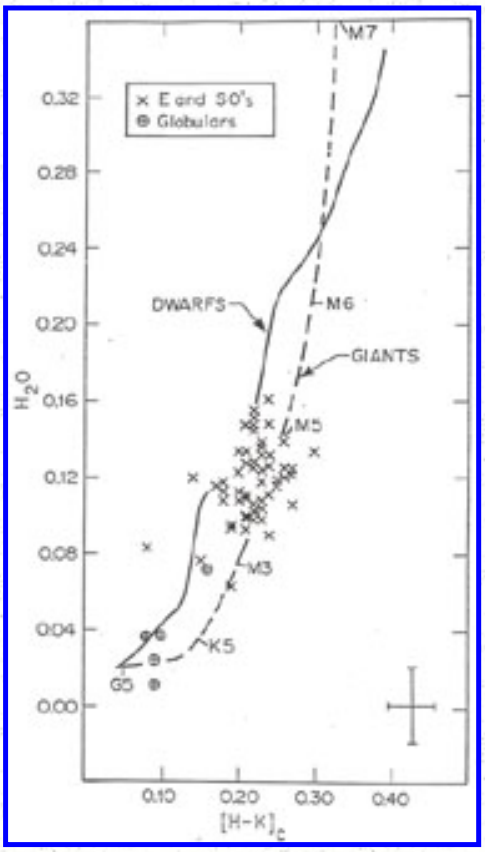

Figure 2. The H_2O indices from Tables 3 and 4 are plotted against the corrected CO indices and broad-band colors from Paper I. Mean relations shown for giant and dwarf stars are taken from Table 2 and from Paper I. The behavior of the mean relationships for dwarf stars is discussed by Persson et al. (1977), and the dependence of J-H on T_{eff} for dwarfs is discussed by Mould and Hyland (1976). The dependences of the H_2O index on colors for late-type stars (M5 and beyond) show large dispersion. Galaxy measurements from Table 3 are not plotted unless data at similar aperture sizes are available from Paper 1. In the H_2O versus V-K plot, all such points lie within the ellipsoid labelled "galaxies."

In order to put this result on a more quantitative basis we compare: the predictions of the models of Tinsley and Gunn (1976, TG, model A) and O'Connell (1976b, OC, model C) with the data of Table 3. This comparison is presented in Table 6, where the mean observed values are from Table 7 of Paper I and from of the present paper. The percentage contributions to the light at 2 μm coming from three stellar "bins" were computed for the two models and the results are listed in the table. As was concluded in Paper I, the relative importance of late M giants in the OC model compared to the TG model leads to better agreement with the observations. For the H_2O

index this occurs because the index increases rapidly in the latest giants.

Table 6. Comparison Between Models and Observations

Index	TG	OC	Observed
H_2O	0.08	0.12	0.12
CO	0.14	0.16	0.16
V - *K*	2.97	3.29	3.33
% Contribution to the 2.2 μm light from:			
M6 III bin	12%	37%	-
KO III to M5 III bins	68%	42%	-
All dwarfs and turnoff stars	20%	21%	-

Note: TG: Tinsley and Gunn (1976), model A; OC: O'Connell (1976b), model C.

Tinsley and Gunn (1976) have suggested that the inclusion of carbon stars could improve the fit of their model. Because of the single sideband nature of the H_2O and CO indices however, a strong temperature sensitive term is included, and the indices do not behave in carbon stars as they do in ordinary late-type giants (see Section III and Tables 1 and 2). Therefore, carbon stars alone cannot help, since the addition of any of these stars will drive the CO index, already too small in the TG model, to even lower values. Because of the large H_2O and CO absorption in Mira stars, it would appear that some contribution from these to the light at 2 μm could be present. However, we find that no combination of Mira and carbon stars added to the TG model produces as good a fit to the infrared data as does the OC model. Furthermore, the allowable contribution of these stars to the TG model cannot be greater than 15% to the light at 2 μm without producing disagreement with the data.

Finally, as was the case for the data of Paper I, we find no sharp discontinuity between the globular clusters and the galaxies in Figure 2; the globular with the strongest H_2O absorption is M69, the most metal-rich one observed. Detailed discussion of the colors and indices of globular clusters and of individual cluster stars will be presented elsewhere.

We thank our colleagues at Caltech and Harvard for their encouragement and for help in making the observations. We also thank an anonymous referee for valuable comments. This work was supported in part by NSF grant AST -74-18555A2 and NASA grant 05-002-207.

REFERENCES

1. Baldwin, J. R., Frogel, J. A., and Persson, S. E. 1973, Ap. J., 184, 427.

2. de Vaucouleurs, G., and de Vaucouleurs, A. 1964, Reference Catalogue of Bright Galaxies (RCBG) (Austin: University of Texas Press).
3. Frogel, J. A. 1971, Ph.D. thesis, California Institute of Technology.
4. Frogel, J. A., and Hyland, A. R. 1972, Proceedings of the Seventeenth International Astrophysical Symposium, Liège, p. 111.
5. Frogel, J. A., Persson, S. E., Aaronson, M., Becklin, E. E., and Matthews, K. 1975a, presented at the Tercentenary Symposium of the Royal Greenwich Observatory.
6. Frogel, J. A., Persson, S. E., Aaronson, M., Becklin, E. E., Matthews, K., and Neugebauer, G. 1975b , Ap. J. (Letters), 195, L15.
7. Frogel, J. A., Persson, S. E., Aaronson, M., and Matthews, K. 1977, submitted to Ap. J. (Paper I).
8. Hartwick, F. D. A., and Sandage, A. 1968, Ap. J., 153, 715.
9. Hesser, J. E., Hartwick, F. D. A., and McClure, R. D. 1976, preprint.
10. Johnson, H. L., and Mendez, M. E. 1970, A. J., 75, 785.
11. Mould, J. R., and Hyland, A. R. 1976, Ap. J., 208, 399.
12. O'Connell, R. W. 1974, Ap. J. (Letters), 193, L49.
13. O'Connell, R. W. 1976a, Ap. J. (Letters), 203, Ll.
14. O'Connell, R. W. 1976b, Ap. J., 206, 370.
15. Persson, S. E., Aaronson, M., and Frogel, J. A. 1977, A. J., (in press).
16. Persson, S. E., Frogel, J. A., and Aaronson, M. 1977, in preparation (Paper III).
17. Tinsley, B. M., and Gunn, J. E. 1976, Ap. J., 203, 52.
18. Whitford, A. E. 1977, Ap. J., 211, 527.

CHAPTER IV
Infrared observations of Bright Galaxies Along the Hubble Sequence

ABSTRACT

Multiaperture J (1.2 μm), H (1.6 μm), and K (2.2 μm) photometric observations are presented for the central regions of 91 galaxies distributed along the Hubble sequence, ranging in morphological type from early spiral to Magellanic irregular. In addition, multiaperture measurements of the luminosity-sensitive 2.3 μm CO absorption feature, and the temperature-sensitive 1.9 μm H_2O absorption feature, are presented for about half the sample.

The main results of this work are: 1) galaxies whose nuclear regions are dominated in the *optical* by a stellar population with mean spectral type ranging from near K to near F have similar stellar compositions in the infrared; and 2) this red stellar component is compatible only with synthesis models characterized by giant branches rich late M stars, flat main-sequence luminosity functions, values of $M / L_V < 10$.

The correlation of the data with parameters - including projected aperture magnitude, and inclination angle - is examined. The relation between U - V and V - K color is discussed and interpreted in terms of simple population and/or metallicity changes. Several non-stellar emission mechanisms are considered in regards to the small subset of galaxies found to have significant 2 μm excesses. Detailed comparison is made with recently published synthesis models of Turnrose and of Williams; the latter author's models are incompatible with the infrared data.

I. INTRODUCTION

Only recently have photometric observations of galaxies in the far red and infrared become available which are of sufficient quality to permit accurate construction of stellar synthesis models for these spectral regions (e.g., O'Connell 1974, 1976a, b; Frogel et al. 1975a, b, c, 1977, hereafter Paper I; Whitford 1977; Aaronson, Frogel, and Persson 1977, hereafter Paper II). However, most of these observations have concentrated on the simplest systems to understand, elliptical galaxies.

In this paper we present multiaperture observations at J (1.2 μm), H (1.6 μm), and K (2.2 μm) for a large number of galaxies distributed in morphological type along the Hubble sequence, from early spiral to Magellanic irregular. addition, we present observations of the 2.3 μm CO absorption band and the 1.9 μm H_2O absorption band, features which are sensitive measures of luminosity and temperature in late-type stars (Johnson and Mendez 1970; Frogel 1971; Baldwin, Frogel, and Persson 1973; Frogel et al. 1975b; Papers I and II). These data provide valuable constraints on both empirical and evolutionary,population models for composite systems with very different star formation histories.

The observational procedures and data reduction are described in Section II. Using U and V measurements obtained from the literature, the relationships between optical and infrared colors with projected aperture size, morphological type, inclination angle, and absolute magnitude are discussed in Section III. The interrelations among the various colors are also examined. In Section IV qualitative interpretation of the results is given in terms of simple population and metallicity effects. A variety of non-stellar emission mechanisms are considered in Section V in regards to the small subset of galaxies found to have significant 2 μm excesses, and the data is compared with several recently published stellar synthesis models in Section VI. Our results are summarized in Section VII. The system of standard magnitudes and colors are reviewed in Appendix A, a brief description of the InSb detector system used in this work is given in Appendix B, and the calibration of V - K color with mean metallicity is discussed in Appendix C.

II. Observations and Data Reduction

a) Equipment

All observations presented in this paper were made with an InSb detector system for which further details are given in Appendix B. The filters used are listed in Table 1, where the effective wavelengths and bandwidths shown were determined from filter scans provided by the manufacturer. The [2.36 μm] - [2.19 μm] color is used to measure the strength of the first overtone absorption bands of CO (bandhead at 2.29 μm). Similarly, the [2.01 μm] - [2.19 μm] color measures the strength of the H_2O absorption feature centered at 1.9 μm.

Table 1. Filters

Name	$\lambda_0(\mu)^*$	$\Delta\lambda(\mu)$

J	1.24	0.28
H	1.65	0.30
K	2.22	0.41
H_2O	2.01	0.07
Continuum	2.19	0.14
CO	2.36	0.08

* Referred to 77° K.

In the course of this work three silicon field lenses optimized for telescope focal ratios of 7.5, 9.6, and 13.5 were employed. An important feature of the InSb dewar was the existence of an external focus mechanism which allowed focusing of the very steep field optics (f / ~ 1 in the most extreme case) with the dewar cold directly at the telescope. A typical example of the relatively flat beam profiles obtained is shown in Figure 1. (Experience proved that a focus change of only ~ 0.01 inch could produce significant degradation of the profiles.)

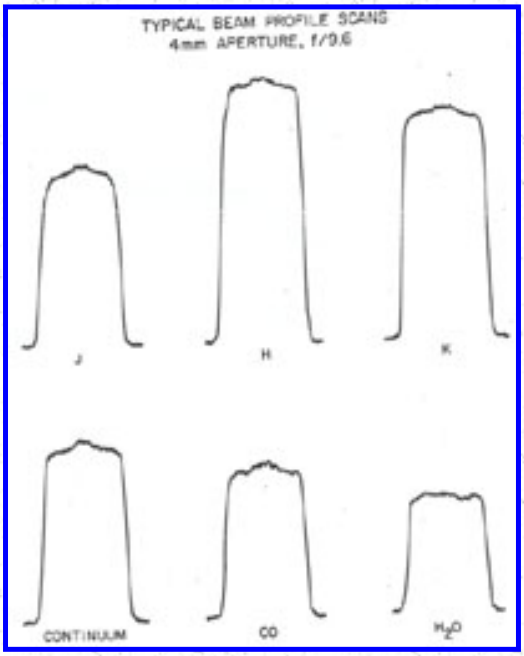

Figure 1. Typical beam profile scans of a star across the aperture are shown for the filters used in this study.

The beam size used was defined by an aperture wheel in the focal plane. The field lens, aperture wheel, filters, and detector were all cooled to pumped nitrogen temperatures (T ~ 60 K). The photometer employed had an offset guider and star-sky chopper consisting of a rotating sector wheel mirror near the focal plane. The telescopes, field lenses, chopper throws, and apertures used, along with the dates of the observations, are listed in Table 2. Chopping was always in the north-south direction. The physical aperture sizes employed were 4.0, 3.0, 2.0, 1.5, and 1.0 mm. However, due to spherical aberration of the plano-convex field lenses, the *effective* aperture sizes were typically 3-6% smaller. Only the effective aperture sizes, determined from the half power points of stellar scans (cf. Figure 1), are listed in Table 2.

Table 2. Observing Log

Telescope	Code	Field Lens	Scale ("/mm)	Dates	Throw* (mm)	Apertures (mm)
Kitt Peak 2.1-m	K84	f/7. 5	12.5	Nov. 75	6	3.8, 2.9
				Mar. 76	6.5	3.0, 1.5
				Nov. 76	6	2.9, 1.9
Mt. Hopkins 60-in	H60	f/9.6	13.7	Dec. 75	6	3.9, 3.0, 2.0, 1.0
				Apr. 76	6	3.9, 3.0, 2.0, 1.5
				Oct. 76	6	3.9, 3.0, 2.0
CTIO 1.5-m	C60	f/7.5	17.7	May 76	6	3.75, 1.9
Las Campanas 40-in	L40	f/0.5	14.3	Feb. 76	9.3	3.9, 2.0
Kitt Peak 0.9-m	K36	f/7.5	28.0	Nov. 75	6	3.9
				Apr. 76	6	3.75
				Oct. 76	6	3.75, 2.9, 1.9

* All chopper throws are in N-S direction.

b) Galaxy Selection

The galaxies observed in this study were selected so as to fulfill one or more of the following criteria: 1) They were bright and could thus be observed in a reasonable amount of integration time - the sensitivity of the InSb detector being such that an object of 9th magnitude at K observed with a 60 inch telescope required typically one hour of integration time to achieve a statistical accuracy of ~ 0.02 mag with the CO filter. 2) They would span a range of morphological type extending from early spiral through Magellanic irregular. 3) They would include objects for which broad band UBV photometry, and/or narrow band optical line indices, and/or detailed synthesis models were available from the literature.

The galaxies selected are listed in column 1 of Table 3. The morphological types, on the modified Hubble system of de Vaucouleurs, are also listed in column l, and were obtained from the *Second Reference Catalogue of Bright Galaxies* (de Vaucouleurs, de Vaucouleurs, and Corwin 1976, hereafter RC2), with but two exceptions: The type for NGC 7316 (not classified in the RC2) is adopted from Huchra (1977a), and the type for NGC 5253 is taken from the original *Reference Catalogue of Bright Galaxies* (de Vaucouleurs and de Vaucouleurs 1964, hereafter RC1), where the galaxy is classified as Im, rather than from the *RC2*, where it is classified as I0. The former classification is considerably more consistent with this galaxy's broad-band colors.

Table 3. Infrared Photometry of Galaxies

Galaxy	b^{II}	Tel.	Aper.	Log	Observed					Corrected for Reddening and Redshift					
type	z	(inches)	(")	A/D_0	K	(J-H)	(H-K)	CO	H_2O	K_c	$(J-H)_c$	$(H-K)_c$	CO_c	H_2O_c	Notes
(1)	(2)	(3)	(4)	(5)	(6)	(7)	(8)	(9)	(10)	(11)	(12)	(13)	(14)	(15)	(16)
NGC 151	-72°	H60	27.4	-0.84	9.81	0.74	0.25	-	-	9.85	0.73	0.21	-	-	
SB(r)bc	0.0122	H60	53.4	-0.55	9.215	0.76	0.215	-	-	9.255	0.755	0.17	-	-	
NGC 157	-71	K36	105	-0.35	8.02	0.71	0.25	-	-	8.04	0.71	0.23	-	-	
SAB(rs)bc	0.0055														
NGC 224	-22	H60	13.7	-2.79	6.95:	0.78	0.24	-	-	6.93:	0.76	0.23	-	-	*
SA(s)b	-0.0010	H60	27.4	-2.49	5.81	0.76	0.23	0.175	0.11	5.79	0.74	0.22	0.17	0.11	
		K84	47.5	-2.25	4.825:	0.79	0.23	0.155	-	4.805:	0.77	0.22	0.15	-	
		H60, K36	53.3	-2.20	4.71	0.77	0.22	0.165	0.11	4.69	0.75	0.21	0.16	0.11	
		K36	107.1	-1.90	3.72	0.78	0.22	0.155	0.11	3.70	0.76	0.21	0.15	0.11	
NGC 253	-88	K36	105	-1.03	5.455	0.94	0.41	0.135	0.165	5.46	0.94	0.41	0.14	0.165	
SAB(s)c	0.0008														
NGC 278	-15	K84	36.3	-0.56	8.75	0.74	0.19	0.10	-	8.73	0.71	0.17	0.115	-	
SAB(rs)b	0.0021	K36	105	-0.10	7.945	0.72	0.27	-	-	7.93	0.69	0.25		-	
NGC 520	-58	K36	105	-0.35	8.575	0.81	0.260	-	-	8.55	0.81	0.23	-	-	*
P	0.0074														
NGC 598	-31	K36	109.2	-1.48	7.71:	0.64	0.21	0.12:	-	7.70:	0.635	0.20	0.12:	-	*
SA(s)cd	-0.0006														

NGC 628	-46	H60	27.4	-1.35	9.81	0.675	0.22	-	-	9.81	0.67	0.21	-	-	
SA(s)c	0.0022	H60	53.4	-1.06	8.97	0.72	0.22	-	-	8.98	0.71	0.21	-	-	
		K36	105	-0.77	8.15	0.73	0.18	-	-	8.155	0.73	0.17	-	-	
NGC 772	-41	H60	27.4	-1.14	9.31	0.745	0.24	-	-	9.33	0.74	0.21	-	-	
SA(s)b	0.0081	H60	53.4	-0.85	8.49	0.75	0.28	-	-	8.51	0.74	0.24	-	-	
		K36	105	-0.56	7.95	0.74	0.21	-	-	7.97	0.73	0.18	-	-	
NGC 891	-17	H60	27.4	-1.31	8.53	1.175	0.59	-	-	8.51	1.15	0.57	-	-	
SA(s)b?sp	0.0017	H60	53.4	-1.02	7.68	1.13	0.55	0.065	0.145	7.67	1.10	0.53	0.075	0.145	
		K36	105	-0.73	6.98	0.99	0.43	0.055	0.145	6.96	0.97	0.41	0.065	0.14	
NGC 936	-55	K36	105	-0.46	7.43	0.73	0.22	-	-	7.45	0.73	0.20	-	-	
SB(rs)0+	0.0045														
NGC 1068	-52	H60	27.4	-1.16	6.80	0.805	0.53	-0.02	0.26	6.815	0.80	0.52	-0.005	0.26	*
(R)SA(rs)b	0.0036	H60	53.4	-0.87	6.34	0.82	0.46	0.03	0.215	6.35	0.82	0.44	0.05	0.215	
		K36	105	-0.58	6.05	0.76	0.40	0.035	0.175	6.06	0.76	0.39	0.055	0.175	
NGC 1084	-57°	H60	27.4	-0.74	9.34	0.75	0.26	-	-	9.35	0.745	0.24	-	-	
SA(s)c	0.0049	B60	41.1	-0.56	8.79	0.73	0.25	0.075	0.105	8.81	0.73	0.23	0.10	0.105	
		K36	105	-0.16	8.04	0.69	0.27	0.135:	0.07:	8.05	0.69	0.25	0.155:	0.07:	
NGC 1232	-58	H60	27.4	-1.22	10.32	0.73	0.17	-	-	10.34	0.73	0.15	-	-	
SAB(rs)c	0.0057	H60	53.4	-0.93	9.35	0.71	0.22	-	-	9.37	0.70	0.195	-	-	
		K36	105	-0.64	8.405	0.70	0.15	-	-	8.425	0.70	0.13	-	-	

NGC 1300	-55	H60	27.4	-1.11	9.775	0.755	0.22	-	-	9.79	0.75	0.20	-	-	
SB(rs)bc	0.0050	H60	53.4	-0.82	9.26	0.71	0.22	-	-	9.28	0.705	0.20	-	-	
		K36	105	-0.53	8.68	0.67	0.22	-	-	8.70	0.67	0.20	-	-	
NGC 1365	-55	L40	28.6	-1.25	7.99	0.88	0.46	-	-	8.01	0.88	0.44	-	-	
SB(s)b	0.0057	L40	55.8	-0.96	7.58	0.805	0.36	0.04	-	7.60	0.80	0.36	0.07	-	
NGC 1398	-53	L40	28.6	-1.12	8.125	0.74	0.17	-	-	8.14	0.74	0.15	-	-	
(R')SB(r)ab	0.0047	L40	55.8	-0.83	7.57	0.70	0.18	0.125	-	7.59	0.695	0.165	0.145	-	
		K36	105	-0.56	7.105	0.72	0.22	0.15	0.105	7.12	0.72	0.20	0.17	0.105	
NGC 1566	-43	L40	28.6	-1.18	8.675	0.74	0.22	-	-	8.69	0.74	0.20	-	-	*
SAB(s)bc	0.0046	L40	55.8	-0.89	8.06	0.74:	0.22	0.115	-	8.07	0.73:	0.20	0.135	-	
NGC 1617	-42	L40	28.6	-0.92	6.67	0.72	0.23	-	-	8.68	0.72	0.22	-	-	
SB(s)a	0.0033	L40	55.8	-0.63	8.10	0.73	0.19	-	-	8.105	0.72	0.17	-	-	
NGC 1637	-30	H60	27.4	-0.85	9.94	0.76	0.24	-	-	9.94	0.745	0.23	-	-	
SAB(rs)c	0.0022	H60	53.4	-0.56	9.29	0.74	0.26	-	-	9.29	0.73	0.24	-	-	
		K36	105	-0.27	8.66	0.78	0.19	-	-	8.66	0.77	0.18	-	-	
NGC 1961	20	H60	27.4	-0.94	9.345	0.86	0.29	-	-	9.37	0.83	0.23	-	-	
SAB(rs)c	0.0129	H60	53.4	-0.65	8.61	0.83	0.34	-	-	8.63	0.80	0.28	-	-	
		K36	105	-0.36	8.09	0.81	0.33	-	-	8.115	0.79	0.27	-	-	
NGC 1964	-27	H60	27.4	-1.04	8.44	0.75	0.28	-	-	8.45	0.73	0.25	-	-	
SAB(s)b	0.0056	H60	53.4	-0.75	8.12	0.78	0.23	0.11	0.10	8.13	0.765	0.20	0.14	0.095	

		K36	105	-0.46	7.86	0.71	0.26	-	-	7.865	0.70	0.23	-	-
NGC 2146	25	H60	27.4	-1.07	8.02	1.08	0.55	-	-	8.01	1.06	0.53	-	-
SB(s) abP	0.0027	H60	41.1	-0.89	7.70	1.02	0.50	0.085	0.195	7.69	1.00	0.48	0.10	0.195
		K36	105	-0.49	7.24	0.91	0.42	0.095	0.15	7.24	0.89	0.41	0.11	0.15
NGC 2217	-18	L40	28.6	-0.99	8.46	0.82:	0.18:	-	-	8.46	0.80:	0.15:	-	-
(R)SB (rs)0$^+$	0.0049	L40	55.8	-0.70	8.03	0.72:	0.235	-	-	8.025	0.695:	0.20	-	-
NGC 2339	12	H60	27.4	-0.76	9.53	0.86	0.34	-	-	9.53	0.81	0.29	-	-
SAB (rs)bc	0.0079	H60	53.4	-0.47	8.90	0.82	0.295	-	-	8.89	0.78	0.25	-	-
		K36	105	-0.18	8.545	0.71	0.32	-	-	8.54	0.67	0.27	-	-
NGC 2403	29°	K36	105	-0.96	7.73	0.70	0.12	-	-	7.72	0.69	0.11	-	-
SAB (s)cd	0.0005													
NGC 2681	40	K84	36.9	-0.78	8.27	0.73	0.22	0.15	0.135	8.27	0.72	0.21	0.165	0.135
(R) SAB (rs)0/a	0.0024	K84	47.5	-0.67	8.14	0.745	0.20	0.155	-	8.145	0.74	0.19	0.165	-
		K36	109.2	-0.31	7.77	0.70	0.21	0.145	-	7.78	0.69	0.20	0.16	-
NGC 2683	39	K84	36.9	-1.05	7.93	0.80	0.23	0.13	0.115	7.93	0.79	0.22	0.14	0.115
SA(rs) b	0.0011	K36	107.1	-0.59	6.85	0.81	0.25	0.125	0.135	6.85	0.805	0.24	0.13	0.135
NGC 2775	34	H60	20.6	-1.09	8.91	0.69	0.22	-	-	8.915	0.68	0.21	-	-
SA(r) ab	0.0038	H60	41.1	-0.79	8.24	0.72	0.22	0.12	0.14	8.25	0.71	0.20	0.135	0.14
		K36	105	-0.39	7.35	0.74	0.24	0.165:	0.125	7.36	0.73	0.22	0.185:	0.125

NGC 2841	44	K84	36.9	-1.04	7.76	0.74	0.19	0.145	0.11	7.77	0.73	0.18	0.155	0.11	*
SA(r)b:	0.0021	K36	109.2	-0.57	6.83	0.72	0.22	0.125	0.13	6.83	0.71	0.21	0.135	0.13	
NGC 2903	45	K84	36.9	-1.24	8.07:	0.76	0.26	0.155	0.13	8.075:	0.75	0.25	0.165	0.13	*
SAB(rs)bc	0.0021	K84	47.5	-1.13	7.77:	0.79	0.27	0.155	-	7.77:	0.79	0.26	0.165	-	
		K36	109.2	-0.77	6.89	0.74	0.26	0.15	0.105	6.89	0.73	0.25	0.16	0.105	
NGC 2976	41	H60	41.1	-0.79	10.03:	0.72	0.14	-	-	10.03:	0.72	0.14	-	-	*
SAcP	0.0001	K36	105	-0.39	8.31	0.71	0.14	-	-	8.30	0.71	0.14	-	-	
NGC 2997	17	C60	33.6	-1.14	8.955	0.79	0.28	-	-	8.945	0.76	0.255	-	-	
SAB(rs)c	0.0036	C60	66.4	-0.85	8.45	0.72	0.25	-	-	8.44	0.69	0.22	-	-	
NGC 3031	41	H60	20.6	-1.81	6.82	0.73	0.245	0.15	0.115	6.82	0.72	0.24	0.15	0.115	
SA(s)ab	-0.0001	K84	36.3	-1.57	6.21	0.73	0.21	0.15	-	6.20	0.72	0.21	0.15	-	
		H60	41.1	-1.51	6.11	0.73	0.23	0.15	0.11	6.10	0.73	0.23	0.15	0.11	
		K36	107.1	-1.10	5.22	0.76	0.21	0.155	0.135	5.21	0.75	0.21	0.155	0.135	
NGC 3034	41	H60	20.6	-1.42	6.39	1.14	0.635	0.14	0.255	6.39	1.13	0.63	0.145	0.255	*
I0 sp	0.0006	H60	41.1	-1.12	5.74	1.08	0.59	0.12	0.22	5.74	1.07	0.59	0.125	0.22	
		K36	105	-0.72	5.08	0.96	0.45	0.13	0.195	5.07	0.96	0.44	0.135	0.195	
NGC 3077	42	H60	41.1	-0.80	9.00	0.68	0.22	-	-	9.00	0.67	0.22	-	-	
I0 P	0.0000														
NGC 3079	48	H60	41.1	-0.88	8.28	1.01	0.49	-	-	8.29	1.00	0.475	-	-	

SB(s) csp	0.0039														
NGC 3245	58	K84	37.5	-0.66	8.50	0.73	0.24	0.13	0.12	8.51	0.73	0.22	0.15	0.12	
SA(r) 0:	0.0042														
NGC 3351	58	H60	20.6	-1.30	8.71	0.75	0.275	-	-	8.72	0.75	0.27	-	-	
SB(r)b	0.0026	K84	37.5	-1.04	8.21	0.75	0.24	0.135	0.13	8.22	0.75	0.235	0.15	0.13	
		H60	41.1	-1.00	8.135	0.76	0.25	0.125	0.125	8.14	0.755	0.24	0.135	0.125	
NGC 3368	57°	K84	37.5	-1.01	7.54	0.75	0.24	0.14	0.115	7.55	0.75	0.23	0.155	0.115	
SAB (rs)ab	0.0031	K36	105	-0.57	6.75	0.76	0.24	0.12	0.145:	6.76	0.755	0.23	0.135	0.145:	
NGC 3521	53	K84	18.8	-1.41	8.11	0.73	0.235	0.145	0.12	8.12	0.73	0.23	0.155	0.12	
SAB (rs)bc	0.0026	H60	20.6	-1.37	8.04	0.73	0.225	-	-	8.045	0.73	0.23	-	-	
		K84	37.5	-1.11	7.47	0.75	0.23	0.135	0.12	7.48	0.745	0.225	0.145	0.12	
		H60	41.1	-1.07	7.38	0.76	0.25	0.11	0.12	7.39	0.76	0.24	0.125	0.12	
		K36	105	-0.67	6.47	0.81	0.26	0.145	0.13	6.475	0.81	0.25	0.16	0.13	
NGC 3556	56	H60	41.1	-0.96	9.07	0.71	0.24	-	-	9.08	0.71	0.23	-	-	*
SB(s) cd sp	0.0023														
NGC 3621	26	C60	33.6	-1.20	9.33	0.725	0.26	-	-	9.32	0.71	0.25	-	-	
SA(s)d	0.0024	C60	66.4	-0.91	8.29	0.745	0.24	-	-	8.285	0.73	0.22	-	-	
NGC 3623	64	K84	37.5	-1.09	7.87	0.72	0.20	0.14	0.10	7.88	0.72	0.19	0.15	0.10	
SAB (rs)a	0.0025														
NGC 3627	64	K84	18.8	-1.37	8.30	0.75	0.265	0.16	0.135	8.31	0.75	0.26	0.17	0.135	

SAB (s)b	0.0024	K84	37.5	-1.07	7.67	0.73	0.24	0.14	0.13	7.68	0.725	0.24	0.15	0.13	
NGC 3628	65	C60	33.6	-1.28	8.31	1.04	0.45	-	-	8.32	1.035	0.44	-	-	
Sb Psp	0.0028	C60	66.4	-0.99	7.555	1.025	0.38	0.095	0.17	7.56	1.02	0.37	0.11	0.17	
NGC 4214	78	H60	41.1	-1.04	10.18	0.57	0.17	-	-	10.18	0.57	0.17	-	-	
IAB(s)m	0.0010														
NGC 4258	69	H60	20.6	-1.64	8.58	0.72	0.265	-	-	8.58	0.715	0.26	-	-	*
SAB (s)bc	0.0015	H60	41.1	-1.34	7.77:	0.72	0.23	0.11	0.125	7.78:	0.72	0.235	0.12	0.125	
NGC 4303	66	C60	33.6	-1.02	8.71	0.69	0.24	-	-	8.73	0.68	0.22	-	-	
SAB (rs)bc	0.0056	C60	66.4	-0.73	8.09	0.69	0.27	-	-	8.11	0.68	0.25	-	-	
NGC 4321	77	K84	37.5	-1.03	8.71	0.71	0.26	0.175	0.12	8.73	0.70	0.245	0.20	0.12	
SAB (s)bc	0.0054														
NGC 4425	75	C60	33.6	-0.67	9.78	0.74	0.17	-	-	9.80	0.735	0.15	-	-	
SB0: sp	0.0063	C60	66.4	-0.38	9.26	0.78:	0.26	-	-	9.28	0.78:	0.23	-	-	
NGC 4429	73	L40	28.6	-0.98	8.33	0.69:	0.27	-	-	8.34	0.69:	0.26	-	-	
SA(r)0+	0.0037	L40	55.8	-0.69	7.73	0.80:	0.25	-	-	7.74	0.80:	0.23	-	-	
NGC 4449	72	H60	20.6	-1.14	10.19	0.64	0.235	-	-	10.19	0.64	0.24	-	-	*
IBm	0.0007	H60	41.1	-0.84	9.24	0.64	0.21	0.10	0.115	9.24	0.64	0.20	0.105	0.115	
NGC 4477	76	L40	28.6	-0.91	8.61	0.71	0.155	-	-	8.62	0.71	0.14	-	-	
SB(s)0:	0.0042	L40	55.8	-0.62	8.07	0.74	0.175	-	-	8.09	0.74	0.16	-	-	

NGC 4490	75°	H60	20.6	-1.17	10.39	0.65	0.12	-	-	10.39	0.65	0.12	-	-	
SB(s)d P	0.0019	H60	41.1	-0.87	9.185	0.64	0.22	0.07	0.075	9.19	0.64	0.21	0.08	0.075	
NGC 4501	77	H60	20.6	-1.24	8.74	0.75	0.25	-	-	8.76	0.74	0.23	-	-	
SA(rs)b	0.0071	H60	41.1	-0.94	7.96	0.76	0.25	0.14	0.13	7.98	0.75	0.23	0.175	0.13	
NGC 4526	70	L40	28.6	-1.06	7.79	0.78	0.25	-	-	7.80	0.78	0.25	-	-	
SAB(s)O:	0.0016	L40	55.8	-0.77	7.25	0.77	0.245	-	-	7.25	0.77	0.24	-	-	
NGC 4565	86	K84	37.5	-1.23	7.64	0.825	0.29	0.115	0.11	7.65	0.82	0.28	0.13	0.11	
SA(s)b: sp	0.0039	K36	105	-0.79	6.70	0.86	0.27	0.125	0.125	6.72	0.855	0.25	0.145	0.125	
NGC 4569	76	C60	33.6	-1.15	8.45	0.77	0.24	-	-	8.45	0.77	0.25	-	-	*
SAB(rs)ab	-0.0010	C60	66.4	-0.86	7.90	0.75	0.29	-	-	7.90	0.75	0.29	-	-	
NGC 4579	74	H60	20.6	-1.17	8.58	0.72	0.25	-	-	8.60	0.715	0.23	-	-	
SAB(rs)b	0.0058	K84	37.5	-0.91	8.025	0.73	0.21	0.12	0.13	8.04	0.725	0.19	0.145	0.13	
		H60	41.1	-0.87	7.95	0.72	0.24	0.12	0.10	7.97	0.71	0.22	0.15	0.105	
		K36	105	-0.47	7.17	0.75	0.23	0.145	0.155:	7.19	0.74	0.21	0.175	0.155:	
NGC 4594	51	K84	18.8	-1.37	7.36	0.75	0.205	0.165	0.10	7.38	0.75	0.19	0.185	0.10	
RA(s)a sp	0.0039	K84	37.5	-1.07	6.66	0.75	0.21	0.15	0.015	6.675	0.75	0.20	0.17	0.105	
		K36	105	-0.63	5.71	0.79	0.23	0.15	0.135	5.72	0.785	0.21	0.165	0.135	
NGC 4631	84	H60	20.6	-1.48	9.50	1.03	0.52	-	-	9.51	1.03	0.51	-	-	*
SB(s)d sp	0.0021	H60	41.1	-1.18	8.44	0.96	0.42	0.08	0.165	8.45	0.96	0.41	0.09	0.165	

NGC 4643	65	H60	20.6	-0.96	8.71	0.70	0.23	-	-	8.73	0.70	0.22	-	-
SB(rs)0/a	0.0048	K84	37.5	-0.70	8.19	0.71	0.195	0.13	0.10	8.205	0.71	0.18	0.155	0.10
		H60	41.1	-0.66	8.10	0.71	0.23	0.17	0.105	8.12	0.705	0.215	0.19	0.105
NGC 4699	54	L40	28.6	-0.85	7.565	0.72	0.22	-	-	7.58	0.72	0.21	-	-
SAB(rs)b	0.0050	C60	33.6	-0.78	7.46	0.70	0.20	-	-	7.47	0.69	0.18	-	-
		L40	55.8	-0.56	7.06	0.70	0.24	-	-	7.07	0.70	0.22	-	-
		C60	66.4	-0.49	6.98	0.70	0.21	0.145	0.125	7.00	0.695	0.19	0.17	0.125
NGC 4725	88	H60	20.6	-1.47	8.67	0.66	0.26	-	-	8.68	0.655	0.25	-	-
SAB(r)ab P	0.0037	K84	37.5	-1.21	8.18	0.695	0.21	0.12	0.07	6.19	0.69	0.20	0.14	0.07
		H60	41.1	-1.17	8.12	0.70	0.23	0.155	0.105	8.135	0.69	0.22	0.175	0.105
NGC 4736	76	K84	18.8	-1.52	6.91	0.72	0.215	0.18	0.105	6.91	0.72	0.21	0.185	0.105
(R)SA(r)ab	0.0010	K84	37.5	-1.22	6.22	0.71	0.22	0.17	0.115	6.225	0.705	0.22	0.175	0.115
		K36	105	-0.78	5.69	0.72	0.21	0.15	0.115	5.59	0.72	0.21	0.155	0.115
NGC 4753	62	C60	33.6	-0.92	7.955	0.77	0.26	-	-	7.97	0.77	0.245	-	-
10	0.0042	C60	66.4	-0.63	7.44	0.77	0.26	0.125	0.165	7.46	0.77	0.24	0.145	0.165
NGC 4826	84°	H60	27.4	-1.26	7.395	0.80	0.31	0.135	0.145	7.40	0.80	0.31	0.14	0.145
(R)SA(rs)ab	0.0012	H60	53.4	-0.97	6.79	0.82	0.28	0.14	0.14	6.79	0.82	0.28	0.145	0.14
NGC 5005	79	H60	20.6	-1.12	8.09	0.78	0.335	-	-	8.10	0.78	0.32	-	-
SAB(rs)bc	0.0034	K84	37.5	-0.86	7.58	0.77	0.285	0.14	0.14	7.59	0.77	0.27	0.16	0.14
		H60	41.1	-0.82	7.50	0.79	0.30	0.125	0.13	7.515	0.79	0.29	0.14	0.13

		K36	105	-0.42	6.83	0.78	0.25	0.11	0.12	6.84	0.775	0.235	0.125	0.12	
NGC 5055	74	K84	37.5	-1.24	7.69	0.76	0.25	0.14	0.10	7.70	0.76	0.25	0.15	0.10	
SA(rs)bc	0.0017	K36	105	-0.80	6.55	0.80	0.24	0.125	0.125	6.56	0.80	0.23	0.135	0.125	
NGC 5128	19	L40	14.3	-1.63	7.45	1.23	0.61	-	-	7.44	1.21	0.59	-	-	*
S0P	0.0016	L40	28.6	-1.33	6.62	1.15	0.52	0.065	0.18	6.61	1.13	0.50	0.075	0.175	
		L40	55.8	-1.04	5.84	1.11	0.47	0.075	-	5.825	1.09	0.45	0.09	-	
NGC 5194	69	K84	37.5	-1.20	7.81	0.71	0.24	0.16	0.11	7.81	0.71	0.23	0.17	0.11	
SA(s)bc P	0.0015	K36	105	-0.76	6.875	0.77	0.24	0.19	0.155	6.88	0.77	0.23	0.195	0.125	
NGC 5195	68	K84	37.5	-0.90	7.53	0.74	0.27	0.14	0.125	7.53	0.74	0.26	0.145	0.125	
I0 P	0.0018	K36	105	-0.46	6.75	0.81	0.24	0.12	0.11	6.75	0.81	0.23	0.125	0.11	
NGC 5236	32	L40	28.6	-1.36	7.365	0.78	0.30	-	-	7.36	0.77	0.29	-	-	
SAB(s)c	0.0017	C60	33.6	-1.29	7.21	0.72:	0.29	0.15	0.155	7.21	0.71:	0.28	0.16	0.155	
		L40	55.8	-1.07	6.85	0.76	0.28	0.115	-	6.85	0.75	0.27	0.125	-	
		C60	66.4	-1.00	6.72	0.725:	0.30	0.15	0.135	6.72	0.715:	0.29	0.16	0.135	
NGC 5253	30	C60	33.6	-0.76	9.52	0.54	0.34	-	-	9.51	0.53	0.33	-	-	*
IBm P	0.0013	L40	55.8	-0.54	9.04	0.60	0.33	-	-	9.03	0.59	0.32	-	-	
		C60	66.4	-0.37	8.96	0.61	0.26	-	-	8.96	0.60	0.25	-	-	
NGC 5457	60	K36	105	-1.19	7.92:	0.78	0.19	-	-	7.92:	0.78	0.185	-	-	*
SAB(rs)cd	0.0009														
NGC 5746	53	C60	33.6	-0.99	8.25	0.80	0.30	-	-	8.27	0.79	0.28	-	-	*

SAB (rs)b? sp	0.0061	C60	66.4	-0.70	7.71:	0.81	0.28	-	-	7.73:	0.80	0.25	-	-	
NGC 5907	51	H60	53.4	-0.94	8.13	0.925	0.39	0.09	0.155	8.14	0.92	0.39	0.10	0.155	
SA(s) c: sp	0.0018														
NGC 6015	44	H60	53.4	-0.70	9.46	0.675	0.19	-	-	9.56	0.67	0.18	-	-	
SA(s) cd	0.0028	K36	105	-0.41	8.86:	0.73:	0.15:	-	-	8.86:	0.73:	0.14:	-	-	
NGC 6384	21	H60	27.4	-1.09	9.57	0.68	0.21	-	-	9.58	0.66	0.18	-	-	
SAB (r)bc	0.0058	H60	53.4	-0.80	8.91	0.70	0.21	-	-	8.91	0.68	0.18	-	-	
		K36	105	-0.51	8.245	0.77	0.25	-	-	8.25	0.75	0.22	-	-	
NGC 6503	31°	K84	37.5	-0.89	8.87	0.72	0.20	0.145:	0.105	8.86	0.71	0.195	0.145:	0.105	
SA(s) cd	0.0001	K36	53.2	-0.74	8.43	0.75	0.18	-	-	8.42	0.74	0.18	-	-	
		K36	105	-0.45	7.72	0.74	0.18	0.13:	0.11	7.71	0.73	0.17	0.13	0.11	
NGC 6643	28	H60	53.4	-0.58	8.985	0.795	0.25	-	-	8.99	0.78	0.23	-	-	
SA(rs) c	0.0051	K36	105	-0.29	8.28	0.71	0.34	-	-	8.29	0.70	0.32	-	-	
NGC 6744	-26	C60	66.4	-1.11	8.31	0.69:	0.17	-	-	8.30	0.68:	0.15	-		
SAB (r)bc	0.0022														
NGC 6814	-16	H60	27.4	-0.84	9.39	0.82	0.31	-	-	9.39	0.79	0.28	-	-	*
SAB (rs)bc	0.0048	H60	53.4	-0.55	8.62	0.78	0.285	-	-	8.61	0.75	0.25	-	-	
		K36	105	-0.26	7.985	0.75	0.33	-	-	7.98	0.73	0.30	-	-	
NGC 6946	12	H60	27.4	-1.37	8.615	0.96	0.39	-	-	8.58	0.92	0.37	-	-	*

SAB (rs)cd	0.0003	H60	41.1	-1.19	8.29	0.94	0.37	0.125	0.15	8.26	0.90	0.35	0.13	0.145	
		K36	105	-0.79	7.215:	0.96	0.34	0.175	0.135	7.18:	0.92	0.315	0.18	0.13	
NGC 7177	-29	H60	27.4	-0.82	8.95	0.75	0.23	-	-	8.95	0.73	0.21	-	-	
SAB (r)b	0.0037	H60	53.4	-0.53	8.50	0.75	0.265	0.11	0.10	8.50	0.74	0.25	0.13	0.10	
		K36	105	-0.24	8.225	0.70	0.21	-	-	8.23	0.69	0.19	-	-	
NGC 7316	-32	K84	36.3	-0.31	10.70	0.685	0.27	-	-	10.755	0.67	0.20	-	-	*
Sc	0.0185														
NGC 7331	-21	K84	23.8	-1.33	7.78	0.745	0.25	-	-	7.77	0.73	0.23	-	-	
SA(s) bc	0.0026	K84	36.3	-1.15	7.38	0.76	0.25	0.15	0.145	7.375	0.74	0.23	0.165	0.14	
		H60	53.4	-0.98	7.04	0.80	0.29	0.14	0.115	7.03	0.78	0.27	0.155	0.115	
		K36	107.1	-0.68	6.50	0.765	0.30	0.115	0.125	6.49	0.75	0.28	0.13	0.125	
NGC 7332	-30	K84	36.3	-0.72	8.58	-	-	0.15	-	8.59	-	-	0.17	-	
S0 P sp	0.0040														
NGC 7465	-40	K84	36.4	-0.37	9.63	0.735	0.29	-	-	9.65	0.73	0.26	-	-	*
(R')SB (s)0^+:	0.0065														
NGC 7620	-34	K84	36.3	-0.35	10.55	0.865	0.31	-	-	10.65	0.84	0.19	-	-	*
Scd:	0.0318														

Notes to Table 3

Measurements listed as 107.1" are-the mean of 109.2" and 105" observations. Those listed as 36.9" are the mean of 37.5" and 36.3" observations. The adopted nominal errors are ± 0.03, 0.03, 0.04, 0.02, and 0.02 mag for K, J - H, H - K, CO, and H_2O, respectively. A colon indicates an error of up to twice the nominal error.

NGC 224 - 53.3" measurement is mean of 53.4" and 53.2" observations. For 47.5" measurement, reference beam correction = 0.37 mag.

NGC 520 - Aperture centered on bright central lump of this morphologically peculiar galaxy, 168" east and 120" north of bright field star to southwest.

NGC 598 - Reference beam correction = 0.18 mag.

NGC1068 - Seyfert galaxy.

NGC1566 - Seyfert galaxy.

NGC2841 - For H_2O index, large aperture measurement is at 105".

NGC2903 - For H_2O index, large aperture measurement is at 105". For 36.9" (47.5") measurement, reference beam correction = 0.24. (0.33) mag.

NGC2976 - Small aperture measurement centered 19" east and 51" north, and large aperture measurement centered 48" east and 25" north, of faint star on southwest edge of galaxy. For 41.1" measurement, reference beam correction = 0.16 mag.

NGC3034 - Centered on infrared peak.

NGC3556 - Aperture centered 18" east and 3" south of superimposed star, which is included in the field. A 13.7" aperture measurement centered on the star gives K = 10.57 mag, J - H = 0.40 mag, and H - K = 0.09 mag.

NGC4258 - For 41.1" measurement, reference beam correction = 0.17 mag.

NGC4449 - Aperture centered on stellar-like nucleus, which is displaced somewhat from geometric center of the overall structure.

NGC4569 - Star projected on nucleus is included in measurement.

NGC4631 - Aperture centered on infrared peak, which is 33" east and 30" south of faint star on northern edge of galaxy. See Aaronson (1977) for further discussion.

NGC5128 - Aperture centered on infrared peak.

NGC5253 - For C60 measurements, photometer was rotated to remove bright star from reference beam.

NGC5457 - Reference beam correction = 0.21 mag.

NGC5746 - For 66.4" measurement, reference beam correction = 0.21 mag.

NGC6814 - Seyfert galaxy.

NGC6946 - For 105" measurement, reference beam correction = 0.17 mag, due to bright star in beam.

NGC7316 - Markarian 307.

NGC7465 - Markarian 313.

NGC7620 - Markarian 321.

The sample in Table 3 includes galaxies in the Local Group, the Virgo cluster, and the general field; galaxies with absolute magnitude M_V primarily between -19 and -23; and galaxies spanning a wide range of inclination angle, from face-on to edge-on. Aside from the criteria discussed above, the sample does not appear to be overly biased in any obvious fashion.

c) Observational Procedure

All galaxy measurements were made only on nights of high photometric quality while guiding on bright stars in nearby offset fields. The focal plane aperture was always centered on the position of peak infrared brightness: the galaxy was first centered visually, and this centering was then checked by maximizing either the 1.6 μm or 2.2 μm signal. A further check on the position observed for galaxies with either very diffuse centers or thick absorption lanes was made by measuring offsets to nearby field stars, and comparing these offsets with published photographs of the galaxy (Sandage 1961; *RC2* and references therein). For all but 6 of the 91 galaxies listed in Table 2, there was clear correspondence between the infrared peak and either the most optically prominent part of the galaxy (i.e., the nucleus), or in the case of a number of edge-on spirals with thick dust lanes, the physical centroid of the spherical component. The exceptions included two well known galaxies with strong imbedded IR sources, NGC 3034 and 5128; three galaxies, NGC 520, 2976, and 3556, having no apparent well-defined intensity peaks - in either the optical or infrared; and NGC 4631, an edge-on spiral where the position of peak infrared intensity lies not on the most optically prominent part of the galaxy, but in the nearby area of strongest dust absorption. The location of this peak is interpreted as the true position of the nucleus (see Aaronson 1977).

d) Photometric Errors and Instrumental Corrections

The adopted photometric errors were a combination of the statistical accuracy of a particular integration, and the nightly photometric quality, as measured by the dispersion of standard star residuals. Typical errors were 0.01 - 0.03 mag. Possible non-linear response of the detector was checked for by comparing measurements of α Lyr relative to much fainter standards on both the Kitt Peak 2.1-m and 0.9-m, but none was found to the 0.01 mag level. However, several sources of systematic error were identified and corrected for:

First, because galaxies are extended objects it is necessary to correct for flux in the reference beam. For a linear

magnitude growth curve and a spherically symmetric galaxy, the size of this correction at a given value of projected aperture size is determined only by the ratio of beam throw to beam diameter. The corrections adopted are illustrated in Figure 2, parameterized by this ratio. The curves shown were calculated using a three-part growth curve: For log $A / D(0) < -1.3$, where A is the aperture size and $D(0)$ is the corrected face-on diameter from the *RC1*, [5] the V growth curve for NGC 224 obtained from published optical data (Section IIe) was used. For $-1.3 \leq \log A / D(0) \leq 0.1$, the K growth curve for elliptical galaxies determined in Paper I was employed. For $\log A / D(0) > 0.1$, the growth curve given by Sandage (1975) for giant ellipticals was adopted. As indicated by Figure 2 and Table 2, the typical reference beam correction ranged from 0.03 - 0.07 mag. The curve labeled 2' in Figure 2 was obtained by rotating the final growth curve about the point at $\log A / D(0) = 0.0$ so that the magnitude change at $\log A / D(0) = -1.0$ was decreased by 0.20 mag. It illustrates that the chopping throws were sufficiently large so that even for significant systematic differences between galaxies in either growth curve or color-aperture relations, the adopted beam corrections introduce an error of only $\lesssim 0.02$ mag.

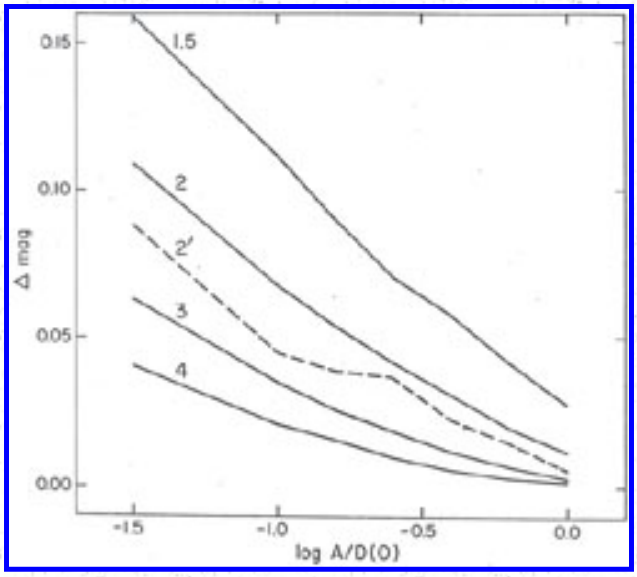

Figure 2. The adopted reference beam corrections are shown as a function of log $A / D(0)$, the ratio of aperture size to corrected face-on diameter from de Vaucouleurs and de Vaucouleurs (1964). Numbers labelling the curves refer to the ratio of beam throw to beam diameter. The curve labelled 2' is explained in the text.

While the growth curves for spiral and elliptical galaxies are similar over the relevant range of aperture sizes and beam throws (*RC2*), we do not expect the corrections in Figure 2 to be appropriate for an inclined spiral with position angle (P.A.) oriented east-west, if we are chopping north-south. As a check on this, and also on the real adequacy of Figure 2 for spirals, a number of measurements of flux in the reference beam itself were taken. (This was not done generally because of the time-consuming nature of the observations.) For $45° \leq$ P.A. $\leq 135°$, the difference between the calculated and observed correction was found to be 0.01 ± 0.015 (24 measurements), while for P.A. $< 45°$ or P.A. $> 135°$, the result was 0.035 ± 0.015 (23 measurements). We have thus adopted the following simple prescription: For spirals with P.A. $< 45°$ or P.A. $> 135°$, or for all spirals with ill-defined P.A.'s because of small inclination angle, the calculated correction (Figure 2) was used directly; but

for spirals with 45° ≤ P.A. ≤ 135° , the calculated correction minus 0.025 mag was used. Position angles were adopted either from Danver (1942), or measured directly from Palomar Observatory Sky Survey or ESO Quick Blue Survey photographs.

For a small number of measurements the above procedure was clearly inadequate, due either to the presence of a bright field star in the reference beam, or to anomalous light distribution of the galaxy itself. In these cases (noted in Table 3), the *measured* reference beam flux at the telescope was the correction used.

Corrections were also applied to account for the rounded nature of, and systematic differences between, the beam profiles of the various filters (Figure 1). Owing to the wavelength-dependent transmission characteristics of the field lens, scans of the H and especially the J filter tended to be more peaked in the center than K filter scans. These effects were accounted for by convolving digitized beam scans with the ellipsoidal luminosity law of de Vaucouleurs (*RC1*). The corrections ranged from 0.0 - 0.02 mag for the K magnitude and H-K color, and from 0.02 - 0.05 mag for the J-H color. No such correction was required for the CO index because of the similarity between the CO and continuum filter scans. However, problems in mounting the H_2O filter resulted in a somewhat altered appearance of the H_2O beam scans (Figure 1). This effect, corrected for as with the broad-band colors, ranged from 0.0 - 0.03 mag. We believe that the uncertainty in these adopted corrections, due to reasonable variation in either the digitized scan or the galaxy surface brightness profile, is ~ 0.01 mag.

Finally, when multiaperture measurements were made, field lens aberration again resulted in aperture dependent corrections. For example, changing from a 4 mm to a 2 mm aperture, the typical correction was 0.02 - 0.03 mag for the K magnitude, and ~ 0.01 mag for the narrow band indices. A 0.03 mag correction was also applied to all J-H colors measured with a 4 mm aperture using the f/7.5 field lens, as in this case only, the effective aperture at J was found to be ~ 0.1 mm smaller than at H or K. We stress that the estimated uncertainties in the sum of all instrumental corrections are only about 0.01 mag for the narrow band indices, and about 0.02 mag for the broad-band magnitudes and colors.

The K magnitude, J-H and H-K colors, and CO and H_2O indices, corrected for all instrumental effects, are listed in columns 6-10, respectively, in Table 2. Preceeding entries in the table are: column 2 - galactic latitude and redshift taken from the *RC2*; column 3 - the telescope used, coded as in Table 2; column 4 - the measured projected aperture in arc sec; and column 5 - the projected aperture in units of D_0. Unless noted otherwise in Table 3, the adopted nominal errors are 0.03, 0.03, 0.04, 0.02, and 0.02 mag at *K, J - H, H - K*; CO, and H_2O, respectively. About half of the measurements were repeated on at least two nights, and the dispersion in these repeated values, after application of instrumental corrections, are consistent with the nominal errors.

---

[5] In this paper $D(0)$ is the corrected face-on diameter taken from the *RC1*, and D_0 is the same quantity but taken instead from the *RC2*. Note that $\log A / D_0 = \log A / D(0) + x$, where $0.0 < x < 0.3$, depending on morphological type (*RC2*). Back.

e) The UVK Colors

To form V-K colors a literature search was made of all published UBV data; some unpublished data was also kindly made available by A. Sandage and by J. Huchra. For each galaxy, the V magnitude and *U - V* colors were plotted as a function of aperture size, and after fitting a smooth curve to the points, values were read off at the apertures corresponding to the infrared measurements. In cases where the optical and infrared aperture ranges did not overlap, no *V - K* color was formed if extrapolation of data greater than 0.2 in log A / D_0, was required, and in only four instances was there extrapolation greater than 0.1 in log A / D_0. The results are presented in Table 4, where UVK colors for 76 galaxies are listed, along with the sources from which the optical data were gathered. Note that for 12 galaxies with only sparse optical data, K magnitudes were interpolated or extrapolated to the optical apertures For these objects there is no correspondence between the values of log A / D_0 in column 2 of Table 4 and column 5 of Table 3.

Table 4.UVK Colors of Galaxies

Name	Log A/D_0	Observed		Corrected for Reddening and Redshift		
		U-V	V-K	$(U-V)_c$	$(V-K)_c$	Notes
(1)	(2)	(3)	(4)	(5)	(6)	(7)
NGC 151	-0.84	1.58	3.35	1.54	3.31	1
	-0.55	1.23	3.22	1.19	3.18	
NGC 157	-0.35	0.71	3.01	0.69	2.99	
NGC 224	-2.79	1.80	3.42:	1.70	3.26:	1,2,3,4
	-2.49	1.77	3.44	1.67	3.28	
	-2.25	1.74	3.55:	1.64	3.39:	
	-2.20	1.74	3.46	1.64	3.30	
	-1.90	1.70	3.37	1.60	3.214	
NGC 253	-1.03	1.55	4.43	1.55	4.43	1
NGC 278	-0.56	-	3.04	-	2.78	1,5
	-0.10	-	2.99	-	2.73	
NGC 598	-1.48	0.52:	2.48:	0.47:	2.40:	2,3
NGC 772	-1.03	1.33	3.48	1.27	3.40	5
	-0.75	1.14	3.48	1.08	3.40	
NGC 936	-0.46	1.59	3.29	1.58	3.27	1,6
NGC 1068	-1.16	0.86:	3.53:	0.85:	3.52:	1,7,8,9
	-0.87	0.82:	3.52:	0.81:	3.51:	10,11
	-0.58	0.81:	3.43:	0.80:	3.42:	
NGC 1084	-0.74	0.71	3.26	0.69	3.25	5
	-0.56	0.60	3.15	0.58	3.14	

NGC 1232	-0.85	1.27	3.10	1.25	3.08	1
NGC 1365	-1.25	-	3.97	-	3.95	1,2,12
	-0.96	-	3.69	-	3.67	13
NGC 1398	-1.03	1.72	3.41	1.71	3.39	5
	-0.75	1.66	3.37	1.65	3.35	
NGC 1566	-1.18	0.92:	3.25:	0.88:	3.20:	8,14
	-0.89	0.95:	3.09:	0.91:	3.04:	15
NGC 1617	-0.92	1.54	3.27	1.50	3.21	6,15,16
	-0.63	1.52	3.24	1.48	3.18	17
NGC 1637	-0.85	1.15	3.40	1.09	3.30	1
	-0.56	1.00	3.17	0.94	3.07	
	-0.27	0.85	3.00	0.79	2.90	
NGC 1961	-0.65	1.43	3.91	1.28	3.69	1
	-0.36	1.21	3.52	1.06	3.30	
NGC 1964	-1.04	1.47	3.33	1.38	3.20	1
	-0.75	1.26	3.28	1.17	3.15	
	-0.46	1.04	3.18	0.95	3.05	
NGC 2146	-0.45	1.10	4.20	1.02	4.06	1
NGC 2217	-0.99	1.76	3.51	1.63	3.29	1,6
	-0.70	1.70	3.42	1.57	3.20	
NGC 2339	-0.47	1.12	3.45	0.88	3.08	1
	-0.18	0.90	3.34	0.66	2.97	
NGC 2681	-0.78	1.22	2.99	1.19	2.93	1
	-0.67	1.20	2.98	1.17	2.92	
NGC 2683	-1.05	1.43	3.62	1.40	3.57	1,18
	-0.59	1.33	3.50	1.30	3.45	
NGC 2775	-0.35	1.37	3.39	1.32	3.30	1
NGC 2841	-1.04	1.61	3.22	1.59	3.17	1,18
	-0.57	1.42	3.20	1.40	3.15	
NGC 2903	-1.24	0.73	3.36:	0.71	3.31:	3,18
	-1.13	0.77	3.38:	0.75	3.33:	
	-0.77	0.82	3.30:	0.80	3.25:	
NGC 2997	-1.14	1.02:	3.51:	0.87:	3.28:	12,13
	-0.85	1.15:	3.39:	1.00:	3.16:	
NGC 3031	-1.81	1.79	3.56	1.76	3.51	2,3,4
	-1.57	1.74	3.49	1.71	3.44	19

	-1.51	1.73	3.44	1.70	3.39	
	-1.10	1.67	3.39	1.64	3.34	
NGC 3077	-0.80	0.47	2.80	0.44	2.75	1,2,20
NGC 3245	-0.66	1.52:	3.20:	1.51:	3.18:	6,21
NGC 3351	-1.30	0.91:	3.38:	0.91:	3.37:	3,22
	-1.04	0.99	3.36	0.99	3.35	
	-1.00	1.02	3.35	1.02	3.34	
NGC 3368	-1.01	1.57:	3.51	1.57:	3.50	3
	-0.57	1.45:	3.32	1.45:	3.31	10,23
NGC 3521	-0.66	1.19	3.52	1.19	3.51	2
NGC 3623	-1.09	1.65	3.29	1.65	3.28	2,10,18,23
NGC 3627	-1.37	1.42	3.41	1.42	3.40	2,10,18
	-1.07	1.32	3.32	1.32	3.31	23
NGC 3628	-0.79	1.41	4.23:	1.41	4.22:	2
NGC 4214	-1.04	-0.01	2.19	-0.01	2.19	2
NGC 4258	-1.64	1.05	3.23:	1.05	3.23:	2,20
	-1.34	1.11	3.23:	1.11	3.23:	24
NGC 4303	-1.02	1.03	3.23	1.01	3.21	18
	-0.73	0.91	3.10	0.89	3.08	
NGC 4321	-1.03	0.69	3.13	0.67	3.11	2,18
NGC 4425	-0.72	1.36	2.98	1.35	2.95	6
NGC 4429	-0.98	1.55:	3.53	1.54:	3.51	6,18
	-0.69	1.51:	3.41	1.50:	3.39	
NGC 4449	-1.14	-0.03	2.22	-0.33	2.22	2,3,5
	-0.84	0.00	2.31	0.00	2.31	
NGC 4477	-0.91	1.55	3.25	1.54	3.23	6,18
	-0.62	1.59	3.25	1.58	3.23	
NGC 4501	-1.24	1.73	3.58	1.71	3.55	2,3
	-0.94	1.59	3.54	1.57	3.51	18
NGC 4526	-1.06	1.58	3.50	1.58	3.49	6,18
	-0.77	1.51	3.39	1.51	3.38	
NGC 4565	-1.23	1.77	4.13	1.76	4.12	2,3
	-0.79	1.60	3.98	1.59	3.97	
NGC 4569	-1.15	1.02	3.29	1.02	3.29	2,18
	-0.86	1.07	3.24	1.07	3.24	

NGC 4579	-1.17	1.54	3.23	1.62	3.21	2,3,18
	-0.91	1.51	3.21	1.49	3.19	
	-0.87	1.50	3.20	1.48	3.18	
	-0.47	1.35	3.22	1.33	3.20	
NGC 4594	-0.62	1.66	3.56	1.65	3.54	2
NGC 4643	-0.96	1.65	3.22	1.64	3.20	3,18
	-0.70	1.62	3.20	1.61	3.18	
	-0.66	1.62	3.22	1.61	3.20	
NGC 4699	-0.85	1.46	3.23	1.44	3.21	3,6
	-0.78	1.44	3.19	1.42	3.17	
	-0.56	1.39	3.22	1.37	3.20	
	-0.49	1.37	3.21	1.35	3.19	
NGC 4736	-1.52	1.32	3.24	1.32	3.24	2,25
	-1.22	1.28	3.22	1.28	3.22	
	-0.78	1.01	3.19	1.01	3.19	
NGC 4753	-0.92	1.73:	3.57	1.72:	3.55	1,2
	-0.63	1.61	3.50	1.60	3.48	
NGC 5005	-1.12	1.48	3.45	1.47	3.44	2,3,26
	-0.86	1.33	3.43	1.32	3.42	
	-0.82	1.32	3.43	1.31	3.42	
	-0.42	1.26	3.50	1.25	3.49	
NGC 5055	-1.24	1.27	3.59	1.27	3.58	2,3,18
	-0.80	1.05	3.48	1.05	3.47	
NGC 5128	-1.86	2.63	6.63	2.52	6.44	13,27
	-1.56	2.34:	6.13:	2.23:	5.94:	28
	-1.27	1.93:	5.69:	1.82:	5.50:	
NGC 5194	-1.20	1.00	3.14	1.00	3.14	2,3,29
	-0.76	0.82	3.14	0.82	3.14	
NGC 5195	-0.90	1.71	3.69	1.71	3.68	2,3,29
	-0.46	1.48	3.62	1.48	3.61	
NGC 5236	-1.36	0.38	3.33	0.33	3.24	2
	-1.29	0.43	3.36	0.38	3.27	7,16
	-1.07	0.56	3.34	0.51	3.25	
	-1.00	0.59	3.36	0.54	3.27	
NGC 5253	-0.76	-0.25	2.18	-0.31	2.09	2,12
	-0.54	-0.09	2.25	-0.15	2.16	16

	-0.37	-0.03	2.22	-0.09	2.13	
NGC 5457	-1.19	0.98	2.98:	0.98	2.98:	2,3,29
NGC 5746	-0.50	1.66	3.95:	1.68	3.93:	2
NGC 5907	-0.94	1.38	4.09:	1.38	4.08:	2,3,18
NGC 6015	-0.40	0.63	2.94	0.61	2.89	2
NGC 6384	-0.50	1.33	3.35	1.21	3.16	2
NGC 6503	-0.89	0.99	3.19	0.93	3.10	2,3
	-0.74	0.92	3.14	0.86	3.05	18
	-0.45	0.79	3.10	0.73	3.01	

Corrections to references at end of Table 4: The missing reference 16 is Bucknell, M. J., and Peach, J. V. 1976, Observatory, 996, 61. Also, reference 30 as listed is wrong. The correct reference is Ables, H. D. 1971, Pub. U. S. Nav. Obs., XX, Part IV.

Since many times considerable scatter was present in the optical measurements, some amount of subjective judgement was necessarily used in forming the UVK colors. The primary sources of data were those available from the work of de Vaucouleurs, Huchra, Sandage and Tifft (cf. Table 4). These data points were given twice the weight as those from the remaining secondary sources, and for all but four galaxies in Table 4 there was at least one measurement available from a primary source. All data from Tifft was transformed to the UBV system using the relations given in Tifft (1973); the agreement between this transformed data and that from the other primary sources was generally acceptable (i.e., within 0.10 mag). As in Paper I, we adopt a nominal error of ± 0.10 mag in the V - K color, unless the error in the K magnitude or the scatter in the V data is exceptionally large, in which case a colon is given after the V - K color and a nominal error of 0.20 is assumed.

f) Reddening and Redshift Corrections

To correct for the effects of interstellar reddening, we have used the absorption free polar-cap model of Sandage (1973) and Van de Hulst curve #15 (Johnson 1968). The adopted corrections are summarized on the left half of Table 5. The values for the color excess ratios E_{H_2O} / A_V and E_{CO} / A_V were obtained by careful interpolation of the reddening curve at the effective wavelengths listed in Table 1. Note that reddening causes an increase in the measured H_2O index, but a decrease in the measured CO index.

Table 5. Adopted Corrections for Reddening and Redshift *

Reddening	Redshift.
$A_V = 0.10(\csc[b] - 1)$, $\lvert b\rvert \leq 50°$	$K_K = -3.25\, z$
$A_V = 0.$, $\lvert b\rvert > 50°$	
$E_{U-V} / A_V = 0.56$	$K_{U-V} = 1.2\, z$, $T \leq 0$†

$E_{V-K} / A_V = 0.91$

$E_{J-H} / A_V = 0.10$

$E_{H-K} / A_V = 0.06$

$E_{H_2O} / A_V = 0.014$

$E_{CO} / A_V = - 0.010$

$= (1.2 + 0.7\ T)\ z, \quad 0 \leq T \leq 3$

$= 3.3\ z, \quad T \geq 3$

$K_{V-K} = 4.9\ z, \quad T \leq 0$

$= (4.9 - 0.45\ T)\ z, \quad 0 \leq T \leq 3$

$= (3.55 - 0.3[T - 3]), \quad T \geq 3$

$K_{J-H} = 0.5z$

$K_{H-K} = 3.6\ z$

$K_{H_2O} = 0.$

$K_{CO} = - 4.8z$

---

*$m_0 = m - A_m - K_m$, $C_0 = C - E_c - K_c$

†T is a morphological type parameter following the notation in the *RC2* ; T = - 5 for type E, T = 0 for type S0/a, T = 5 for type Sc, etc.

The adopted redshift corrections are listed on the right side of Table 5. The redshift corrections for the optical colors are taken from Pence (1976), and given as a function of morphological type parameter T following the notation in the *RC2*, where T = - 5 is for type E, T = 0 for type S0/a, T = 5 for type Sc, etc. The redshift corrections for the infrared colors are discussed in and adopted from Papers I and II. Although these corrections were based on measurements of elliptical galaxies, we have used them for spirals because, as we show below, the infrared colors depend very weakly on morphological type.

Only nine galaxies in Table 3 have galactic latitude less than 20°, the galaxy with the smallest value being NGC 6946, with b^{II} = 12° . No galaxies in Table 3 for which CO and H_2O indices were observed, and only four galaxies for which JHK colors were measured, have redshift z > 0.01, the largest value being that for NGC 7520, with z = 0.032. Thus, uncertainties in either the redshift or reddening corrections will not affect the conclusions of this paper.

g) Comparison with Previous Results

The majority of observations in Papers I and II were made with a completely independent set of filters and detector (the CIT system). The J - H and H - K transformations between that system and the present one (the HCO system) are discussed in Appendix A. No transformation is necessary between the systems for the K magnitudes, or the CO and H_2O indices. For comparison purposes a number of galaxies were measured in common with the two systems using the same or similar apertures. The results, after application of all instrumental effects and transformations, are summarized in Table 6. We conclude from this Table that no statistically significant calibration differences exist between the data of Papers I and II and the present paper.

Table 6. Comparison of Galaxy Observations on the HCO and CIT Systems

---

Number of Observations	Feature	Mean Δ *
3	K	-0.013 ± 0.014
6	J-H	-0.007 ± 0.009
6	H-K	-0.010 ± 0.010
9	CO	0.002 ± 0.004
3	H_2O	0.005 ± 0.005

* $\Delta \equiv (\text{color})_{HCO} - (\text{color})_{CTT}$, after transformation of the CIT data to the HCO system and application of all instrumental corrections.

III. Results

Columns 11 - 15 of Table 3 contain the K magnitude, K colors, and CO and H_2O indices *corrected for reddening and redshift.* Columns 5 and 6 of Table 4 contain U - V and V - K colors also corrected for reddening and redshift.

a) Color-Aperture Relations

In Figures 3 - 9 the measurements from Tables 3 and 4 are plotted against log A / D_0. [6] The galaxies have been separated into seven groups: S0, S0$^+$, and I0; S0/a, Sa, Sab; Sb; Sbc; Sc; Scd, Sd, and Im; and "2.2 μm excess." Preliminary plots of the J - H color against H - K for all multiaperture data revealed a small number of galaxies with very red colors distinctly segregated from the region of general scatter of the remaining galaxy points. The term "2.2 μm excess" has been adopted in referring to these 12 objects, and these galaxies have been grouped separately because in the discussion to follow we are primarily interested in galaxian infrared colors as they relate to the stellar population, and not to the various non-stellar effects which produce, the anomalously red colors (Section V).

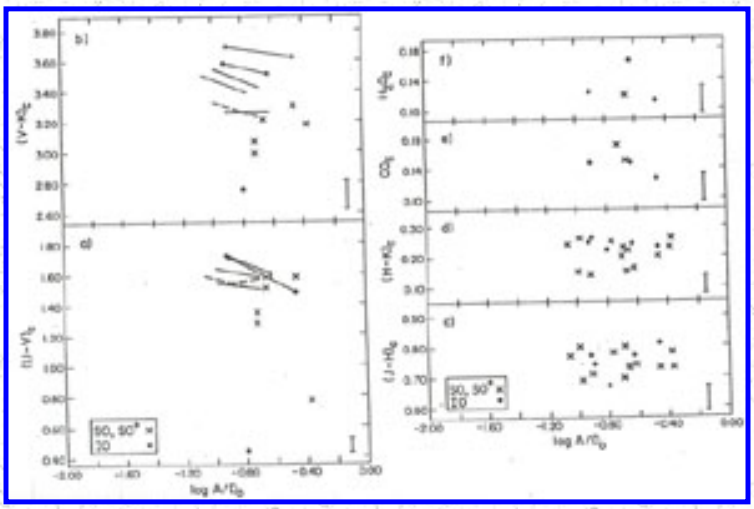

Figure 3. The colors for S0, S0$^+$, and I0 galaxies from Tables 3 and 4, corrected for reddening and redshift, are shown as a function of log A / D_0, the ratio of aperture size to corrected face-on diameter from de Vaucouleurs, de Vaucouleurs, and Corwin (1976). The lines shown in a) and b) connect multiaperture observations of a particular galaxy. Data points for the multiaperture observations are plotted only to distinguish among morphological types. The error bars shown in this and all succeeding figures are the adopted nominal errors from Tables 3 and 4. When two lines intersect, one is shown as dashed.

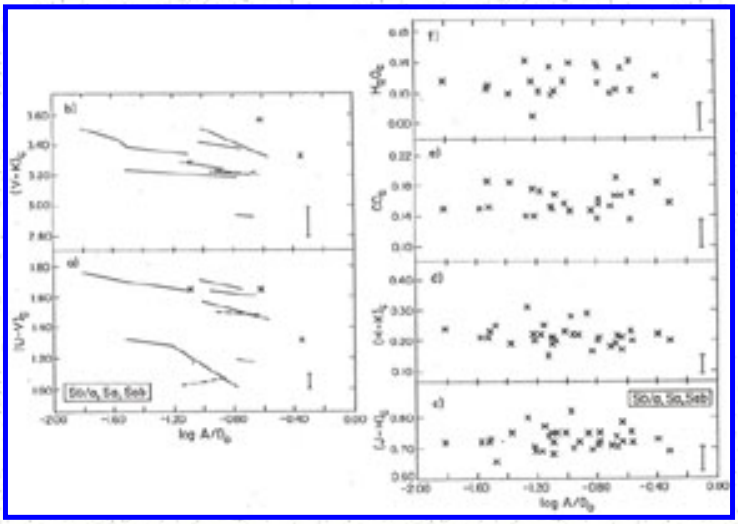

Figure 4. Same as Figure 3, for galaxy types S0/a, Sa, and Sab.

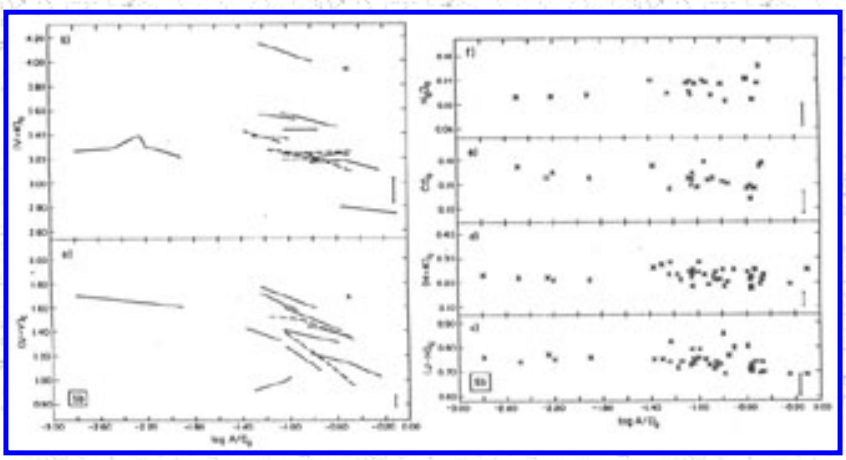

Figure 5. Same as Figure 3, for galaxy type Sb.

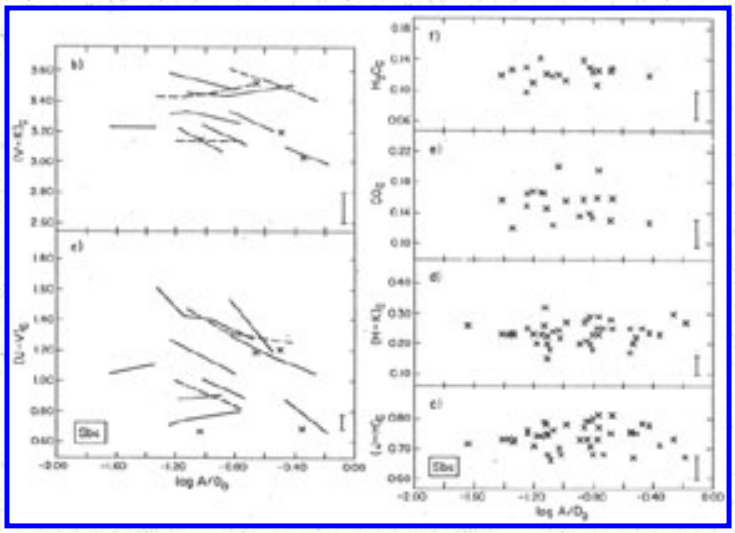

Figure 6. Same as Figure 3, for galaxy type Sbc.

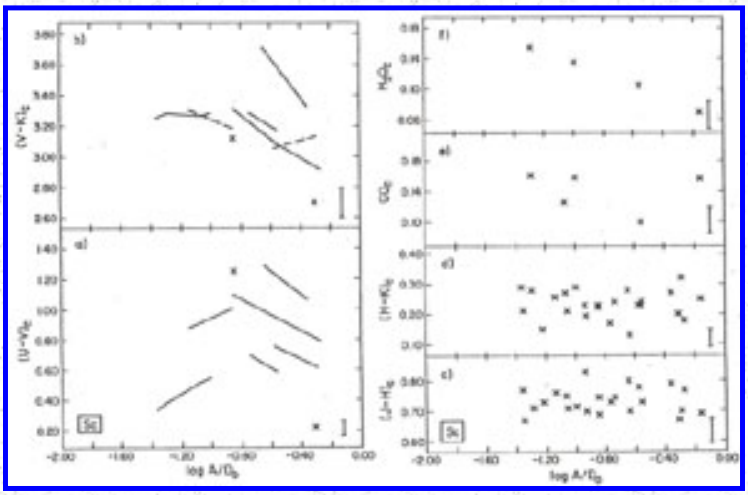

Figure 7. Same as Figure 3, for galaxy type Sc.

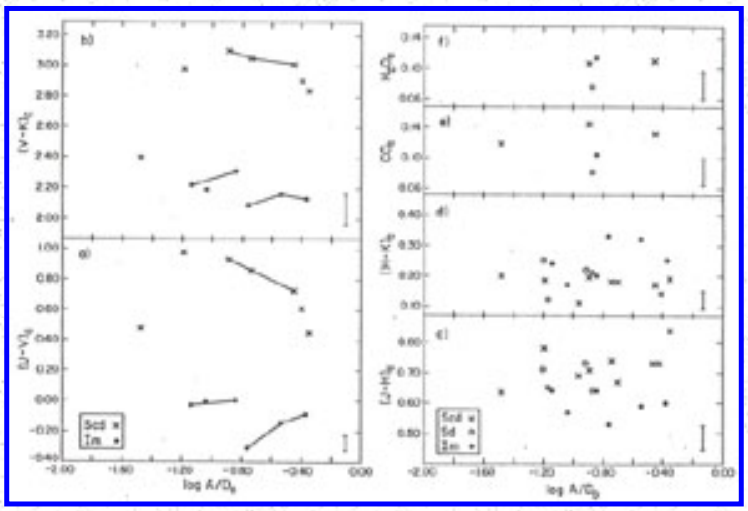

Figure 8. Same as Figure 3, for galaxy types Scd, Sd, and Im.

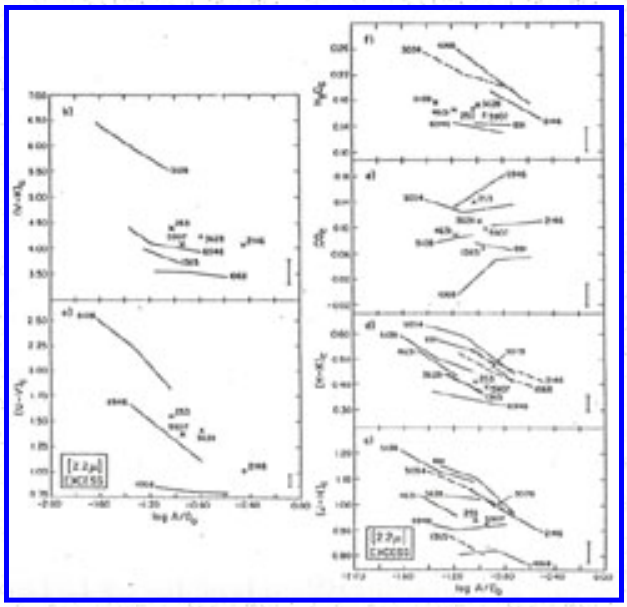

Figure 9. Same as Figure 3, for galaxies with a significant 2.2 μm excess. Lines connect all multiaperture observations in a) - f). The NGC numbers of the galaxies are also shown.

Ideally, to determine mean color-aperture relations, a "color growth curve" should be constructed in a manner analogous to that in which a normal magnitude growth curve is made. Such a construction was in fact attempted, but because the data is scattered over a large range of log A / D_0 mostly from -0.2 to -1.6, while the data for almost all galaxies individually extends over less than half this range, unambiguous results could not be achieved. We have instead followed the same procedure as in Paper I: Multi-aperture data for each galaxy was fit with a least squares line, and the slopes so determined were averaged together. While UBV color-aperture curves apparently flatten out at very large and very small apertures (*RC2*), such curves are in fact approximately linear over the predominant range of aperture sizes in this paper, and so we have some confidence that our own forced linear fits will not be too misleading.

The resulting mean color-aperture slopes are summarized in Table 7, and confirm the qualitative impressions of Figures 3 - 9: First, excluding the 2.2 μm excess galaxies, no statistically significant radial color gradients are found in spirals for either the J - H and H - K colors, or the CO and H_2O indices. Second, significant U - V and V - K color gradients do exist for galaxies of all types, and are correlated in the sense that smaller: apertures generally imply redder colors. Considering the small sample size, the U - V gradients listed in Table 7 are consistent with the linear U - V fits found by de Vaucouleurs and de Vaucouleurs (1972). Third, galaxies with a 2.2 μm excess exhibit large radial gradients in all colors and indices, in the sense of redder broad-band colors, larger H_2O absorption, and smaller CO absorption, at smaller aperture sizes. The behavior of the narrow-band indices is as expected from reddening effects (Section IIf).

Table 7. Color-Aperture Relations *

CO	H_2O	U-V	V-K	J-H	H-K

	N	Slope	± σ_m	N	Slope	± σ_m	N	Slope	± σ_m	N	Slope	± σ_m	N	Slope	± σ_m	N	Slope	± σ_m
All E and S0 Papers I and II	33	0.00	0.02	16	-0.04	0.02	32	-0.13	0.03	32	-0.11	0.05	37	-0.08	0.04	37	-0.04	0.03
S0/a, Sa, Sab	8	0.015	0.02	6	0.015	0.02	8	-0.16	0.06	8	-0.16	0.05	12	0.02	0.02	12	-0.02	0.03
Sb	6	-0.01	0.02	6	0.03	0.01	12	-0.32	0.09	13	-0.13	0.03	14	-0.01	0.01	14	-0.02	0.02
Sbc	6	-0.02	0.02	6	0.00	0.02	11	-0.36	0.13	11	-0.22	0.07	14	0.00	0.03	14	-0.01	0.02
Sc, Scd, Sd	3	0.02	0.06	3	-0.05	0.03	7	-0.26	0.20	7	-0.42	0.20	12	-0.03	0.04	12	0.01	0.04
Im	-	-	-	-	-	-	2	0.43	0.33	2	0.24	0.06	2	0.12	0.12	2	-0.18	0.04
I0	1	-0.05	-	1	-0.03	-	2	-0.47	0.06	2	-0.20	0.04	2	0.08	0.08	2	-0.04	0.03
All but 2 μm excess	24	0.00	0.01	22	0.00	0.01	-	-	-	-	-	-	-	-	-	-	-	-
2.2 μm excess	6	0.04	0.02	5	-0.08	0.03	3	-0.75	0.33	4	-0.87	0.30	9	-0.19	0.04	9	-0.24	0.02
Blue†	-	-	-	-	-	-	7	0.38	0.08	7	-0.09	0.07	7	0.03	0.05	7	-0.06	0.04

* The least-squares slope Δ color / ($\Delta \log A / D_0$) is given for various galaxy bins.

† This bin includes all galaxies for which $\Delta U - V / (\Delta \log A / D_0) > 0.10$.

The U - V and V - K color gradients for early type spirals are similar to those of E and S0 galaxies found in Paper I, as is the lack of significant radial gradients in either the CO or H_2O indices. On the other hand, no significant radial gradients are bound in spirals for either the J - H or H - K color, a result that is perhaps in contra-distinction with the case for the early-type Paper I galaxies. However, since the typical range in log A / D_0 for a particular galaxy is only about 0.4, a systematic error of just 0.03 mag need exist *between* the J magnitudes, for instance, of Paper I and in this paper, to produce a 0.07 mag discrepancy per unit log A / D_0 in color. Given the instrumental problems associated with measuring J (e.g., Section IId this paper, Section IIc in Paper I), such a systematic error cannot be ruled out.

We note that the results in Table 7 *are not* field lens dependent. In particular, for types S0/a to Sd the J - H color gradient determined using just multiaperture data obtained with the f/9.6 and f/13 field lenses yields a slope of 0.00 ± 0.02 (for $N = 29$), while the same quantity for the f/7.5 field lens is 0.01 ± 0.02 (for $N = 23$).

Cursory examination of Figures 3 - 9 reveals considerable dispersion in the visual correlation in aperture changes between U - V and V - K; in many cases the colors anti-correlate. In the last line of Table 7 we have grouped together all galaxies with a "blue" U - V color gradient (i.e., bluer U - V colors at smaller aperture sizes) greater than 0.10 mag per unit log A / D_0. The mean V - K color gradient of this group, although small, is still in the opposite sense. Interpretation of this point, and of the general relation between U - V and V - K, is postponed to Section IV.

---

[6] The observations for NGC 520, 2976, and 3556 have been excluded from this discussion (cf. Section IIc). Back.

b) Integrated Properties

To study general galaxian properties, we assign to every galaxy a representative value of each color. For the CO and H_2O indices, a weighted average of all aperture measurements was formed, since in all but the 2.2 μm excess objects the measuring error is at least as large as the allowable radial variation. For the broad-band colors, the data has been referenced to a fiducial value of log A / D_0 equal to -0.6 because 1) this value involves minimal extrapolation of the measurements, and 2) the galaxies in Paper I which were assigned integrated colors at log $A / D(0)$ = - 0.3 can be compared directly to those in the present study, since for early type galaxies $D_0 \simeq D(Q) + 0.3$ (*RC2*).

For galaxies with multiaperture measurements straddling log A / D) = - 0.6, we have interpolated the data to -0.5. For the remaining galaxies, we have adopted the colors at the projected aperture size closest to -0.6. The final integrated colors are presented in Table 8, binned by morphological type. Note that the value of log A / D_0 listed in column 2 refers to the U - V and V - K colors only. In a few cases a value for U - V is listed in Table 8 where no values were given in Table 5. For these instances the scatter in published U - V was deemed too great for reliable determination of a color gradient, but did allow assignment of an integrated value.

Table 8. Integrated Colors of Galaxies

Name	Log A/D_0 *	$(U-V)_c$	$(V-K)_c$	$(J-H)_c$	$(H-K)_c$	CO_c	H_2O_c	Yerkes Class
S0, $S0^+$:								
NGC 936	-0.5	1.58	3.27	0.73	0.20	-	-	k
NGC 2217	-0.8	1.60	3.24	0.74	0.19	-	-	-
NGC 3245	-0.7	1.51	3.18	0.73	0.22	0.15	0.12	gk
NGC 4425	-0.7	1.35	2.95	0.75	0.17	-	-	-
NGC 4429	-0.7	1.50	3.39	0.77	0.24	-	-	k

NGC 4477	-0.6	1.58	3.23	0.74	0.16	-	-	k
NGC 4526	-0.8	1.51	3.38	0.77	0.24	-	-	k
NGC 7332	-0.7	1.28	3.04	0.71	0.08	0.17	-	k?
NGC 7465	-0.4	0.77	3.14	0.13	0.26	-	-	-
S0/a, Sa, Sab:								
NGC 1398	-0.8	1.65	3.35	0.72	0.18	0.16	0.105	k
NGC 1617	-0.6	1.49	3.19	0.72	0.19	-	-	-
NGC 2681	-0.7	1.18	2.92	0.73	0 20	0.165	0.135	fg
NGC 2775	-0.4	1.32	3.30	0.72	0.21	0.14	0.13	k
NGC 3031	-1.1	1.64	3.34	0.74	0.22	0.15	0.12	gk
NGC 3368	-0.6	1.47	3.33	0.75	0.23	0.145	0.125	gk
NGC 3623	-1.1	1.65	3.28	0.72	0.19	0.15	0.10	gk
NGC 4569	-0.9	1.07	3.24	0.76	0.28	-	-	f
NGC 4594	-0.6	1.65	3.54	0.78	0.20	0.175	0.11	k
NGC 4643	-0.7	1.61	3.20	0.70	0.20	0.17	0.105	k
NGC 4725	-	-	-	0.69	0.21	0.155	0.085	gk
NGC 4736	-0.8	1.01	3.19	0.72	0.21	0.175	0.11	g
NGC 4826	-	-	-	0.82	0.29	0.145	0.14	fg
Sb:								
NGC 224	-2.0	1.62	3.25	0.76	0.22	0.16	0.11	gk
NGC 278	-0.6	0.33	2.78	0.71	0.21	0.115		f
NGC 772	-0.7	1.08	3.40	0.74	0.21	-	-	g
NGC 1964	-0.6	1.06	3.10	0.73	0.23.	0.14	0.095	g
NGC 2683	-0.6	1.35	3.51	0.80	0.23	0.135	0.125	g
NGC 2841	-0.6	1.42	3.16	0.72	0.20	0.145	0.12	k
NGC 3351	-1.0	1.02	3.34	0.75	0.24	0.14	0.13	g
NGC 3627	-1.1	1.32	3.31	0.73	0.24	0.16	0.13	g
NGC 4501	-0.9	1.57	3.51	0.74	0.23	0.175	0.13	g
NGC 4565	-0.8	1.59	3.97	0.85	0.26	0.14	0.12	gk
NGC 4579	-0.6	1.40	3.19	0.73	0.22	0.155	0.125	k
NGC 4699	-0.6	1.39	3.19	0.70	0.20	0.17	0.125	k
NGC 5746	-0.5	1.68	3.93	0.80	0.26	-	-	gk
NGC 7177	-0.6	1.16	3.15	0.73	0.22	0.13	0.10	g
Sbc:								

NGC 151	-0.6	1.30	3.21	0.74	0.19	-	-	fg
NGC 157	-0.4	0.69	2.99	0.71	0.23	-	-	a
NGC 1300	-	-	-	0.69	0.20	-	-	g
NGC 1566	-0.9	0.91	3.04	0.74	0.20	0.135	-	-
NGC 2339	-0.3	0.77	3.02	0.79	0.27	-	-	af?
NGC 2903	-0.9	0.78	3.29	0.75	0.25	0.165	0.12	f
NGC 3521	-0.7	1.19	3.51	0.82	0.24	0.145	0.125	f
NGC 4258	-1.3	1.11	3.23	0.72	0.24	0.12	0.125	g
NGC 4303	-0.7	0.89	3.08	0.68	0.24	-	-	f
NGC 4321	-1.0	0.67	3.11	0.70	0.24	0.20	0.12	fg
NGC 5005	-0.6	1.28	3.46	0.78	0.27	0.14	0.13	gk
NGC 5055	-0.8	1.05	3.47	0.80	0.23	0.14	0.11	g
NGC 5194	-0.8	0.82	3.14	0.77	0.23	0.18	0.12	fg
NGC 6384	-0.5	1.21	3.16	0.72	0:20	-	-	gk
NGC 6744	-	-	-	0.68	0.15	-	-	-
NGC 6814	-0.6	1.16	3.48	0.75	0.27	-	-	fg
NGC 7331	-0.7	1.28	3.50	0.75	0.27	0.15	0.125	gk
Sc, Scd, Sd:								
NGC 598	-1.5	0.	2.40	0.64	0.20	0.12	-	f
NGC 628	-	-	-	0.72	0.19	-	-	fg
NGC 1084	-0.6	0.64	3.20	0.73	0.24	0.115	0.095	a?
NGC 1232	-0.8	1.25	3.08	0.70	0.15	-	-	f
NGC 1637	-0.6	0.94	3.09	0.74	0.22	-	-	f
NGC 1961	-0.5	1.17	3.50	0.80	0.26	-	-	f
NGC 2403	-	-	-	0.69	0.11	-	-	f
NGC 2976	-	-	-	0.71	0.14	-	-	a
NGC 2997	-0.8	1.00	3.16	0.73	0.23	-	-	f
NGC 3621	-	-	-	0.73	0.23	-	-	a
NGC 4490	-	-	-	0.64	0.21	0.08	0.075	a
NGC 5236	-1.0	0.54	3.27	0.74	0.28	0.15	0.145	fg
NGC 5457	-1.2	0.98	2.98	0.78	0.18	-	-	f
NGC 6015	-0.4	0.61	2.89	0.70	0.17	-	-	af
NGC 6503	-0.6	0.80	3.03	0.74	0.18	0.14	0.11	g?
NGC 6643	-0.6	0.75	3.01	0.78	0.23	-	-	af

NGC 7316	-0.3	0.22	2.70	0.67	0.20	-	-	-
NGC 7620	-0.4	0.45	2.82	0.84	0.19	-	-	-
Im:								
NGC 4214	-1.0	-0.01	2.19	0.57	0.17	-	-	a
NGC 4449	-0.8	0.00	2.31	0.64	0.21	0.105	0.115	a
NGC 5253	-0.6	-0.15	2.16	0.58	0.32	-	-	-
I0:								
NGC 3077	-0.8	0.44	2.75	0.67	0.22	-	-	-
NGC 4753	-0.6	1.60	3.48	0.77	0.24	0.145	0.165	g
NGC 5195	-0.6	1.55	3.63	0.79	0.25	0.135	0.115	f?
2.2 - μm Excess:								
NGC 253	-1.0	1.55	4.43	0.94	0.41	0.14	0.165	af
NGC 891	-	-	-	0.97	0.41	0.07	0.14	g?
NGC 1068	-0.6	0.83	3.48	0.77	0.41	0.03	0.215	g
NGC 1365	-1.0	0.83	3.67	0.80	0.36	0.07	-	fg
NGC 2146	-0.5	1.02	4.06	0.92	0.43	0.105	0.17	k?
NGC 3034	-	-	-	0.95	0.44	0.135	0.225	-
NGC 3079	-	-	-	1.00	0.47	-	-	fg
NGC 3628	-0.8	1.41	4.22	1.02	0.37	0.11	0.17	g?
NGC 4631	-	-	-	0.96	0.43	0.09	0.165	af
NGC 5128	-1.3	1.82	5.50	1.09	0.45	0.085	0.175	-
NGC 5907	-0.9	1.38	4.08	0.92	0.39	0.10	0.155	g?
NGC 6946	-0.8	1.11	3.93	0.92	0.32	0.155	0.135	af

* Refers to U-V and V-K colors only.

In Figures 10 - 13, the colors from Table 8 of this study, from Table of Paper I, and from Table 3 of Paper II [7] are shown as a function of morphological type. To assist interpretation of these figures the mean colors as a function of type are presented in Table 9.

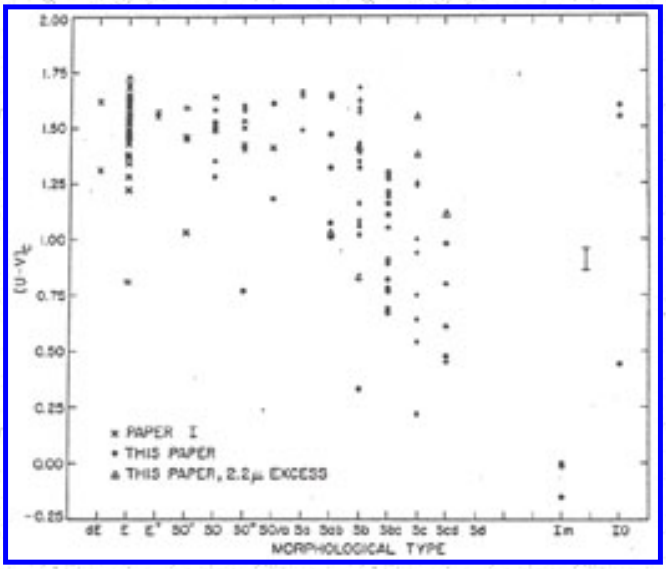

Figure 10. The U - V colors from Table 4 of Paper I and from Table 8 of this paper are shown as a function of morphological type. Note that the points for the two 2.2 μm excess Sb galaxies, NGC 1068 and 1365, overlap at U - V = 0.83.

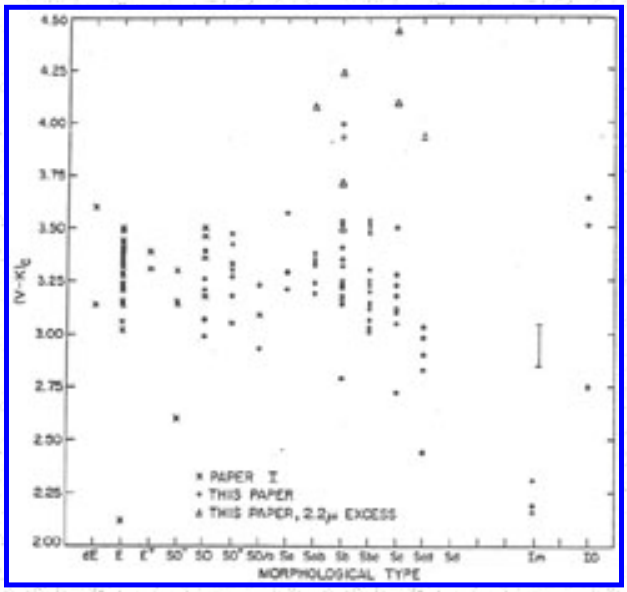

Figure 11. The V - K colors from Table 4 of Paper I and Table 8 of this paper are shown as a function of morphological type. The point for NGC 5128 lies off the plot, and for this reason the point was also excluded from Figure 10.

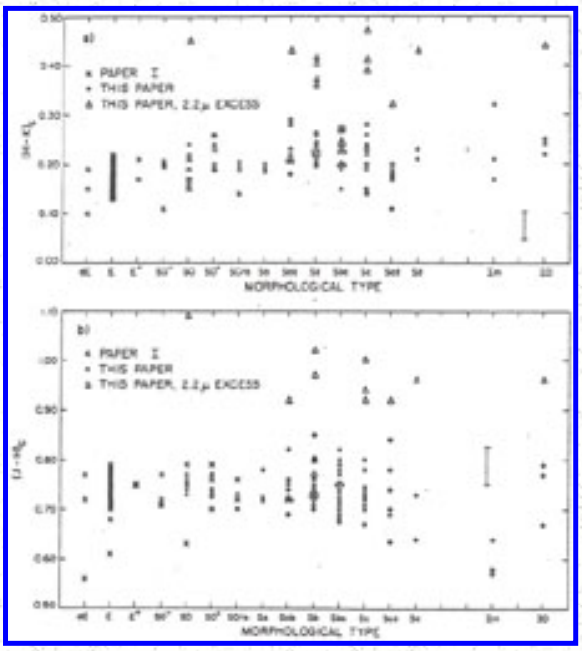

Figure 12. The J - H and H - K colors from Table 4 of Paper I and from Table 8 of this paper are shown as a function of morphological type.

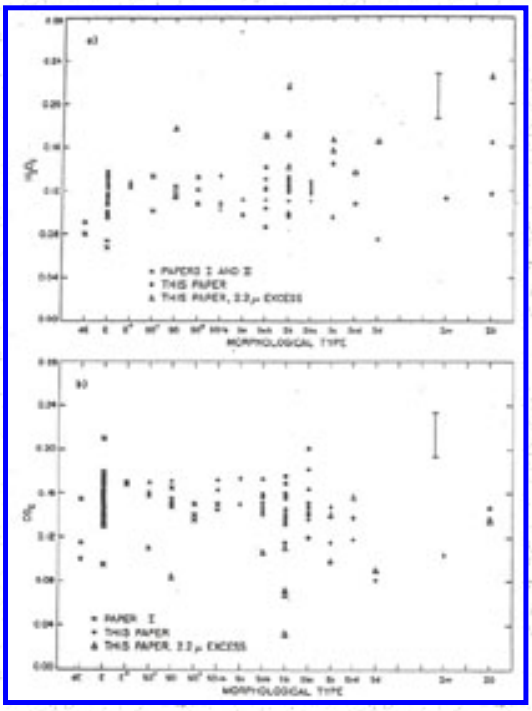

Figure 13. The H_2O indices from Table 3 of Paper II and Table 8 of this paper are shown as a function of morphological type. b) The CO indices from Table 4 of Paper I and from Table 8 of this paper are shown as a function of morphological type.

In computing the mean E and S0 colors, the color-luminosity effects found in Paper I were explicitly ignored, except that data for the very blue dwarf galaxies NGC 205 and 404 were excluded. For the five spiral bins we have considered two samples of the U - V and V - K color data. First there is the "full" sample, which includes the observations for all galaxies. However, this sample is biased by both color-aperture and inclination effects (Table 7 and Section IIIc). We have thus formed a "restricted" sample, which includes only those galaxies with integrated values at $\log A / D_0 > -0.9$, and values of $\csc(i) < 5$, where i is the inclination angle (Section IIIc). The latter constraint excludes only two galaxies, NGC 4565 and 5746, both from the Sb bin. The mean U - V and V - K colors for the restricted (full) sample are given in the upper (lower) entries in Table 9.

Table 9. Mean Colors of Morphological Types

	N	$(U-V)_c$	σ_m	N	$(V-K)_c$	σ_m	N	$(J-H)_c$	σ_m	N	$(H-K)_c$	σ_m	N	CO_c	σ_m	N	H_2O_c	σ_m
E, Papers I and II	34	1.51	0.02	34	3.29	0.02	37	0.74	0.01	37	0.18	0.01	37	0.155	0.01	27	0.115	0.01
S0, Papers I and II	11	1.49	0.02	11	3.28	0.05	12	0.74	0.01	12	0.19	0.01	12	0.155	0.01	10	0.12	0.01
S0, this paper	9	1.41	0.09	9	3.20	0.05	8	0.75	0.01	8	0.21	0.01	2	0.16	0.01	1	0.12	-
S0/a, Sa, Sab*	9	1.38	0.08	9	3.25	0.06	13	0.74	0.01	13	0.22	0.01	11	0.155	0.01	11	0.115	0.01
	11	1.43	0.08	11	3.26	0.05												
Sb*	9	1.20	0.12	9	3.22	0.08	14	0.75	0.01	14	0.22	0.01	12	0.145	0.01	11	0.12	0.01
	14	1.29	0.09	14	3.34	0.08												
Sbc*	13	1.03	0.06	13	3.26	0.06	17	0.74	0.01	17	0.23	0.01	9	0.155	0.01	8	0.12	0.01
	15	1.01	0.06	15	3.25	0.05												
Sc*	7	0.85	0.13	7	3.11	0.09	10	0.73	0.01	10	0.21	0.01	2	0.13	0.02	2	0.12	0.02
	8	0.81	0.12	8	3.13	0.08												
Scd, Sd*	3	0.62	0.10	3	2.91	0.06	8	0.72	0.03	8	0.18	0.01	3	0.11	0.02	2	0.09	0.02
	5	0.66	0.10	5	2.82	0.11												
Im	3	-0.05	0.05	3	2.22	0.05	3	0.60	0.02	3	0.23	0.05	1	0.105	-	1	0.115	-
I0	3	1.20	0.38	3	3.29	0.27	3	0.74	0.03	3	0.24	0.01	2	0.14	0.01	2	0.14	0.02
2.2 μm excess	8	1.24	0.13	8	4.17	0.22	12	0.94	0.03	12	0.41	0.01	11	0.10	0.01	10	0.17	0.01

* Upper U-V and V-K entries are for the restricted sample, and lower entries are for the full sample. See text for details.

Several results are apparent from Figures 10 - 13 and Table 9. First, the well-known U - V color-morphological type relation (de Vaucouleurs 1961; de Vaucouleurs and de Vaucouleurs 1972) is readily visible in Figure 10 and from column 2 of Table 9. Note, however, that considerable dispersion exists in the U - V color at a given morphological type. Second, excluding the 2.2 μm excess objects, the mean V - K color of spiral galaxies is the same as for ellipticals through types Sbc, where it then becomes increasingly bluer for types Sc to Im. The mean V - K color of the I0, galaxies is consistent with the interpretation from optical data alone that this class is more similar to disturbed, dusty, early-type galaxies than to type Im. While previous authors (e.g., Grasdalen 1975; Pacholczyk and Tarenghi 1975) have commented on the large scatter in V - K color for spiral galaxies, we note that for the restricted sample the scatter in V - K color at a given type is comparable with the nominal error. In particular, even for the full sample, at a given morphological type *the dispersion in V - K color is comparable with the dispersion in U - V color.*

Turning to Figures 12 and 13, we see that the mean J - H color as a function of morphological type is essentially constant, becoming significantly blue only for types Im. The mean H - K color is also mostly independent of morphological type, although middle spirals tend to have redder H - K colors than other types. The mean CO index remains constant with morphology through type Sbc, where it then appears to decrease, the mean CO index being only 0.118 ± 0.010 for six galaxies of type Sc or later, compared to a mean of 0.153 ± 0.008 for nine galaxies of type Sbc. On the other hand, the mean H_2O index appears to be less dependent on morphology than the CO index - the mean H_2O index for five galaxies of type Sc and later is 0.108 ± 0.012, compared to 0.122 ± 0.002 for eight Sbc galaxies. While the scatter at a given type in Figures 12 and 13 is generally comparable to the nominal errors, there are clearly some instances of real dispersion. Note particularly the broad band colors of the Magellanic irregular NGC 5253, which are extremely blue in all cases except H - K, whose value of 0.32 is quite *red*.

The agreement in mean UVK colors between the S0 sample in Paper I and in this paper (cf. Table 9) is reasonable given the peculiar way in which the latter sample is biased: Most of these galaxies were originally excluded from Paper I because they had been classified by Sandage (1976, private communication) as spirals. However, in the *RC2* these same galaxies are classified as S0, and for consistency we have adopted them as such.

The mean infrared colors for the galaxies with a 2.2 μm excess are substantially reddened in all cases. (The dichotomy visible in Figure 12 between this sample and the other galaxies is even more striking when just nuclear colors alone are plotted.) On the other hand, the U - V colors of galaxies in this sample cannot be well characterized, and in relation to their types, four are very red (NGC 253, 5128, 5909, and 6946), three are blue (NGC 1068, 1365, and 2146), and one (NGC 3628) has atypical color (cf. Figure 10).

The mean colors from Table 8 are presented as a function of Yerkes class in Table 10. The Yerkes form classification system (Morgan and Mayall 1957; Morgan 1958, 1959, 1962), which is based primarily on the degree of central concentration of the galaxian light, has been shown by Morgan to correlate closely with the mean spectroscopic stellar population. As Table 8 shows, the correlation Between the Yerkes and Hubble systems is not perfect. However, a comparison between Tables 9 and 10 indicates that the correlation between the infrared colors and either system is comparable.

Table 10. Mean Colors of Yerkes Classes *

Class	N	$(U-V)_c$	σ_m	N	$(V-K)_c$	σ_m	N	$(J-H)_c$	σ_m	N	$(H-K)_c$	σ_m	N	CO_c	σ_m	N	H_2O_c	σ_m
k	12	1.49	0.04	12	3.27	0.04	11	0.73	0.01	11	0.20	0.01	8	0.16	0.01	7	0.115	0.01
gk	5	1.35	0.06	5	3.33	0.07	11	0.75	0.01	11	0.23	0.01	9	0.15	0.01	9	0.115	0.01
	10	1.49	0.06	10	3.44	0.09												
g	9	1.19	0.09	9	3.32	0.07	13	0.74	0.01	13	0.22	0.01	11	0.145	0.01	11	0.12.	0.01
	12	1.18	0.07	12	3.31	0.05												
fg	4	1.11	0.10	4	3.19	0.11	8	0.75	0.01	8	0.24	0.01	5	0.165	0.01	5	0.13	0.01
	6	0.95	0.13	6	3.19	0.08												
f	10	1.02	0.10	10	3.24	0.08	13	0.74	0.02	13	0.22	0.01	5	0.135	0.01	3	0.12	0.00
	12	0.93	0.12	12	3.14	0.10												
af	3	0.71	0.05	3	2.97	0.04	3	0.76	0.03	3	0.22	0.03	-	-	-	-	-	-
a	4	0.33	0.19	4	2.67	0.25	7	0.68	0.02	7	0.20	0.01	3	0.100	0.01	3	0.095	0.01

* The mean colors given are based on the data in Table 8, excluding the 2.2 μm excess sample. For bins gk - f, upper (lower) U-V and V-K entries are for the restricted (full) sample.

Morgan and Osterbrock (1969) have spectroscopically characterized galaxian stellar populations by three general categories: the amorphous population (spectral type near K), present in ellipticals and the central bulges of early-type spirals; the intermediate population (spectral type near F). present in middle spirals and showing the largest degree of compositeness; and the Orion population (spectral type near B), present in irregulars rich in H II regions and blue giants. Furthermore, as with the Yerkes form system, the population does not correlate perfectly with Hubble morphology. For example, the mean spectral type for the two Sa galaxies NGC 2681 and 4594 are F5 and K0, respectively. The large scatter in U - V color at a.given morphological type commented on above would seem to partially reflect such population differences. However, Figures 12 and 13 and Tables 9 and 10 clearly indicate that *all galaxies whose central regions are dominated optically by a population ranging from amorphous to intermediate have similar stellar compositions in the infrared.*

---

[7] A weighted mean of the H_2O indices for each galaxy in Table 3 of Paper II was adopted. Back.

c) Color-Inclination Relations

Knowledge of internal absorption in galaxies is important for proper interpretation of color-aperture effects (Section IIIa), color-luminosity relations (Section IIId), stellar synthesis models (Section VI), and in determinations of the Hubble constant H_0 which use spiral galaxies as calibrators (Sandage and Tammann 1974;

Tully and Fisher 1977). Previous investigators (Holmberg 1958, 1969; Heidmann, Heidmann, and de Vaucouleurs 1971a, b) have attempted to calibrate intrinsic reddening with inclination angle, but the usefulness of these results has been questioned recently (Sandage and Tammann 1974; Tully 1972).

The ratio $E(V - K) / E(B - V) = 2.8$ given by the Van de Hulst reddening curve (Johnson 1968) implies that infrared photometry should be a very useful technique for investigating the behavior of color with inclination. *We caution that although the data in the present sample are both limited and severely biased by aperture effects, a preliminary investigation of this question seems worthwhile.*

Following Holmberg (1958), least square solutions were fit to color residuals as a function of two quantities, csc (i) - 1 and 1 - b / a, where i is the inclination angle and a / b is the major to minor axis ratio. csc(i) = a / b was adopted, as for an infinitely thin disk, and the values of a / b given in the *RC1* were used, which are partially corrected for projection effects (cf. Sandage and Tammann 1974). Note that in our-notation, $i = 90°$ for a face-on galaxy, and $i = 0°$ for an edge-on galaxy. Color excess residuals were formed for six morphological bins - E; S0; S0/a, Sa, Sb; Sb; Sbc; and Sc - using the data from Table 4 of Paper I and Table 8 of this paper. For each galaxy, U - V, V - K, and V - H color residuals were calculated by subtracting the mean colors for the particular morphological type, as given in Table 9 for the restricted sample, from the observed colors. Six galaxies (NGC 253, 1068, 1365, 2146, 3628, and 5907) with 2.2 μm excesses, and having V - K colors, were now included in the spiral bins. V - H was also solved for in addition to V - K because as is shown in Section V, the 2.2 μm light from some galaxies is probably affected by non-stellar emission. Finally, in the solutions for early-type galaxies data for the dwarfs NGC 205 and 404, and the Markarian galaxy NGC 7465, were excluded, as the very blue colors of these objects are clearly unrelated to inclination effects.

The results are presented in Figures 14 and 15, and in Table 11. In computing the quoted errors of the least-squares slopes, the error in the inclination parameter was adjusted to give a reduced chi-squared value of 1. The solutions for 1 - b / a can be compared directly with the calculations of Holmberg (1958). The "predicted Holmberg solutions" were found by first taking a weighted mean from Holmberg's Table 4, where values of the color-inclination slope are given for the color index C. I. on the international system. Adopting C. I. $\simeq B - V$, the Van de Hulst reddening curve (Johnson 1968) was then used to obtain the values given in Table 11.

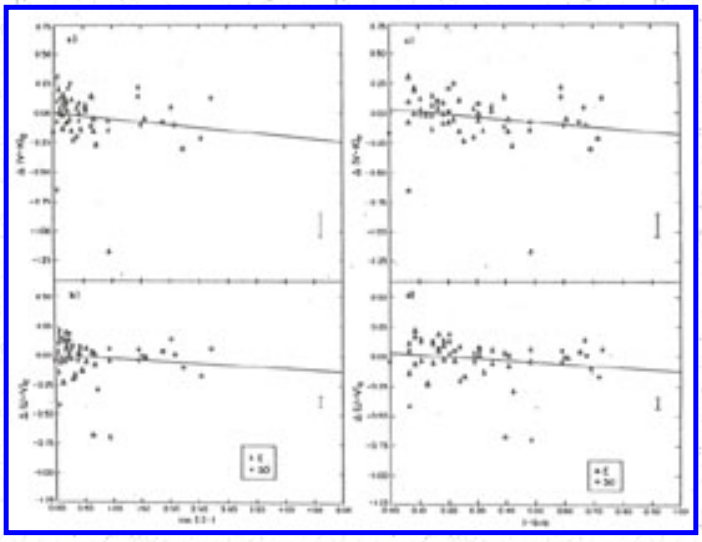

Figure 14. The U - V and V - K color residuals for the elliptical and lenticular galaxies from Table 4 of Paper I and from Table 8 of this paper are plotted against two inclination angle parameters: csc(i) - 1 and 1 - b / a. Also shown are the least squares fits to the data. The residuals for NGC 205, 404, and 7645, although plotted in the figure, has been excluded from the least square solutions. See text for further details.

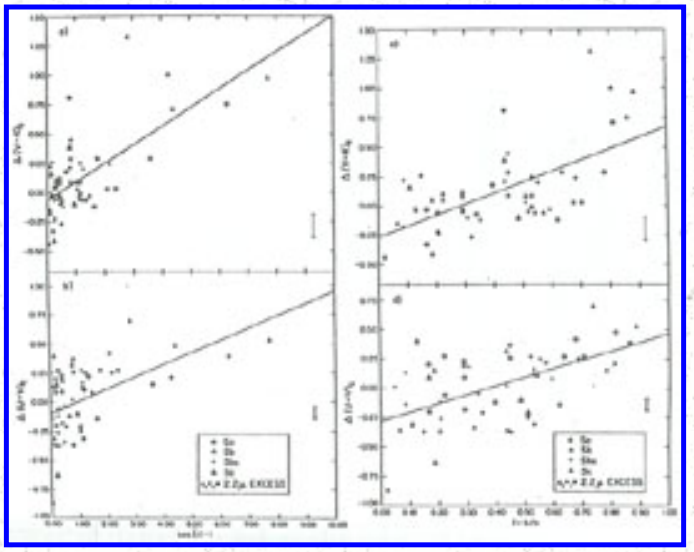

Figure 15. Same as Figure 22, for the spiral galaxy sample in Table 8.

The results in Table 11 show that a significant correlation exists between all colors and inclination angle in spiral galaxies, while only a marginal result is present for the E and S0 galaxies. The negative solutions for the E and S0's (i.e., bluer colors with smaller i) are apparently due to a slight dependence of inclination on absolute magnitude in the sample.

Table 11. Color-Inclination Correlations

		$\Delta U - V$		$\Delta V - K$		$\Delta V - H$			
	N	Slope	R	Slope	R	Slope	R	$(\text{Slope})_{V-K}$ / $(\text{Slope})_{U-V}$	$(\text{Slope})_{V-K}$ / $(\text{Slope})_{V-H}$
Solutions with csc(i) - 1									
E-S0	53	-0.03 ± 0.02	0.18	-0.05 ± 0.03	0.25	-0.04 ± 0.03	0.23	1.7	1.2
Sa-Sc	54	0.10 ± 0.03	0.52	0.16 ± 0.02	0.69	0.14 ± 0.02	0.71	1.6	1.1
Sa-Sc, i > 17.°5 only	47	0.20 ± 0.07	0.39	0.125 ± 0.06	0.30	0.12 ± 0.05	0.34	0.6	1.0

		Solutions with 1 - b/a							
E-S0	53	-0.12 ± 0.07	0.22	-0.19 ± 0.09	0.29	-0.18 ± 0.08	0.29	1.6	1.1
Sa-Sc	54	0.75 ± 0.16	0.56	0.95 ± 0.17	0.62	0.87 ± 0.14	0.65	1.3	1.1
Sa-Sc, Predicted Holmberg	155	0.24	-	0.39	-	0.36	-	-	-
Sa-Sc, $i > 17.°5$ only	47	0.62 ± 0.21	0.39	0.45 ± 0.17	0.36	0.44 ± 0.15	0.41	0.7	1.0

* The least-squares slope Δ(color residual) / Δ(inclination parameter) is given for two measures of inclination, csc(i) - 1 and 1 - b / a. R is the correlation coefficient. See text for further details.

The ratios in the last two columns of Table 11 are consistent, within the statistics, with the values expected from the Van de Hulst curve, which are 1.6 for $U - V / V - K$, and 1.1 for $V - K / V - H$. However, our results are 2 to 3 times larger than the predicted Holmberg solutions. We interpret this difference as due at least partly to an aperture effect: The Holmberg data are corrected to a value of $\log A / D_0 \simeq 0.2$, while our own data are mostly at $\log A / D_0 \simeq - 0.6$. Because highly reddened galaxies tend to have strong color gradients (Section IIIa), the size of the color-inclination effect is expected to be inversely correlated to the diameter of the projected aperture.

Holmberg (1958) found that the size of the color-inclination effect decreased in going from early to late type spirals. To check this, we have calculated least square solutions for the individual galaxy bins separately. Unfortunately, owing to the small and differing number of highly inclined objects in each bin, the answers were somewhat ambiguous, and Holmberg's result could not be reproduced.

Figures 14 and 15 also illustrate a point discussed in Section IIIb, namely, that galaxies with a significant 2.2 μm excess - as measured by their JHK colors - are not necessarily distinguished by their UVK colors. On the other hand, the two highly inclined spirals NGC 4565 and 5746, which have fairly normal JHK colors and only slightly reddened U - V colors, have V - K,excesses comparable to the galaxies with 2.2 μm excesses. We shall come back to this point in Section V.

If the spirals are excluded for which $1 - b / a > 0.7$, or $i < 17.5°$, the significance of the color-inclination effect decreases in all cases. The data are in fact consistent with an interpretation in which the effect is important only for highly inclined galaxies, a conclusion consistent with the results of Holmberg (1958, 1969). *We thus consider it inappropriate to attempt any correction of the colors for inclination.*

d) Color-Absolute Magnitude Relations

In Figure 16 we have plotted various colors of spiral galaxies against absolute magnitude M_V. The latter was determined as in Paper I: Values of V at $A / D(0) = 1$ were obtained from the *RC1*, redshifts corrected for motion relative to the Local Group of galaxies were taken from the *RC2*, and a value of $H_0 = 50$ km/sec/Mpc was assumed. For galaxies in small groups (de Vaucouleurs 1975), the mean redshift of the group was used, but all galaxies in the Virgo cluster were assigned the same redshift, and the distance moduli for local group galaxies

(NGC 224, 598) were obtained from van den Bergh (1975).

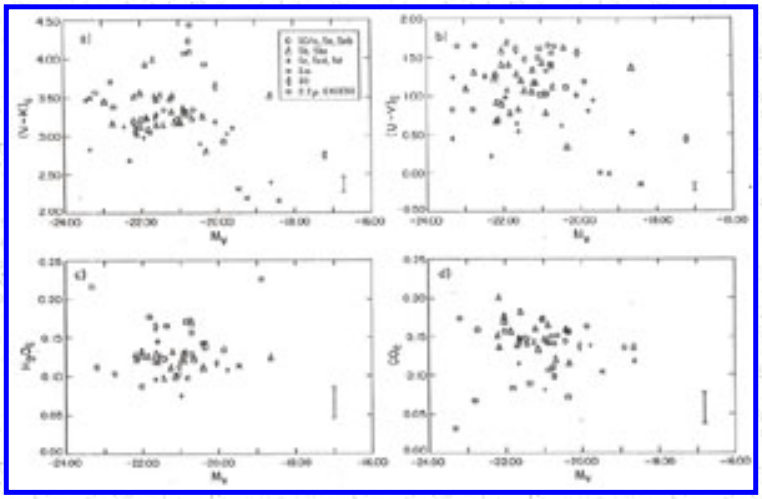

Figure 16. Various colors for the sample of spiral galaxies in Table 8 are shown as a function of absolute magnitude.

In Table 12 we have compared least square solutions of the various colors with absolute magnitude for both ellipticals and spirals. The E - S0 group includes the data from Papers I and II and the S0's from this paper. For the S0/a - Sd group, the full sample is used for the CO and H_2O solutions, while the restricted sample is used for the broad-band color solutions. Since the upper limit of M_V for types Im is about -20 (van den Bergh 1977), to avoid introducing a false correlation these types were excluded from the solutions.

Table 12. Correlations with Absolute Magnitude *

	All E and S0 ($-23.5 \lesssim M_V \lesssim -13.5$) †	S0/a-Sd ** ($-23.5 \lesssim M_V \lesssim -18.5$)
N	56	41
b_{U-V}	-0.06(± 0.02)	-0.03(± 0.05)
R	0.62	0.08
N	56	41
b_{V-K}	-0.07(± 0.02)	-0.02(± 0.03)
R	0.62	0.12
N	50	37
b_{CO}	-0.0.06(± 0.015)	-0.009(± 0.035)
R	0.59	0.40
N	36	34

b_{H_2O}	-0.0.06(± 0.029)	0.002(± 0.041)
R	0.46	0.11

---

* Least-squares solutions b_{color} are given for the relation (*color*) = $b_{color} \times M_V$ + *constant*. *R* is the correlation coefficient.

† For H_2O only, $-23.5 \lesssim M_V \lesssim 18$.

** Full sample for CO and H_2O, restricted sample for U-V and V-K.

In Paper I a correlation for early-type galaxies between V - K and M_V was found comparable to the well-known correlation between U - V and M_V (de Vaucouleurs 1961; de Vaucouleurs and de Vaucouleurs 1972; Sandage 1972). For spirals, we find no significant correlation with M_V in either color (Table 12). Solutions were also found for three subsets of the spiral sample - S0/a, Sa, Sab, Sb, Sbc; and Sc, Scd, Sd - but again no significant correlations were discovered. These results are consistent with the lack of correlation between optical colors and luminosity found by de Vaucouleurs and de Vaucouleurs (1972) for a much larger sample of spirals. Finally, no significant correlation between the CO and H_2O indices and luminosity is found for either spirals or ellipticals, a result perhaps expected in view of the severe restriction of the samples at the faint end.

e) Color-Color Relationships

i) CO and H_2O Indices

The CO and H_2O indices for the spiral galaxy sample in Table 8 are plotted against U - V color in Figure 17, against V - K color in Figure 18, and against J - H and H - K colors in Figure 19. In Figure 20 we show the H_2O index plotted against the CO index. The mean stellar color relations in these figures are adopted from Paper I, and transformed to the HCO system (Section IIg and Appendix A).

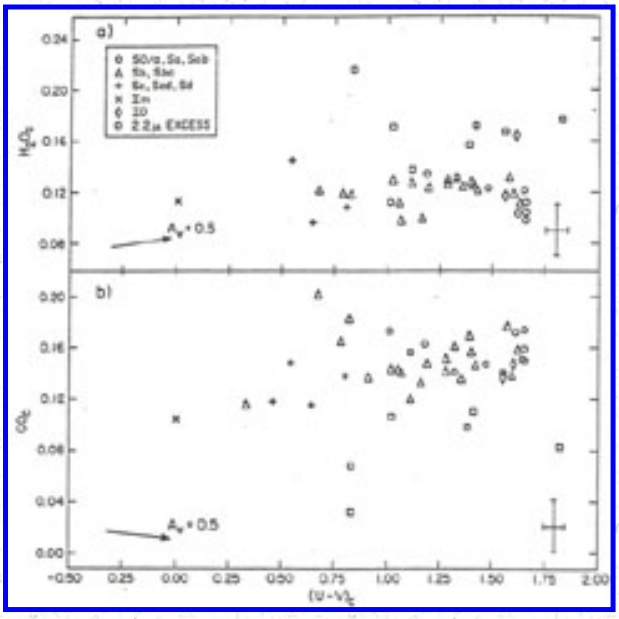

Figure 17. The H_2O and CO indices are plotted against U - V for the spiral galaxy data in Table 8.

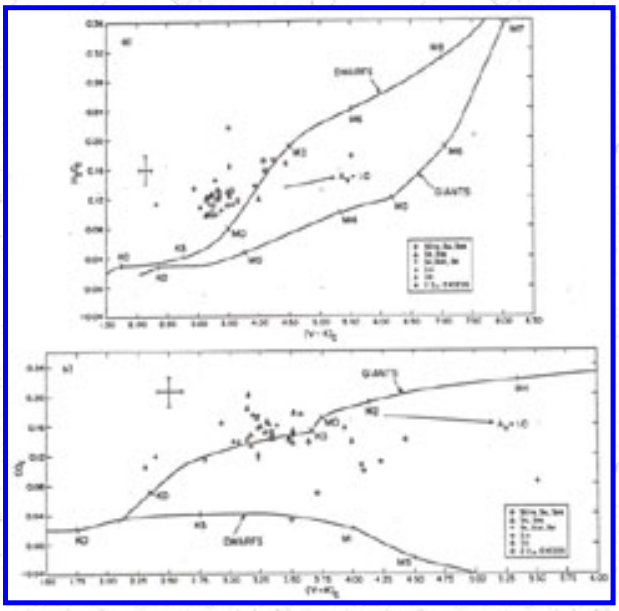

Figure 18. The H_2O and CO indices are plotted against V - K for the spiral galaxy data in Table 8. Also shown are the mean color relations for dwarf and giant stars.

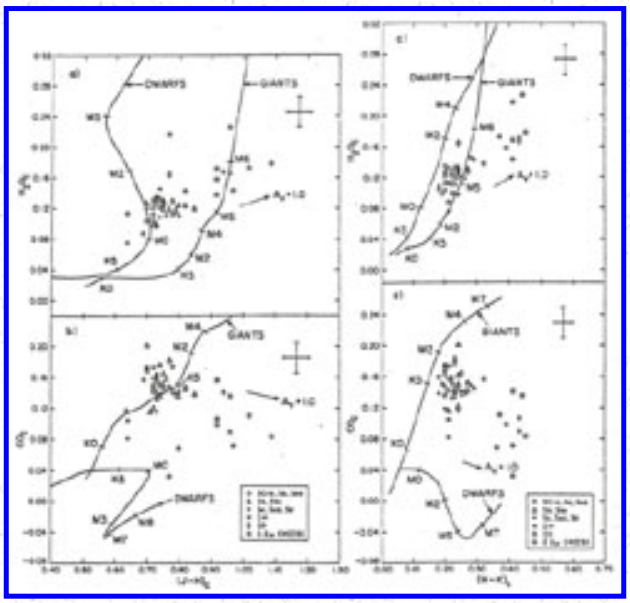

Figure 19. The H_2O and CO indices are plotted against the J - H and H - K colors for the spiral galaxy data in Table 8. Also shown are the mean color relations for dwarf and giant stars.

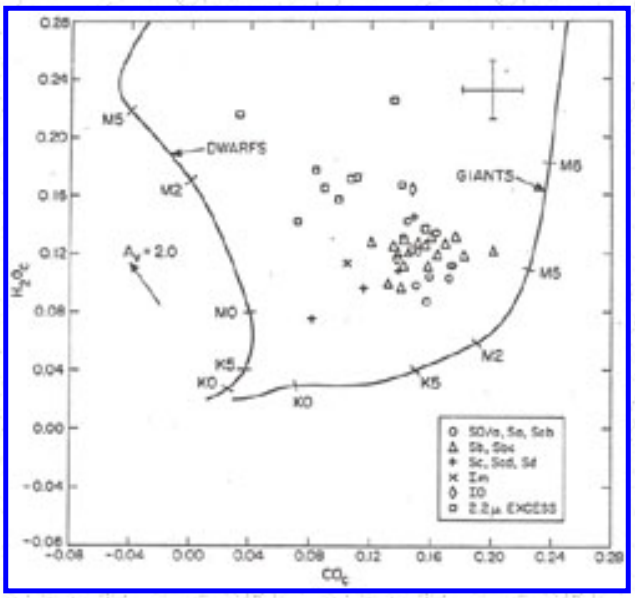

Figure 20. The H_2O index is plotted against the CO index for the spiral galaxies in Table 8. Also shown are the mean color relations for dwarf and giant stars.

As expected from the similarity of mean colors between spirals and ellipticals, the appearance of these plots is generally the same as in similar plots for early type galaxies presented in Papers I and II: First, the CO indices of the sample indicate that the 2 μm light is dominated by giant stars. Second, the H_2O indices show that at 2 μm a significant number of these giants are late M in spectral type. Third, Figures 17 - 20 illustrate the composite nature of the galaxian flux, in that the mean giant colors of V - K, J - H, CO, H - K, and H_2O correspond to spectral types K4, K4, K6, M3, and M5. Thus, as the observational baseline shifts redward, so does the dominating stellar component. This effect, discussed also by Stebbins and Whitford (1948), explains the general displacement of the points in the figures from the mean giant star relations. For two colors dominated by a similar mean stellar component, this displacement will be small (e.g., Figures 18b, 19b, c); for two colors dominated by different mean stellar components, the displacement will be large (e.g., Figures 18a, 19a, 20). Similarly, the CO and H_2O indices in Figure 17, which are determined by the reddest stars, depend very weakly on the U - V color, which is determined by the bluest stars.

As expected from Table 9, there is little segregation with morphological type in these figures, and the scatter of points is generally comparable with the measuring errors, except for 1) the 2.2 μm excess objects, which are well separated from the other galaxies in roughly the direction of the reddening line, and 2) the small number of late-type galaxies with bluer colors and smaller narrow-band indices.

ii) The JHK Plane

In Figure 21 we have plotted the J - H color against H - K. The JHK colors alone provide little information on the giant-to-dwarf ratio. However, since the strength of the CO absorption requires a giant dominated spectrum, the displacement of points from the mean giant line can again be understood as being due to the composite nature of the giant branch. We again see as before the separation of the 2.2 μm excess objects in the figure. There is also a large scatter in the remaining points, due partly to residual reddening, and partly to the blue

colors of late-type galaxies.

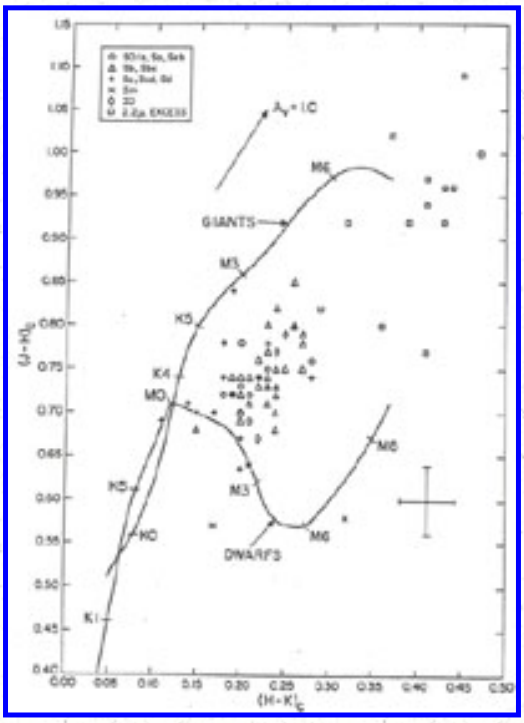

Figure 21. The J - H color is plotted against H - K for the spiral galaxies in Table 8. Also shown are the mean color relations for dwarf and giant stars.

iii) The UVK Plane

In Figure 22 the U - V color is plotted against V - K for all galaxies in Table 4 of Paper I and in Table 8 of this paper, and for the globular clusters in Table 2 of Paper I. There are two significant results apparent from this figure. *First, as we advance in morphological type, the galaxies fall along a generally well-defined and continuous sequence. Second, this morphological sequence is well separated from the sequence defined by the dwarf ellipticals and globular clusters.* The second result cannot be due to just an internal reddening effect, since as Figure 22 shows, the reddening line is essentially parallel to the elliptical galaxy sequence.

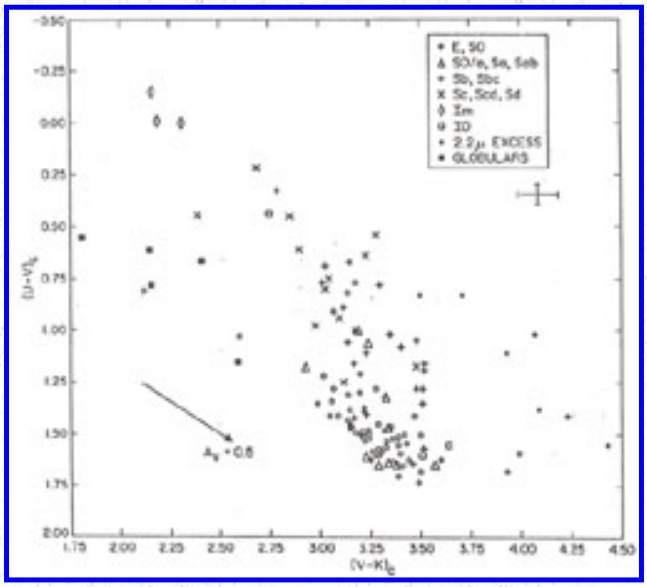

Figure 22. The U - V color is plotted against V - K for all galaxies in Table 4 of Paper I and Table 8 of this paper, and for the globular clusters in Table 3 of Paper I. The point for NGC 5128 lies off the plot.

IV. DISCUSSION

In this section we shall attempt to interpret the color-color and color-aperture results presented above in terms of simple stellar population and/or metallicity considerations.

a) Integrated Colors

The bifurcation seen in Figure 22 between the elliptical and morphological galaxy sequences indicates that a fundamental difference exists between the two distributions. That the former is probably a metallicity sequence was shown in Paper I, where it was found that 1) the V - K color depended on luminosity to as comparable a degree as the U - V color, and 2) the elliptical galaxy distribution in a UVK color-color plot was continuous with a globular cluster sequence that was ordered by metallicity (cf. Figure 22). Previous studies of optical line indices by McClure and van den Bergh (1968) and by Faber (1973) also indicated that the UBV color-luminosity relation in ellipticals (e.g., de Vaucouleurs 1961; de Vaucouleurs and de Vaucouleurs 1972; Sandage 1972) is most likely explained by an increase of mean metallicity with luminosity. (Further discussion of the relation between UVK colors and metallicity is given in Appendix C.)

On the other hand, the spectroscopic work of Morgan (Section IIIb) clearly demonstrates that the UBV color-morphological distribution of galaxies is primarily a stellar population sequence. We shall show that simple populations changes can also account for the nature of the morphological sequence apparent in Figure 22.

In Figure 23a we have plotted the mean U - V and V - K colors from Table 9, using values for the restricted sample only far types Sa - Sd. The heavy line connecting these points is labelled log A / D_0 = - 0.6. Also shown

is a second sequence labelled log $A / D_0 = -0.2$, which at a projected aperture size corresponding approximately to Palomar Observatory Sky Survey spiral galaxy diameters, is more representative of the total integrated galaxian light. This latter sequence was determined as follows: For V - K, an extrapolation was made using values at log $A / D_0 = -0.6$ and the mean color gradients from Table 7. For U - V, integrated colors from a compilation by Huchra (1977a), were used. These values, based on a sample of data from de Vaucouleurs (1961) about three times larger than the present one, and requiring little aperture extrapolation, are corrected for reddening and redshift (but not for inclination effects) using essentially the same relationships as in this paper. If we instead extrapolate the mean U - V colors from Table 9 to log $A / D_0 = -0.2$ using the color gradients in Table 7, the difference $(U - V)_{extrapolated} - (U - V)_{Huchra}$ is 0.00, 0.03, 0.14, 0.12, 0.10, 0.13, 0.07, and -0.11 for galaxy types E, S0, S0/a - Sab, Sb, Sbc, Sc, Scd - Sd, and Im, respectively. While the agreement is encouraging, the U - V colors of our spiral sample do appear to be systematically 10% redder than in Huchra's larger sample, a result we believe is compatible with the allowable sampling error.

Figure 23a shows that the mean integrated V - K color remains essentially constant from types E to Sbc, changing by only 0.08 mag; whereas the U - V color changes by 0.66 mag over this same range. However, from types Sbc to Im, the V - K color changes by 0.85 mag, while the U - V color now changes by only 0.56 mag. This behavior can be well understood in terms of the composite effect of mixing red and blue stars. This point is illustrated in Figure 23b where we have plotted a "mixture line" obtained by combining together various proportions of an A0 dwarf (U - V = V - K = 0.) and an MO giant (U - V = 3.43, V - K = 3.74). At the tick mark labelled 0.2, 200 of the V light is contributed by the dwarf; at 0.3, 30% is from the dwarf, etc. Also shown in the figure are the mean integrated colors from Figure 23a at log $A / D_0 = -0.2$. Our simple two component model reproduces the morphological sequence quite well: As we add blue colors to a red object, the blue color of the composite mixture is primarily affected - from 0.2 to 0.5 along the mixture line, $\Delta U - V = 0.7$ and $\Delta V - K = 0.3$. Similarly, as red colors are added to a blue object, the red color of the composite mixture is primarily affected - from 0.8 to 0.5 along the mixture line, $\Delta U - V = 0.5$ and $\Delta V - K = 1.0$. We de not consider the systematic difference between the mixture line and the early-type galaxies significant in view of the simple nature of the model.

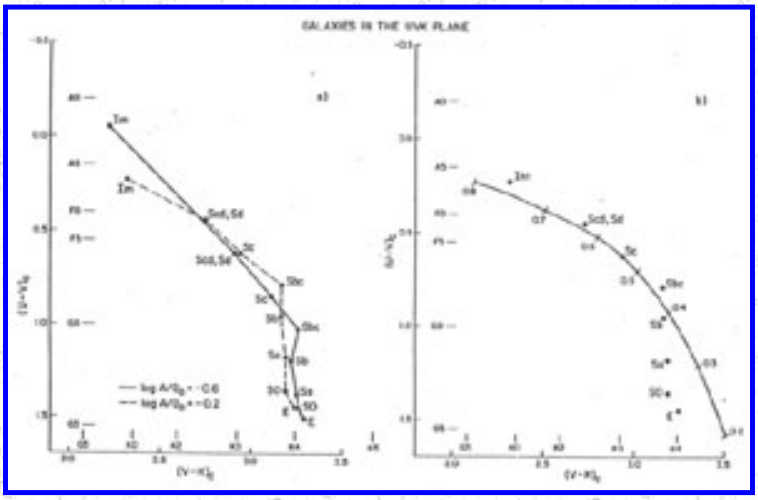

Figure 23. a) The mean U - V and V - K colors as a function of morphological type are shown for the restricted sample of galaxies from Table 8 in this paper, and for the galaxies in Table 4 of Paper I, for two values of log A / D_O. The horizontal and vertical spectral type scales are for giant stars and are adopted from Johnson (1966a). See text for further details. b) The heavy line shows the locus of various mixtures of an A0 V and an MO III star. At the tick mark labelled 0.2, 20% of the light at V is contributed by the dwarf star; at 0.3, 30% of the V light is from the dwarf star, etc. Also shown are mean integrated colors at log A / D_0 = - 0.2, grouped by morphological type as in Figure 23 a).

Our two-component model is also generally consistent with the relation of purely infrared colors with morphological type, as the following table shows:

V flux	J - H	H - K	CO
100% M0 III	0.79	0.16	0.17
50% M0 III, 50% A0 V	0.75	0.15	0.16
20% M0 III, 80% A0 V	0.65	0.14	0.15

The model predicts that only in the latest-type galaxy will the J - H color become blue, while the H - K color, still dominated by the M giant, will not change significantly, in agreement with the results in Tables 9 and 10. However, the model does not appear to adequately account for the apparent decrease in the CO index seen in the latest-type galaxies (Tables 9 and 10).

There are two ways a decrease in the CO index can occur: either the giant branch luminosity function becomes dominated by hotter stars, or the giant-to-dwarf ratio changes. The first effect will lower both the CO and H_2O indices and result in bluer J - H and H - K colors; while the second effect will lower just the CO index, actually *raise* the H_2O index, give a bluer J - H color, and leave the H - K color-relatively unchanged - as the mean stellar relations in Figures 18 - 21 indicate. If both effects are operating, the CO index and J - H color will decrease significantly more than the H_2O index or H - K color, which is just what is observed. In particular, the two (non 2.2 μm excess) galaxies in Table 8 with the smallest CO indices, NGC 4449 and 4490, are also the two latest galaxies morphologically for which the narrow-band indices were measured. The mean CO index of these two galaxies, 0.095, is ~ 6% less than in earlier-type galaxies; while the mean H_2O index, also 0.095, is only ~ 2% lower than in earlier-type galaxies.

Now recent evolutionary studies of galaxies based on theoretical stellar tracks (e.g., Tinsley 1972; Searle,

Sargent and Bagnuolo 1973; Huchra 1976; Larson and Tinsley 1977) suggest that all galaxies are approximately the same age, but differ in the time dependence of their star formation rates. In elliptical galaxies, the bulk of star formation is thought to have occurred within a short period (~ 10^9 years), some 10^{10} years ago; while in the latest-type spirals, the star formation is believed to be roughly uniform over the galaxian lifetime. In the latter case, both effects discussed above for lowering the CO index will be operating: First, the high mass objects from newborn generations that are dominating the light spend a proportionately smaller part of their lifetimes as evolved M stars; while second, many successive generations of M dwarfs will have piled up along the main sequence. On the other hand, the high mass stars will lead to a larger proportion of supergiants among the evolved M stars that *are* present, which will act to raise the narrow-band indices (Appendix A). The ultimate effect on the narrow-band indices is thus uncertain. Clearly, both detailed evolutionary models, and a significant increase in the observational material for late-type galaxies, would be of interest.

Published evolutionary star formation models (cf. Huchra 1977; Larson and Tinsley 1977) are largely based on UBV colors alone, and so, for instance, cannot well distinguish between truly young galaxies, and older galaxies with a recent star formation burst. Such models also have difficulty in disentangling metallicity and/or reddening effects, since these tend to parallel the UBV color-morphology sequence. The appearance of Figure 22 suggests that studies of star formation in the UVK plane, or in UBVK space, should prove very fruitful.

b) Color Gradients

Radial UVK color gradients found in Paper I for ellipticals and in this paper for early-type spirals, coupled with observations of radial CN gradients (Welch and Forrester, 1972; McClure, 1969; Spinrad et al., 1971; Spinrad, Smith, and Taylor, 1972) suggest the presence of metallicity gradients in galaxies dominated by an amorphous population. Now both the mean U - V and V - K color gradients in galaxies of type Sa are similar to those in E and S0 galaxies (Table 7). However, the large increases in the U - V gradient for types Sb and Sbc probably reflects the color transition from the red bulge component to the blue disk component, rather than metallicity effects. That the mean V - K gradients in these types (and in the bin labelled "blue" in the last line of Table 7) are smaller than the population-driven U - V gradients can again be understood as the composite result of mixing red and blue objects. In this case, as emission from blue disc stars (and perhaps gas) is introduced to the red bulge component, blue colors (i.e., U - V) are primarily affected. In fact, the mean V - K gradient in the Sb sample is similar to that in earlier-type galaxies, and may thus be indicative of a comparable metallicity change in the bulge component. Tifft's (1963) suggestion that color gradients in early type spirals result from a radial increase in dust absorption' does not seem tenable, since from the reddening law we would expect $\Delta V - K / \Delta U - V > 1$, which is in fact seen for only 20% of the total S0/a - Sbc sample.

Unfortunately, straightforward interpretation of the UVK gradients in the latest-type galaxies is difficult in view of the large dispersion of color gradient means.

The lack of radial gradients in the JHK colors for the spiral galaxy sample (Table 7) suggests that radial population and/or metallicity changes are most evident at wavelengths shortward of 1.2 μm. The large J - K gradient found in Paper I implied just the opposite to be true for E and S0 galaxies. However, the latter result seems difficult to understand in light of recent globular cluster measurements (Appendix C) which indicate that a metallicity driven color gradient should lead to $\Delta J - K / \Delta V - K \simeq 0.3$, whereas in Paper I we found $\Delta J - K / \Delta V - K \simeq 1.1$. As discussed in Section II, serious systematic errors may be present in the J measurements. On

the other hand, the possibility exists that linearly extrapolated calibrations based on metal-pool galactic globular clusters are simply inadequate for describing metal-rich systems.

V. NON-STELLAR EFFECTS

The large color gradients found in galaxies with 2.2 μm excesses imply that the source of the excess is located primarily within the nucleus. In the following discussion we shall assume that the galaxian flux can be decomposed into a nuclear source with an infrared excess, and an extended source with normal galaxy colors. For these fiducial colors we adopt 3.3, 0.74, 0.20, 0.16, and 0.12 for V - K, J - H, H - K, CO and H_2O, respectively, which are appropriate values for all but very late-type galaxies (Table 9). We shall first briefly discuss the various non-stellar effects to be compared with the data. Note that the color of the different emission mechanisms to be considered were calculated by adopting the flux calibration of Wilson et (1972) for JHK, and the flux calibration of Johnson (1966a) for U and V. For the CO and H_2O indices, it was assumed that at the effective wavelengths of the narrow band filters given in Table 2, α Lyr could be represented by a 10000 K black body.

a) Dust Absorption

For purely absorbing (zero albedo) dust, completely external to the emitting source, we have

$$I_\nu = I_0 e^{-\tau_\nu}. \tag{1}$$

For dust that is uniformly mixed with the emitting source,

$$I_\nu = \frac{I_0}{\tau_\nu}(1 - e^{-\tau_\nu}). \tag{2}$$

In both eq. (1) and (2) τ is the optical depth of the dust and I_0 is the intensity of the emitting source if no dust were present. For $\tau\nu$ we adopt the Van de Hulst reddening curve (Johnson 1968), which is essentially the same reddening curve discussed by Whitford (1956). Note that for small values of $\tau\nu$, the reddenings given by eqs. (1) and (2) are similar. Observational evidence for reddening from "well-mixed" dust has been presented by Leibowitz (1973) in galactic planetary nebulae, by O'Connell (1970) in the galaxy NGC 3034 (M82), and by Turnrose (1976) in the galaxy NGC 2903.

b) Dust Emission

For emission by dust grains, we have

$$I_\nu = \epsilon_\nu B_\nu(T).$$

The dust is expected to be a combination,of graphite and silicates, with emissivity $\epsilon \propto 1/\lambda^x$, and $0 \lesssim x \lesssim 3$ (Werner and Salpeter 1969, Aannestad 1975). We assumed $x = 2$, as for a uniform conducting sphere of radius

a, with $a << \lambda$ (Van de Hulst 1946).

c) Gaseous Emission

For optically thin free-free emission, we have simply

$$I_\nu \propto e^{-h\nu/kT} / \sqrt{T}.$$

Thermal emission from gas, as in a typical H II region, includes free-free, free-bound, bound-bound, and two photon processes. We have assumed T_e = 8000 K, and calculated the gaseous JHK colors from the formulae in Willner, Becklin, and Visvinathan (1972). The V - K color was calculated using the absolute magnitude calibration in Huchra (1977b) appropriate for Huchra's standard line ratio set, composed of mean line ratios in LMC H II regions and Orion. The U - V color was also adopted from Huchra (1977b). The CO and H_2O indices appropriate for an H II region were estimated by interpolation of the broad-band gaseous flux dependence. The adopted final colors are given in Table 13.

Table 13. Table 13. Adopted Gaseous Emission Colors

U-V	-0.87
V-K	0.56
J-H	0.43
H-K	0.70
CO Index	-0.12
H_2O Index	0.18

It is well known that gaseous excitation conditions differ between the nuclear and outer regions of spiral galaxies (Morgan and Osterbrock 1969; Spinrad and Peimbert 1975). The purely infrared colors, being mostly unaffected by line emission, are largely insensitive to excitation changes (Willner et al. 1972). However, 70% of the gaseous V flux is contributed by line emission , while-only 30% is from the continuum (Huchra 1977b), and the same is not true for the UVK colors. Nevertheless, the colors in Table 13 will not differ by more than 30% for reasonable excitation variations (Huchra 1977b) and are thus of sufficient accuracy for the purposes of this discussion. Note that the gaseous H - K color is considerably redder, while the gaseous J - H color is considerably bluer, than typical galaxy JHK colors.

d) Non-Thermal Emission

For a pure non-thermal spectrum, we adopt

$$I_\nu = I_0 \nu^{+n}$$

In a color-color diagram, the locus of different n values is then a straight line.

e) Discussion

The different non-stellar effects discussed above are illustrated in Figures 24 and 25, where various colors are plotted against H - K, our primary indicator of a galaxian 2.2 μm excess. (The V - H rather than V - K color is plotted in Figure 25c to avoid false correlation with H - K.) Also shown are the multiaperture data from Tables 3 and 5 for galaxies with a 2.2 μm excess, for the anomalously colored galaxy NGC 5253, and for the two Sb galaxies with largest inclination angle, NGC 4565 and 5746. Morphologically, the 12 galaxies in the 2.2 μm excess sample include 6 spirals (NGC 253, 891, 3079, 3628, 4631, and 5907) with large inclination angle, 3 objects (NGC 2146, 3034, and 5128) of a distinctly peculiar morphological character, and three comparatively normal looking galaxies (NGC 1068, 1365, and 6946). The relatively normal colors of such galaxies as NGC 520, 2976, 4490, and 5195 suggest that morphological peculiarities alone do not lead to a large 2.2 μm excess.

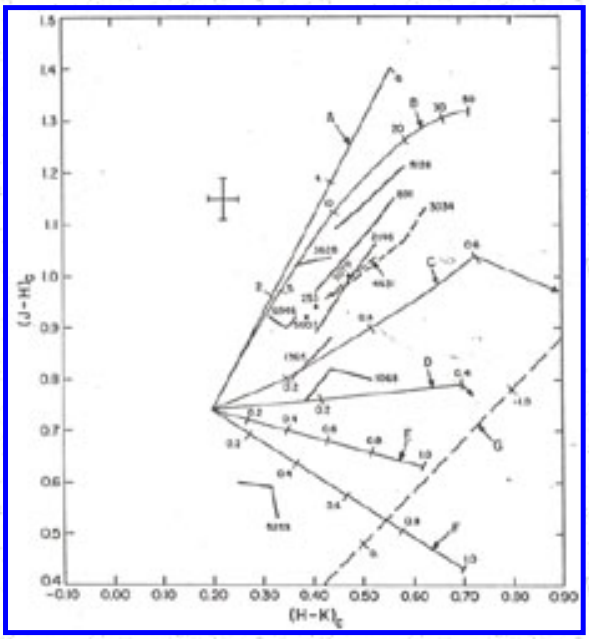

Figure 24. The J - H color is plotted against H - K for the galaxies with a 2.2 μm excess, using the data from Table 3. Also shown is the anomalously colored galaxy NGC 5253. Using fiducial colors of J - H = 0.74 and H - K = 0.20, various non-stellar effects have been illustrated and are denoted as follows: A - reddening from a dust screen, labelled by optical depth at V, τ_V. B - reddening from dust completely mixed with the stars, labelled by τ_V. C - dust emission with emissivity $\epsilon \propto 1 / \lambda^2$ and temperature T = 600 K; labelled by the fractional contribution of the dust to the 2.2 μm light. The arrow points to the position

the tick mark labelled 0.6 would have for dust with grey body emissivity. D - same as C, but for dust with T = 1000 K. E - the effect of increasing the contribution from free-free emission with T_e = 20000 K to the 2.2 μm light. F - the effect of increasing the contribution from "H II region" emission with T_e = 8000 K to the 2.2 μm light. G - a pure power law spectrum labelled by n, where $I\nu \propto$. See text for further details.

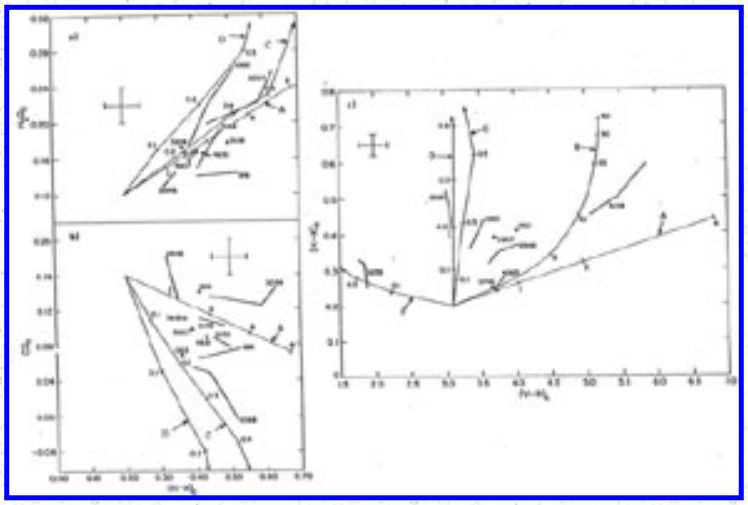

Figure 25. - a) and b) The CO and H_2O indices are plotted against H - K color for galaxies with a 2.2 μm excess, using the data in Table 3. Using fiducial values of CO index = 0.16, H_2O index = 0.12, and H - K = 0.20, the non-stellar effects illustrated are: A - reddening from a dust screen. C - dust emission, with T = 600 K. D - dust emission, with T = 1000 K. The tick marks and arrows have the same meaning as in Figure 24. c) The H - K color is plotted against V - H for the galaxies with a 2.2 μm excess using the data in Tables 3 and 4. Also shown is the anomalously colored galaxy NGC 5253, and two Sb galaxies of large inclination angle, NGC 4565 and 5746. Because the H - K and V - K colors for NGC 5746 are referred to different apertures, the point plotted for this galaxy is only a limit, in the sense suggested by the arrow. Using fiducial values of H - K = 0.2 and V - H = 3.1, the various non-stellar effects illustrated are: A - reddening from a dust screen. B - reddening from dust well-mixed with the stars. C - dust emission with T =

600 K. D - dust emission with T = 1000 K. F - H II region emission. The tick marks and arrows have the same meaning as in Figure 24.

It appears from Figures 24 and 25 that the Van de Hulst reddening curve does not adequately fit the color excesses. There are several ways to account for the discrepancies:

First, the Van de Hulst curve may simply not apply in external galaxies. However, no physically plausible reddening curve could reproduce the color residuals in at least two galaxies, NGC 1068 and 1365. Furthermore, color residuals in the two highly inclined spirals NGC 4565 and 5746, with V - H excesses comparable to those in most of the 2.2 μm excess objects, are well matched by the Van de Hulst curve. The bulge-to-disc ratio in these two galaxies are larger than in the other objects, and so in this respect are better fit by the simple dust screen model.

A second possibility is that the assumed fiducial colors are inappropriate. However, the intrinsic colors which would produce agreement, J - H $\simeq$ 0.6 and V - H $\simeq$ 1.0, are far too blue.

A third possibility is that as the wavelength is decreased, the flux is weighted more and more by unobscured stars, while as the wavelength is increased, the flux is weighted more and more by regions that are visually optically thick. Under these circumstances, the value of A_V calculated for a given color residual will increase as the baseline shifts redward - which is precisely the effect observed. For instance, the color residuals E(V - H), E (J - H), and E(H - K) for the group of galaxies NGC 253, 5907, and 6946 lead to A_V values of ~ 1, 2, and 3, respectively. Simple numerical models indicate that for small values of central source reddening ($A_V \lesssim 3$), E(V - H) / E(J - H) $\simeq$ E(V - H) / E(H - K) $\simeq$ 2, while much larger values of central source reddening ($A_V \sim 10$) are required to produce E(H - K) / E(J - H) $\simeq$ 1.5. It thus seems likely that this effect plays a role in Figure 25c, but not in Figure 24.

The final possibility we shall consider is that one of the emission mechanisms discussed above is occurring. Now the colors in Table 13 rule out any significant contribution from H II region emission. For instance, using the data for NGC 253 as an example, if the measured JHK colors are a combination o,f a normal stellar component (U - V ~ 1., V - K ~ 3.3) and an H II region contributing about 20% of the 2.2 μm flux, all reddened by $A_V = 2$, the resulting U - V color should be ~ 0.5, as opposed to the observed value of 1.5. Similar problems occur in trying to fit the other color residuals. Furthermore, even in the bluest Markarians, galaxies which are optically the most dominated by gaseous emission, the contribution to the V flux by such emission is no more than 30% (Huchra 1977b), which amounts to only a 1% contribution at 2.2 μm.

The presence of a dust emission component can well. account for the displacement of the points in both Figures 24 and 25, and seems an especially appealing explanation for the color residuals in three galaxies - NGC 1068, 1365, and 5253. Published 3.5 μm, 5 μm, 10 μm, and 20 μm photometry is available for some of the galaxies measured in this paper (e.g. Rieke and Low 1972; Kleinmann and Wright 1974; Becklin et al. 1971; Becklin, Fomalont, and Neugebauer 1973; Glass 1973, 1976; Penston et al. 1974), including six of the galaxies in Figure 24 - NGC 253, 1068, 3034, 5128, 5253, and 6946. In fact the first five of these objects are among the brightest 10 μm extragalactic sources known, so there is clearly some correlation between H - K color excess and 10 μm

emission. If the infrared radiation is in fact due to dust, the 2 - 10 μm spectra can generally not be fit by a single blackbody temperature, implying instead a dust shell with a range of temperatures, in analogy with galactic H II regions (cf. Becklin and Wynn-Williams 1974). Now the dust temperatures implied by the JHK excesses are in the range 600 - 1000 K, but because of uncertainties in A_V, unambiguous color temperatures cannot be formed. The K - L (3.5 μm) color would be very useful in this respect, but the available data is mostly at much smaller aperture sizes and much lower statistical accuracy than are the observations in this paper. Nevertheless, in all cases published K - L colors for the galaxies in Figure 24 indicate the presence of non-stellar emission, at least at L. Extrapolated to the aperture sizes in this paper, available K - L colors do provide a lower limit of ~ 600 K to the temperature of any dust component that is emitting as much as 10% at 2.2 μm. There is no physical problem in forming such a warm dust component, since relevant condensation temperatures are > 1000 K (Gilman 1969).

If we assume a value of 1 for $\rho a / Q$ (the ratio of grain mass times grain radius to grain absorption efficiency), the required warm dust masses seem physically plausible. Taking NGC 1068 as an example, with $A_V = 0$ the JHK color residuals can be fit with a dust component having $T \sim 700$ K and contributing 30% of the 2.2 μm flux in a 27" beam. At a distance modulus of 31.29 (Sandage and Tammann 1975), this leads to a mass of $\sim 2 \times 10^3$ $M_\odot$, compared to a dust mass of $\sim 5 \times 10^4$ $M_\odot$ estimated by Rees et al. (1969) on the basis of the 2 - 20 μm spectrum, and a mass of 1×10^8 $M_\odot$ for a 30 K dust component estimated on the basis of the submillimeter spectrum by Hildebrand et al. (1977). For NGC 5253, with $A_V = 0$, the K - K color residual can be fit by a 10% contribution from 700 K dust to the 34" 2.2 μm measurement, which at a distance modulus of 29.49 (Sandage and Tammann 1975) leads to a dust mass of ~ 10 $M_\odot$. Warm dust mass estimates for the other galaxies are ambiguous because of previously mentioned uncertainties in A_V, but appear to be mostly in the range 10 - 100 $M_\odot$.

Three Seyfert galaxies were measured in this study - NGC 1068, 1566, and 6814. The measured J - H colors for all three are normal, while the measured H - K color advances from normal in NGC 1566, to somewhat red in 6814, to very red in 1068. Our results are thus consistent with the work of Penston et al. (1974), who in a study of 11 Seyferts also found a range of H - K colors from normal to very red, with NGC 1068 having the largest excess of all.

Because the CO and H_2O indices are so affected by reddening (Figures 25a, b), it is difficult to recover any useful information about possible differences in the stellar luminosity function between galaxies with a 2.2 μm excess and "normal" galaxies. However, the case of NGC 3034 seems noteworthy: relative to the other 2.2 μm excess objects with the reddest JHK colors, *both* the CO and H_2O indices are very large, which suggests that above normal numbers of late-type giants and/or supergiants are present. O'Connell (1970), in an optical study of the stellar content in this galaxy, reached a similar conclusion.

VI. COMPARISON WITH STELLAR SYNTHESIS MODELS

In Papers I and II, published evolutionary models of Tinsley and Gunn (1976) and empirical models of O'Connell (1976) for the central regions of bright ellipticals were compared with the infrared observations. In both cases, the best fitting models were similar in that at 2 μm, only 20% of the light was contributed by dwarf and evolving stars, while 80% was contributed by stars from the giant branch. However, the O'Connell model,

with a 37% contribution from M6 giants, agreed significantly better with the data than did the Tinsley and Gunn model, with only a 12% contribution from such stars.

The model fitting work of Tinsley and Gunn (1976), O'Connell (1976b), Frogel et al. (1975a) and in Papers I and II has established that the CO and H_2O indices and the V - K color provide strong constraints on both the dwarf-to-giant ratio and the shape of the giant branch luminosity function in elliptical galaxies. The data are most consistent for elliptical galaxy models with an initial mass function slope x (following the notation of Tinsley 1968, 1972) in the range $0 \lesssim x \lesssim 1$, giant branches rich in late M stars, and mass-to-light ratios $M / L_V < 10$. However, the very latest M giants - such as Miras and carbon stars - do. not appear to contribute more than about 15% to the 2 μm light (cf. Paper II). The data presented in this paper suggest that similar constraints apply to the nuclear regions of all galaxies dominated optically by populations ranging in mean spectral type from near K to near F.

While a number of empirical synthesis models for galaxies measured in this study have been published in recent years (e.g. Tifft 1963; Johnson 1966b; Wood 1966; McClure and van den Bergh 1968; Lasker 1970; Spinrad and Taylor 1971; Faber 1972; Andrillat, Souffrin, and Alloin 1972; Alloin 1973; Joly 1973, 1974; Joly and Andrillat 1976), comparison with such models is generally not instructive because either M giants were ignored completely, or they were included in only an ad hoc fashion - for instance, by lumping all stars into a single M5 bin. However, recent empirical models by Williams (1976) of mostly amorphous population galaxies, and by Turnrose (1976) of intermediate population galaxies, treat M giants in a somewhat more rigorous manner. Using the stellar-calibrations in Johnson (1966a), Papers I and II, and in Appendix A, the infrared colors of the models presented by these authors were calculated and compared with the available infrared data from Papers I and II and in this paper.

Williams (1976) has presented synthesis models for NGC 221, 224, 584, 3031, 3115, 3379, 4594, and 5194. Except for 5194, in these models the contributions from M dwarfs range from 22% to 63% of the 2 μm light, the contributions from late M giants range from 11% to 39%, and the mass-to-light ratios range from 17 to 81. Excluding NGC 5194, *these models are incompatible with the data.* Typically, the V - K colors are 0.5 to 1.0 mag too red, the CO indices are 0.05 to 0.10 mag too small, and the H_2O indices are 0.10 to 0.15 mag too large. As an example, comparison of the observations with three of the models is made in Table 14. The model colors are quite sensitive to the V - K color adopted for Williams' late M giant bin, as apparent in Table 14. However, the discrepancies cannot be accounted for by variation in this V - K color: an increase above 7.20 drives the model V - K color, already too red, to even redder values; while a decrease below 7.20 drives the CO index, already too low, to even lower values. The major problem with the models is the excessive numbers of M dwarfs, which produce the rather high M / L_V values. Only in the model for NGC 5194, which at 2 μm has a 1% contribution from late M dwarfs, a 35% contribution from late M giants (assuming V - K for this bin = 7.20), and an M / L_V of 1.2, is there reasonable agreement with the data.

Table 14. Comparison with Stellar Synthesis Models of Williams

Color	NGC 3031		NGC 4594		NGC 5194	
	Observed	Model*	Observed	Model*	Observed	Model*

U - V	1.76	1.49	1.65	1.45	1.00	1.12
V - K	3.51	3.84 - 4.09	3.54	4.42 - 4.68	3.14	3.16 - 3.68
J - H	0.72	0.67 - 0.73	0.75	0.68 - 0.73	0.71	0.76 - 0.83
H - K	0.24	0.23 - 0.26	0.19	0.26 - 0.28	0.23	0.19 - 0.25
CO	0.15	0.06 - 0.10	0.17	0.04 - 0.09	0.18	0.15 - 0.19
H_2O	0.12	0.18 - 0.22	0.11	0.21 - 0.24	0.12	0.12 - 0.21
M/L_V	-	36	-	81	-	1.2

* The left hand values for the model infrared colors were obtained by assuming V - K = 7.20 (i.e. that for an M6 III) for Williams' late M giant bin. The right-hand values were found by assuming V - K = 8.30 (i.e. that for an M7 III) for this bin.

The galaxies modeled by Turnrose (1976) include NGC 1084, 1637, 2903, 4321, and 5194. Typically, at 2 μm the models have a $\lesssim$ 1% contribution from late M dwarfs, a 15 - 30% contribution from late M giants, and M / L_V, values < 2. In addition, these models also contain substantial numbers of upper main sequence stars and M supergiants, the contribution of the former ranging from 20 - 60% at V, and of the latter from 0 - 20% at 2 μm.

Within the uncertainties (see below), the CO and H_2O indices for the Turnrose models are generally compatible with the observations. However, interpretation of the V - K color in these models is ambiguous for a number of reasons. To begin with, as usual the 2 μm luminosity is quite sensitive to the mean V - K color adopted for the M6 - M8 III bin. Now because of the large upper main sequence contribution, the intrinsic V - K colors of the models are very blue. On the other hand, Turnrose finds *internal* reddening values of 0.3 - 0.4 in E(B - V), which leads to corrected V - K colors about 1 mag redder. In other words, if Turnrose's internal reddening values are correct, the mean V - K colors in intermediate population spirals are deter- mined mostly by reddening effects, and not by the stellar population, as was implied in Section IV.

Adopting a V - K color of 8.3 for the M6 - M8 III bin leads to model V - K colors in the range 2.0 to 2.5, and with the Turnrose reddening corrections there is acceptable agreement with the data. However, in light of the generally large V - K color gradients in these spirals (Table 7), and of the fact that Turnrose's aperture size was 7", whereas the smallest available aperture sizes for the infrared data are typically 4 - 5 times larger, the agreement would seem to be somewhat fortuitous. It furthermore seems surprising that the intrinsic V - K colors in these galaxies should be as blue as in Magellanic irregulars, i.e., galaxies with little internal reddening (Holmberg 1975) but presumably richer upper main sequences than in the Sc's. The explanation may simply be that Turnrose's 7" data is more heavily weighted by intense star formation regions than is the much larger aperture infrared measurements. Infrared observations at Turnrose's aperture size might resolve the dilemma.

VII. SUMMARY

In this paper we have presented new broad-band infrared colors and CO and H_2O absorption indices for a number of galaxies distributed in morphological type along the Hubble sequence. The data indicate that a fundamental similarity exists in the nuclear red stellar component of all galaxies dominated optically by a stellar

population with mean spectral type ranging from near K to near F. This component appears compatible only with stellar synthesis models characterized by giant branches rich in late M stars, flat main-sequence luminosity functions, and values of $M / L_V < 10$. In only the latest-type galaxies is there perhaps some evidence for a decrease in the influence of late M giants on the 2 μm light. The well-defined morphological distribution that was found for galaxies in the UVK plane should prove particularly useful for future evolutionary star formation studies.

In combination with previously obtained results for ellipticals, we have examined the correlation of the various colors with galaxian luminosity, inclination angle, and projected aperture size. The elliptical colors correlate more strongly than the spiral colors with luminosity, while the reverse is true for inclination. While no radial gradients are found in the spiral sample for the purely infrared colors, both U - V and V - K color gradients appear to be present in all morphological types and generally tend to redden with decreasing aperture size.

Several emission mechanisms have been considered in relation to the small subset of galaxies found to have nuclear 2.2 μm excesses. A warm dust component (with $T \sim 700$ K) seems likely to be present in at least a few cases. Accurate measurements at L (3.5 μm) would be very useful in this regard. Detailed comparison was made with recently-published synthesis models by Turnrose (1976) and Williams (1976); the latter author's models were found to be incompatible with the infrared data.

Appendix A
The Stellar Calibration

The standard star system, selected calibrating stars, and mean stellar color relationships have been presented and discussed in Papers I and II and in Persson, Aaronson, and Frogel (1977). The observations in these papers were made with two independent InSb detector systems in use at the Harvard College Observatory (the HCO system) and at the California Institute of Technology (the CIT system). For K magnitudes, and CO and H_2O indices, intercomparison of measurements on the two systems have revealed no systematic differences greater than 0.01 mag for either dwarf stars, giant stars, or galaxies. However, the following transformations were found for the J - H and H - K colors:

$$[J - K]_{HCO} = 1.09\,[J - H]_{CIT} \qquad \text{(A1)}$$

and

$$[H - K]_{HCO} = [H - K]_{CIT} - 0.02, \quad ([H - K]_{CIT} \gtrsim 0.15) \qquad \text{(A2)}$$

Equation (Al) is well explained by a difference in effective wavelength between the J_{HCO} and J_{CIT} filters. The reason for the transformation indicated by equation (A2) is less clear, as the H_{HCO} and H_{CIT} filters are identical. [8]

In Table A1 the J - H colors are given for standard stars from Paper I independently set up on the HCO system. All stars have been observed between one and three times on at least 5 different nights, and the internal accuracy of the system is 0.02 mag. The colors of additional standards set up for this study are listed in Table A2, and are

of comparable internal precision as the standards of Table Al and in Papers I and II. The V magnitudes in Table A2 are adopted from the *Catalogue of Bright Stars* (Hoffleit 1964).

Table A1.J-H Colors of Standards on the HCO System

Name	J-H	Name	J-H
BS 0134	0.49	4689	0.02
BS 0923	0.56	6092	-0.07
BS 1698	0.59	6136	0.72
BS 3304	0.73	6228	0.78
BS 3403	0.68	7001	0.00
BS 4550	0.44	8498	0.70

Table A2. Additional Standards

Name	Spectral Type	V	K	J-H	H-K	CO	H_2O	Notes*
BS 1453	gG6	4.50	2.19	0.53	0.07	0.045	0.02	S
BS 1953	K4III	5.18	2.66	0.54	0.08	0.06	0.025	S
BS 3903	G8III	4.12	2.02	0.47	0.07	0.03	0.03	S
BS 4167	F2+A3	3.83	3.13	0.13	0.01	-0.02	0.005	S
BS 4954	K5III	4.74	1.29	0.76	0.14	0.155	0.035	N
BS 6072	G8III	4.01	1.65	0.54	0.09	0.07	0.03	S

* N = northern hemisphere standard; S = southern hemisphere standard.

In Table A3 the colors are listed for some additional calibrating stars not included in Papers I or II. (As discussed in Paper II, the CO and H_2O indices for most carbon stars are in the opposite sense expected due to the single sideband nature of the absorption measurements.) Using the extra data in Table A3, we have rederived the mean stellar relation for the H_2O index in M giants. As shown in Table A4, the revised calibration does not differ significantly from the calibration used in Paper II. The errors given for types M6 and M7 in Table A4 reflect the large dispersion of the H_2O absorption strength found in giant stars of very late spectral type.

Table A3.

Table A4. Mean H_2O Indices for M Giants

Spectral Type	V-K	Paper II Calibration	Calibration This Paper
M3	4.63	0.08	0.07
M4	5.34	0.10	0.09
M5	6.20	0.12	0.11
M6	7.20	0.20	0.18 ± 0.05
M7	-	0.36	0.36 ± 0.05

The adopted mean CO and H_2O indices of M supergiants are listed for synthesis purposes in Table A5. The spectral type, V - K relationship is taken from Lee (1970). At a given spectral type, the CO index is 0.10 mag stronger in supergiants than in giants, while the H_2O index varies from being only marginally stronger at type M0, to 0.12 mag stronger at type M4 - results roughly consistent with the earlier work of Baldwin et al. (1973).

Table A5. Mean CO and H_2O Indices for M Supergiants

Spectral Type	V-K	CO Index	H_2O Index
MO	3.82	0.26	0.07
M1	3.98	0.28	0.09
M2	4.31	0.29	0.16
M3	4.91	0.31	0.19
M4	5.52	0.32	0.21

J and K magnitudes for many stars observed in this study were also measured by Johnson et al. (1966). Allowing for the value of J (α Lyr) = K (α Lyr) = 0.02 mag given by Johnson et al., a comparison of these measurements yields

$$J_{HCO} - J_{Johnson} = 0.002 \pm 0.03 \quad (13 \text{ stars})$$

and

$$K_{HCO} - K_{Johnson} = 0.008 \pm 0.04 \quad (16 \text{ stars}),$$

where the quoted errors are dispersions of the mean. Thus, except for a zero-point shift, the J and K values in this paper are on the same infrared photometric system described by Johnson (1966a).

[8] Note that equation (A2) was derived by an intercomparison of dwarf stars and galaxies only, because an insufficient number of late-type giant stars were observed in common at H on the two systems. The mean H - K color relation for giant stars adopted in this paper is taken directly from Table A3 in Paper I, without applying a transformation. Furthermore, to transform the mean H - K color relation for dwarf stars listed in the aforementioned Table A3 to the HCO system, equation (A2) should be applied to *all* the values of H - K. Back.

Appendix B
The InSb Detector System

All of the observations in this paper were made with an InSb detector system built by the author. The preamplifier used follows the design of Hall et al. (1975): the detector (supplied by Santa Barbara Research Center) is externally biased to 0 volts, and radiation is detected by measuring the variation in generated current. The only noise source is then random thermal electron motion (Johnson noise), for which the noise current is proportional to the square root of the ratio of detector temperature to impedance.

The detector is operated at pumped nitrogen, temperatures ($T \sim 60$ K). Prior to pump-down, and following a technique discovered by K. Matthews at Caltech, the detector is flashed by exposing it to extremely intense 1.2 μm radiation for several minutes, The apparent effect of this bizarre procedure is to remove a surface charge layer that builds up on the protective oxide coating of the InSb crystal, thereby eliminating a spurious conduction current from the oxide to the p/n junction (K. Matthews 1976, private communication). Typical results of flashing are an increase in detector impedance from a value of 3×10^9 ohms to 10^{11} ohms. The system noise is thus determined not by the detector, but by the feedback resistor, whose resistance of 10^{10} ohms is the highest stable value that is available commercially.

At 2.2 μm, the system NEP is $\lesssim 10^{-15}$ watts / $(\mathrm{Hz})^{1/2}$, and using a focal plane chopper, the system is background noise limited (in the K-band) on the Mt. Hopkins 60-inch telescope at f/10 with a 2 mm aperture. Using the 60-inch, an object having a K magnitude of 9 can be measured (at K) to a statistical level of ~ 1% in one minute of integration time. This represents about a tenfold improvement in signal-to-noise over the best previously available PbS system.

Appendix C
Metallicity Calibration and the V - K Color

As previously discussed, a change in mean metallicity is the most likely explanation for the UVK color-aperture and color-luminosity effects found in early-type,galaxies. In this Appendix we shall attempt to estimate quantitatively the implied variation in metallicity, as measured by $\mathrm{Fe/H} \equiv (\mathrm{Fe/H})_{\mathrm{obs}} / (\mathrm{Fe/H})_{\odot}$.

The UVK colors of a stellar ensemble composed of a single generation of stars will become bluer with decreasing metallicity because of three reasons: First, the ultraviolet line blanketing will decrease; second, the horizontal branch will shift to the blue; and third, the giant branch will steepen. Now it is well known that the position of the horizontal branch does not correlate perfectly well with metal abundance. Furthermore, Peterson (1976) has shown that changes in CN band strength, through variations only in the nitrogen abundance, can alter

the U - V color by several tenths of a magnitude, for the same value of Fe/H. Thus, we expect the V - K color, which depends primarily on just the giant branch morphology, to be a superior indicator of mean metallicity than the U - V color. Recent infrared observations of globular clusters (Malkan, Aaronson, and Kleinmann 1977; Aaronson and Malkan 1977) have in fact demonstrated that as an accurate measure of metallicity, the V - K color is comparable to the best purely optical techniques.

We shall thus use the V - K color as our metallicity indicator. It is first necessary to determine the ratio $\Delta\log(Fe/H) / \Delta V - K$. Using the luminosity function of M3, and theoretical evolutionary tracks of Rood (1972), Strom et al. (1976) found that $\Delta\log(Fe/H) / \Delta V - K \simeq 1.2$, with $V - K \simeq 3.15$ as the solar abundance value. The globular cluster observations of Aaronson and Malkan (1977) provide a strictly empirical calibration. Preliminary results indicate that $\Delta\log(Fe/H) / \Delta V - K \simeq 2.$, with $V - K = 3.0$ as the solar abundance value.

In Paper I the mean V - K color at $\log A / D_0 = - 0.6$ in elliptical galaxies was found to vary from 3.15 to 3.33, for a change in absolute magnitude of from -19 to -23. The calibrations discussed above imply a concomitant change in Fe/H of 1.6 - 2.3. This result is completely consistent with the work of Faber (1973), who estimated a factor of 2 change in Fe/H was required to explain the change in optical line indices between her group 2 and group 5 galaxies, which cover about the same magnitude range as the Paper I sample. (It was in fact shown in Paper I that the UVK colors correlate quite well With Faber's $CN_0 - Mg_0$ index.) Furthermore, the V - K colors suggest a mean value of Fe/H of 1 to 2 at $M_V = - 19$, and-2 to 4 at $M_V = - 23$, amounts again consistent with Faber's estimates.

A mean radial color change $\Delta V - K / \Delta \log A / D(0)$ of ~ 0.1 was found for elliptical galaxies in Paper I and for the bulges of early-type spirals in this paper. This suggests a typical change in Fe/H of 1.5 to 2 over a range of -0.3 to -1.3 in $\log A / D_0$, a value that appears to be within the limits of the theoretical collapse models discussed by Larson (1974, 1975, 1976).

We caution that the above estimates depend on linear extrapolation of calibrations based on metal-poor galactic globular clusters to seemingly metal-rich composite galaxian systems. Better knowledge of the end points of giant star evolution coupled with detailed synthesis models which include chemical evolution may be needed to confirm the validity of this assumption.

REFERENCES

1. Aannestad, P. A. 1975, Ap. J., 200, 30.
2. Aaronson, M. 1977 (in preparation).
3. Aaronson, M., Frogel, J. A., and Persson, S. E. 1977, Ap. J. (in press, Paper II).
4. Aaronson, M., and Malkan, M. 1977 (in preparation).
5. Alloin, D. 1973, Astr. and Ap., 27, 433.
6. Andrillat, Y., Souffrin, S., and Alloin, D. 1972, Astr. And Ap., 19, 405.
7. Baldwin, J. R., Frogel, J. A., and Persson, S. E. 1973, Ap. J., 184, 427.
8. Becklin, E. E., Fomalont, E. B.; and Neugebauer, G. 1973, Ap. J. Letters, 181, L27.
9. Becklin, E. E., Frogel, J. A., Kleinmann, D. E., Neugebauer, G., Ney, E. P., and Strecker, D. W. 1971, Ap. J. Letters, 170, L15.

10. Danver, C. G. 1942, Ann. Lund. Obs., No. 10.
11. de Vaucouleurs, G. 1961, Ap. J. Suppl., 5, 233.
12. de Vaucouleurs, G. 1975, in Stars and Stellar Systems, vol. 9, Galaxies and the Universe, ed. A. and M. Sandage and J. Kristian (Chicago: University of Chicago Press), p. 557.
13. de Vaucouleurs, G., and de Vaucouleurs, A. 1964, Reference Catalogue of Bright Galaxies (Austin: University of Texas Press).
14. de Vaucouleurs, G., and de Vaucouleurs, A. 1972, Mem. R. A. S., 77, 1.
15. de Vaucouleurs, G., de Vaucouleurs, A., and Corwin, H. G. 1976, Second Reference Catalogue of Bright Galaxies (Austin: University of Texas Press).
16. Faber, S. M. 1972, Astr. and Ap., 20, 361.
17. Faber, S. M. 1973, Ap. J., 179, 731.
18. Frogel, J. A. 1971, Ph.D. thesis, California Institute of Technology.
19. Frogel, J. A., Persson, S. E., Aaronson, M., Becklin, E. E. and Matthews, R. 1975a, presented at Tercentenary Symposium of the Royal Greenwich Observatory.
20. Frogel, J. A., Persson, S. E., Aaronson, M., Becklin, E. E., Matthews, R., and Neugebauer, G. 1975b, Ap. J. Letters, 195, L15.
21. Frogel, J. A., Persson, S. E., Aaronson, M., Becklin, E. E., Matthews, R., and Neugebauer, G. 1975c, Ap. J. Letters, 200, L123.
22. Gilman, R. C. 1969, Ap. J. Letters, 155, L185.
23. Glass, I. S. 1973, M. N. R. A. S., 164, 155.
24. Glass, I. S. 1976, ibid., 175, 191.
25. Grasdalen, G. L. 1975, Ap. J., 195, 605.
26. Hall, D. N. B., Aikens, R. S., Joyce, R., and McCurnin, T. N. 1975, Ap. Optics, 14, 450.
27. Heidmann, J., Heidmann, N., and de Vaucouleurs, G. 1971a, Mem. R. A. S., 75, 85.
28. Heidmann, J., Heidmann, N., and de Vaucouleurs, G. 1971b, ibid. 75, 121.
29. Hildebrand, R. H., Whitcomb, S. E., Winston, R., Stiening, R. F., Harper, D. A., and Moseley, S. H. 1977, Ap. J. (in press).
30. Hoffleit, D. 1964, Catalogue of Bright Stars (3d ed.; New Haven: Yale University Observatory).
31. Holmberg, E. 1958, Medd. Lunds. Obs., Ser. 2, No. 158.
32. Holmberg, E. 1969, Arkiv For Astronomi, Band 5 nr 20.
33. Holmberg, E. 1975, in Stars and Stellar Systems, vol. 9, Galaxies and the Universe, ed. A. and M. Sandage, and J. Kristian (Chicago: University of Chicago Press), p. 123.
34. Huchra, J. P. 1977a, Ap. J. Suppl.(in press).
35. Huchra, J. P. 1977b, Ap. J. (in press).
36. Hulst, H. C. van de. 1949, Rech. Astr. Obs. Utrecht, 11, Part 1, 1.
37. Johnson, H. L. 1966a, Ann. Rev. Astr. and Ap., 4, 193.
38. Johnson, H. L. 1966b, Ap. J., 143, 187.
39. Johnson, H. L. 1968, in Stars and Stellar Systems, vol. 7, Nebulae and Interstellar Matter, ed. B. M. Middlehurst, and L. H. Aller (Chicago: University of Chicago Press), p. 167.
40. Johnson, H. L., and Mendez, M. E. 1970, A. J., 75, 785.
41. Johnson, H. L., Mitchell, R. I., Iriarte, B., and Wisniewski, W. Z. 1966, Comm. L. P. L., No. 63.
42. Joly, M. 1973, Astr. and Ap., 33, 177.
43. Joly, M. 1974, ibid., 37, 57.

44. Joly, M., and Andrillat, Y. 1976, Astr. and Ap., 50, 279.
45. Kleinmann, D. E., and Wright, E. L. 1974, Ap. J. Letters, 191, L19.
46. Larson, R. B. 1974, M. N. R. A. S., 166, 585.
47. Larson, R. B. 1975, ibid., 173, 671.
48. Larson, R. B. 1976, ibid., 176, 31.
49. Larson, R. B., and Tinsley, B. M. 1977, Ap. J. (in press).
50. Lee, T. A. 1970, Ap. J., 162, 217.
51. Liebowitz, E. M. 1973, Ap. J., 186, 899.
52. Malkan, M., Aaronson, M., and Kleinmann, D. 1977, Bull. A. A. S., 9, 294.
53. McClure, R. D. 1969, A. J., 74, 50.
54. McClure, T. D., and van den Bergh, S. 1968, A. J., 73, 313.
55. Morgan, W. W. 1958, P. A. S. P., 70, 364.
56. Morgan, W. W. 1959, ibid., 71, 394.
57. Morgan, W. W. 1962, Ap. J., 135, 1.
58. Morgan, W. W., and Mayall, N. U. V. 1957, P. A. S. P., 69, 291.
59. Morgan, W. W., and Osterbrock, D. E. 1969, A. J., 74, 515.
60. O'Connell, R. W. 1970, Ph.D. thesis, California Institute of Technology.
61. O'Connell, R. W. 1974, A p. J. Letters, 193, L49.
62. O'Connell, R. W. 1976a, ibid., 203, Ll.
63. O'Connell, R. W. 1976b, Ap. J., 206, 370.
64. Pacholczyk, A. G., and Tarenghi, M. 1975, Mem. Soc. Astron. Italiana, 46, 199.
65. Pence, W. 1976, Ap. J., 203, 39.
66. Penston, M. V., Penston, M. J., Selmes, R. A., Becklin, E. E, and Neugebauer, G. 1974, M. N. R. A. S., 169, 357.
67. Persson, S. E., Aaronson, M., and Frogel, J. A. 1977, A. J. (in press)
68. Peterson, R. 1976, Ap. J. Suppl., 30, 61.
69. Rees, M. J., Silk, J. I., Weemer, M. W., and Wickramasinghe, N. C. 1969, Nature, 223, 788.
70. Rieke, G. H., and Low, F. J. 1972, Ap. J. Letters, 176, L95.
71. Rood, R. T. 1972, Ap. J., 177, 681.
72. Sandage, A. 1961, The Hubble Atlas of Galaxies (Washington, D.C.: Carnegie Institution Publ. no. 618).
73. Sandage, A. 1972, Ap. J., 176, 21.
74. Sandage, A. 1973, ibid., 183, 711.
75. Sandage, A. 1975, ibid., 202, 563.
76. Sandage, A., and Tammann, G. A. 1974, Ap. J., 194, 559.
77. Sandage, A., and Tammann, G. A. 1975, ibid., 196, 313.
78. Searle, L., Sargent, W. L. W.; and Bagnuolo, W. G. 1973, Ap. J., 179, 427.
79. Spinrad, H., Gunn, J. E., Taylor, B. J., McClure, R. D., and Young, J. W. 1971, Ap. J., 164, 11.
80. Spinrad, H., and Peimbert, M. 1975, in Stars and Stellar Systems, vol. 9, Galaxies and the Universe, ed. A. and M. Sandage, and J. Kristian (Chicago University of Chicago Press), p. 37.
81. Spinrad, H., Smith, H. I., and Taylor, D. J. 1972, Ap. J., 175, 649.
82. Spinrad, H., and Taylor, B. J. 1971, Ap. J. Suppl., 22, 445.
83. Stebbins, J., and Whitford, A. E. 1948, Ap. J., 108, 413.

84. Strom, S. E., Strom, K. M., Goad, J. W., Vrba, F. J., and Rice, W. 1976, Ap. J., 204, 684.
85. Tifft, W. G. 1963, A. J., 68, 302.
86. Tifft, W. G. 1973, P. A. S. P., 85, 283.
87. Tinsley, B. M. 1968, Ap. J., 151, 547.
88. Tinsley, B. M. 1972, Astr. and Ap., 20, 383.
89. Tinsley, B. M., and Gunn, J. E. 1976, Ap. J., 203, 52.
90. Tully, R. B. 1972, M. N. R. A. S., 159, 35P.
91. Tully, R. B., and Fisher, J. R. 1977, Astr. and Ap., 54, 661.
92. Turnrose, B. E. 1976, Ap. J., 210, 33.
93. van den Bergh, S. 1975, in Stars and Stellar Systems, vol. 9, Galaxies and the Universe, ed. A. and M. Sandage, and J. Kristian (Chicago: University of Chicago Press), p. 50
94. van den Bergh, S. 1977, Evolution of Galaxies and Stellar Populations (New Haven: Yale University Observatory, in press).
95. Welch, G. A., and Forrester, W. T. 1972, A. J., 77, 333.
96. Werner, M. W., and Salpeter, E. E. 1969, M. N. R. A. S., 145, 249.
97. Whitford, A. E. 1958, A. J., 63, 201.
98. Whitford, A. E. 1977, Ap. J., 211, 527.
99. Williams, T. B. 1976, Ap. J., 209, 716.
100. Willner, S. P., Becklin, E. E., and Visvanathan, N. 1972, Ap. J., 175, 699.
101. Wilson, W. J., Schwartz, P. R., Neugebauer, G., Harvey, P. Becklin, E. E. 1972, Ap. J., 177, 523.
102. Wood, D. B. 1966, Ap. J., 145, 36.
103. Wynn-Williams, C. G., and Becklin, E. E. 1974, P. A. S. P., 86, 5.

CHAPTER V
Identification of the Nucleus in the Spiral Galaxy NGC 4631

ABSTRACT

We present broad band infrared photometry of the edge-on spiral galaxy NGC 4631. The position of peak infrared intensity is found to lie not on the most optically prominent part of the galaxy, but in the nearby area of strongest dust absorption. This position is discussed in relation to the rotation curve measured by G. and A. de Vaucouleurs, and the radio continuum maps of Pooley. We conclude that the location of the infrared peak is probably the true position of the nucleus.

Key words: galaxies - infrared photometry

Running title: Identification of the Nucleus in NGC 4631

I. INTRODUCTION

NGC 4631 is an edge-on spiral galaxy classified as "probably late Sc" by Sandage (1961), and as a barred-Sd by G. and A. de Vaucouleurs (1963), with the bar oriented end-on along the line of sight. Optical photographs of

this object show a patchy distribution of stars, H II regions, and dust (Figure 1), but reveal no obvious nuclear feature. The absence of a well-defined nucleus hinders understanding of the rotation curve measured by G. and A. de Vaucouleurs (1963), and of the radio continuum maps of Pooley (1969).

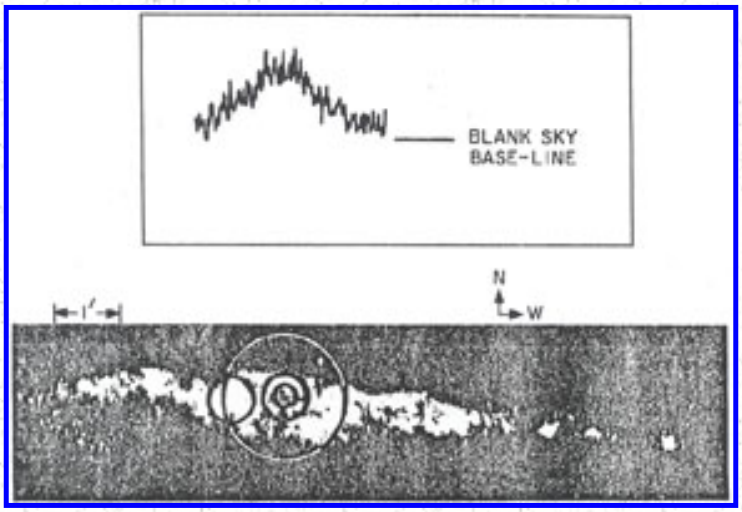

Figure 1. The circles superimposed on an optical photograph of NGC 4631 indicate the positions and sizes of the beams used to collect the photometric data in Table 1. The inset shows a section of an east-west 2.2 μm scan with a 41" beam across the galaxy at the declination of the infrared peak. Both the scan and the photograph are shown at the same scale.

NGC 4631 was first observed by the author in the course of surveying the infrared colors of a large number of spiral galaxies (Aaronson 1977, hereafter Paper IV). 2.2 μm scans along the major axis revealed that the peak infrared intensity lay not on the most optically prominent part of the galaxy, but in the nearby area of strongest dust absorption (Figure 1) The observations are presented in Section II, and the location of the infrared peak is discussed in Section III in relation to the aforementioned work of the de Vaucouleurs' and of Pooley.

II. OBSERVATIONS

The infrared observations were made on two nights in April, 1976 and one night in June, 1977 with the Mt. Hopkins 60-inch (1.5 m) Tillinghast reflector; and on one night in June, 1-977 with the Kitt Peak National observatory #1 36-inch (0.9m) telescope. The Harvard College Observatory InSb photometer was used, with filters and focal plane apertures cooled to solid nitrogen temperatures. The effective wavelengths and bandwidths of the filters employed are: J - 1.24 μm (0.28 μm), H - 1.65 μm (0.30 μm), K - 2.22 μm (0.41 μm), and L - 3.49 μm (0.54 μm). The photometric system (called the HCO system) and set of standard stars to which the measurements are referred are described fully by Frogel et al. (1977, hereafter Paper I) and in Paper IV. In this system, which is close to the original photometric system of Johnson (1966), α Lyr has magnitude 0.00 at all wavelengths.

The photometric results are presented in Table 1. The data consists of 21", 41", and 107" aperture JHK

measurements, and a 21" L measurement, all centered on the position of peak infrared intensity, and also a 41" JHK measurement centered on the brightest optical patch, which has been designated point A, following the notation of G. and A. de Vaucouleurs (1963). The position and sizes of the measuring beams are superimposed on an optical photograph of the galaxy in Figure 1.

Table 1. Infrared Photometry of NGC 4631

	Position* 1950			Aperture					
	α	δ	Telescope	(")	log A / D_0	K†	J-H	H-K	K-L
Infrared Peak	$12^h39^m40.^s9$	32° 49'19"	MH60	21	-1.48 9.51	1.03	0.51	0.83 ± 0.15	
			MH60	41	-1.18	8.45	0.96	0.41	-
			KP36	107	-0.77	7.34	0.87	0.34	-
Point A	$12^h39^m44.^s7$	32° 49'16"	MH60	41	- 9.25	0.78	0.37	-	
Mean spiral**	-	-	-	-	-	-	0.72 ± 0.03	0.18 ± 0.01	0.22 ± 0.1

* Positions were determined by offsetting to nearby field stars, and have an accuracy of ± 5" in each coordinate.

† Nominal errors for K, J-H, and H-K are ± 0.03,± 0.04, and ± 0.03 mag, respectively.

** Quoted values for J-H and H-K are the mean and dispersion of colors for 8 Scd and Sd galaxies (Aaronson 1977). The K-L color is an unpublished measurement of M31 with a 27" aperture.

The chopping throws used were 82" at Mt. Hopkins and 252" at Kitt Peak. Because all chopping was in the north-south direction, and the galaxian spindle is aligned almost exactly east west, corrections for extended flux in the reference beam are negligible. However, following the precepts in Papers I and IV, corrections were applied for beam profile and aperture effects, although the largest such correction was only 0.04 mag. Since the galactic latitude of NGC 4631 is $b^{II} = 84°$, no correction has been applied for interstellar reddening. With the formulae in Paper I, and a redshift of z = 0.0021 (de Vaucouleurs, de Vaucouleurs, and Corwin 1976), the redshift corrections to the stellar component of the flux are all < 0.01 mag.

The statistical accuracy of the JHK measurements was always < 0.02 mag. The adopted nominal errors given in Table 1 for the JHKL data are generally equal to or larger than the nightly variations, after application of all instrumental corrections.

III. DISCUSSION

For comparison purposes, we have listed in the last line of Table 1 the mean J - H and H - K colors for eight late-type spirals (Paper IV), and the K - L color for the nucleus of M31 (unpublished measurements). In Figure 2 we

have plotted the K magnitude - aperture relations for the infrared peak in NGC 4631, for the Sd galaxy NGC 4490 (Paper IV), and for a standard bright elliptical (Paper I).

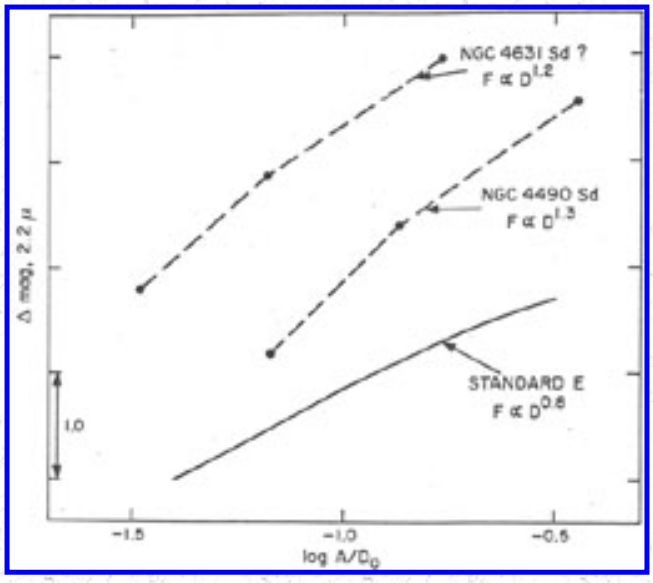

Figure 2. The R magnitude growth curves are shown for the possible Sd galaxy NGC 4631, for the Sd galaxy NGC 4490 (Aaronson 1977), and for a standard elliptical galaxy (Frogel et al. 1977). Log A/D_0 is the ratio of aperture size to corrected face-on diameter (from de Vaucouleurs, de Vaucouleurs, and Corwin 1976). The three curves have been shifted vertically an arbitrary amount, and an approximate flux-diameter relation is given next to each one.

Several results are apparent from Table 1 and Figure 2. First, the K magnitude of point A, the most optically prominent part of the galaxy, is 0.8 mag fainter than that of the infrared peak, through identical measuring apertures. Second, all colors of NGC 4631 are considerably redder than the "mean spiral" colors. Third, a significant radial color variation is seen in the J - H and H - K nuclear colors; such a color gradient is characteristic of galaxies with nuclear 2.2 μm excesses (Paper IV). Finally, the magnitude aperture relation for NGC 4631 is similar to that of NGC 4490, and not to that of an elliptical galaxy.

If the "mean spiral" colors are adopted as the true colors of NGC 4631 corrected for inclination effect, the resulting color residuals cannot be fit by a single value of internal absorption, using the Van de Hulst reddening curve (Johnson 1968). For instance, the implied values of A_V in the 21" aperture from E (J - H), E (H - K), and E (K - L) are 3.2 mag, 5.8 mag, and 15.2 mag, respectively. In particular, the excess at L indicates the presence of significant non-stellar emission. In this regard, the infrared peak in NGC 4631 is similar to the well known imbedded infrared sources in the galaxies NGC 253 (Becklin, Fomalont, and Neugebauer 1973), NGC 3034 (Kleinmann and Low 1970), and NGC 5128 (Becklin et al. 1971).

Assuming the J - H color excess is primarily due to internal absorption (i.e. $A_v \simeq 3$), the remaining H - K and K - L residuals can be fit if ~ 15% of the 2.2 μm flux is from warm dust emission with temperature $T \simeq 700$ K and $1 / \lambda^2$ emissivity. Using a distance modulus of 30.15 (Sandage and Tammann 1975), and a value of 1 for $\rho a / Q$ (the ratio of grain mass times grain radius to grain absorption efficiency), the required mass of warm dust emitting in the 21" beam is only ~ 20 $M\odot$. This value seems reasonable, for instance, in relation to a dust mass of ~ 5×10^4 $M\odot$, estimated by Rees et al. (1969) for the galaxy NGC 1068 on the basis of the 2 - 20 μm spectrum. The red H - K color of point A, which is probably an H II region on the foreground side of the galaxy, implies that such a warm dust component, if present, is not confined solely to the location of the infrared peak. Observations of NGC 4631 at longer wavelengths than L would clearly be of interest.

The center of the NGC 4631 rotation curve measured by G. and A. de Vaucouleurs (1963) lies about 80" west of point A (see their Figures 3 and 6). However, on the basis of the overall luminosity distribution, G. and A de Vaucouleurs placed the center of, their conjectured bar only about 40" west of point A, and cited an analogy with the Large Magellanic Cloud, where the center of the bar also appears to be displaced from the center of the velocity curve (de Vaucouleurs 1960; Feast, Thackeray, and Wesselink 1961). G. and A. de Vaucouleurs have interpreted the considerable scatter of points about their rotation curve as being due to streaming motions of gas from the ends of the bar, although this picture has been questioned on physical grounds by Burbidge, Burbidge, and Prenderghast (1964). In any event, the maximum negative residual velocity (i.e., motion toward the observer) of the scatter corresponds to a spot that is also about 40" west of point A (cf. Figure 6, G. and A. de Vaucouleurs 1963).

Pooley (1969) has presented high resolution continuum maps of NGC 4631 at 408 and 1407 MHz that indicate the presence of non-thermal radio emission from a narrow region corresponding roughly with the optical galaxian outline. Pooley further states that "the center of the brightest radio emission peak coincides closely with the position of the center of the rotation curve . . . but there are no features clearly related to the position of the bar . . ." However, careful inspection of Pooley's Plate I and Figure 1, and G. and A. de Vaucouleurs' Figure 6, reveals that Pooley has in fact misplotted the center of rotation adopted by the de Vaucouleurs': the position of peak radio emission given by Pooley lies about 50" west of point A, and not 80" west, the aforementioned location of the rotation curve center.

In Figure 3 we have plotted the position of peak infrared intensity, and of the rotation curve center, relative to the 1407 MHz map of Pooley (1969). It is clear that 1) the peak infrared and radio positions closely correspond; and 2) these peak positions are near the location predicted by G. and A. de Vaucouleurs (1963) to be the center of the end-on bar (which as discussed above is also the point of maximum negative velocity residual). Furthermore, it appears both from Figure 3 and the 2.2 μm scan shown in Figure 1 that the rotation curve center chosen. by the de Vaucouleurs' bears little physical relation to the galaxy itself.

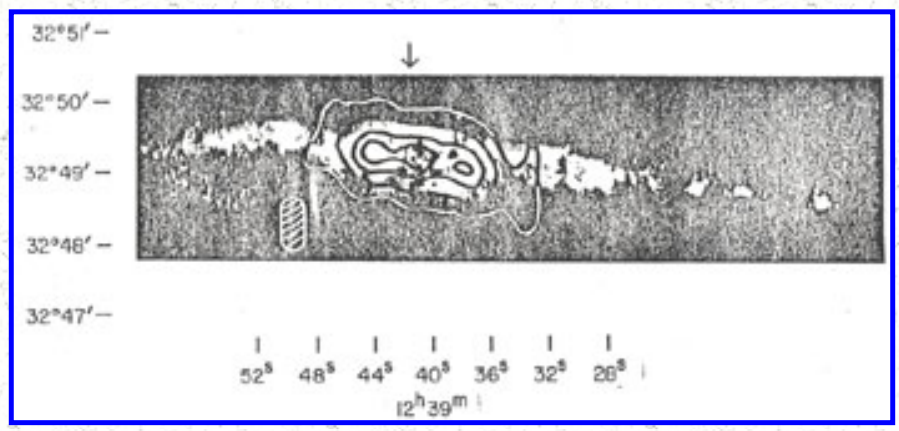

Figure 3. The 1407 MHz map of Pooley (1970, Plate I) is superimposed on an optical photograph of NGC 4631. The small ellipse to the lower left is the beam size used by Pooley The cross (+) is placed at the position of peak infrared intensity; the triangle (Δ) marks the rotation curve center adopted by G. and A. de Vaucouleurs (1963); and the arrow (↓) lies at the right ascension predicted by. those authors to be the true nuclear location.

The K magnitude of the infrared peak was found to increase with aperture size in a manner- similar to that for the Sd galaxy NGC 4490 (Figure 2). Given also the proximity of the peak infrared intensity with both the peak radio intensity and the geometric center of the overall luminosity distribution, we conclude that the location of the infrared peak is probably the true position of the nucleus

We caution that the infrared measurements do not distinguish between a bar seen end-on, and a simple spherical nucleus. The data is consistent with the streaming model proposed by G. and A. de Vaucouleurs (1963), but does not confirm it - perhaps a high resolution 2 μm map might do so. However, in light of the observations presented in this paper, a reexamination of the NGC 4631 rotation curve does seem warranted.

We thank Bruce Carney, Mat Malkan, Steve Perrenod, and Bas van't Sant for their assistance at the telescope, Eric Persson and Herb Gursky for helpful discussions, and the Center for Astrophysics for generous financial support.

REFERENCES

1. Aaronson, M. 1977 (in preparation, Paper IV)
2. Becklin, E. E., Fomalont, E. B., and Neugebauer, G. 1973, Ap. J. Letters, 181, L27.
3. Becklin, E. E., Frogel, J. A., Kleinmann, D. E., Neugebauer, G., Ney, E. P., and Strecker, D. W. 1971, Ap. J. Letters, 170, Ll.
4. Burbidge, E. M., Burbidge, G. R., and Prenderghast, K. H. 1964, Ap. J, 140, 1620.
5. de Vaucouleurs, G. 1960, Ap. J., 131, 265.
6. de Vaucouleurs, G. and A. 1963, Ap. J., 137, 363.
7. de Vaucouleurs, G., de Vaucouleurs, A., and Corwin, H. G. 1976, Second Reference Catalogue of Bright

Galaxies (Austin: University of Texas Press).
8. Feast, M. W., Thackeray, A. D., and Wesselink, A. J. 1961, M.N.R.A.S., 122, 433.
9. Frogel, J. A., Persson, S. E., Aaronson, M., and Matthews, K. 1977, Ap. J. (in press, Paper I).
10. Johnson, H. L. 1966, Ann. Rev. Astron. Astrophys., 4, 193.
11. Johnson, H. L. 1968, in Stars and Stellar Systems, vol. 7, Nebulae and Interstellar matter, ed. B. M. Middlehurst, and L. H. Aller (Chicago: University of Chicago Press), p. 167
12. Kleinmann, D. E., and Low, F. J. 1970, Ap. J. Letters, 161, L203.
13. Pooley, G. G. 1969, M.N.R.A.S., 144, 143.
14. Rees, M, J., Silk, J. I., Weemer, M. W., and Wickramasinghe, N. C. 1969, Nature, 223, 788.
15. Sandage, A. 1961, The Hubble Atlas of Galaxies (Washington, D. C.: Carnegie Institution Publ. No. 618).
16. Sandage, A., and Tammann, G. A. 1975, Ap. J., 196, 313.

CHAPTER VI
Closing Thoughts

The development of InSb detectors highly sensitive in the 1 - 5 μm region has finally permitted detailed photometric study of the red stellar population in external galaxies. This thesis is the result of such an investigation. we have shown that the red stellar component appears to be fundamentally similar in the central regions of bright galaxies of all but perhaps the latest morphological types, we have learned that this component is compatible only with stellar synthesis models having small mass-to-light ratios - models that are rich in late M giants, but which have only a minor contribution from late M dwarfs. The relation of infrared and optical colors between ellipticals and globular clusters was found to provide further support for the hypothesis that the color-luminosity distribution in early type galaxies is a metallicity sequence. on the other hand, the U - V, V - K color-morphology distribution that was identified here for the first time could be well reproduced by a simple population model.

A number of interesting problems remain: Detailed empirical or evolutionary models which fully incorporate the infrared data are certainly warranted. Evolutionary models coupled with additional infrared observations of very blue galaxies may clarify the question of whether there. are truly young galaxies, or just old galaxies with recent star formation bursts. A survey of UVK colors in galaxy clusters of varying richness might reveal interesting differences in star formation history between such clusters. Detailed point mapping of CO and H_2O indices off the nucleus might better indicate whether broad band galaxian color, gradients are primarily population or metallicity driven. Assuming the latter is the case in early-type galaxies, whether our knowledge of giant branch evolution can properly account for either the V - K color-aperture or color-luminosity relations discovered in this study is presently unclear. Finally, exploitation of new infrared spectral features which, could better pin dawn the nature of the very latest M stars in galaxies would be extremely useful.